Investigating Key Parameters Affecting Slurry Pipeline Erosion

by

Ardalan Sadighian

A thesis submitted in partial fulfillment of the requirements for the degree of

Doctor of Philosophy

In

Chemical Engineering

Department of Chemical and Materials Engineering
University of Alberta

Abstract

Slurry pipelines are widely utilized in most mining operations to transport the raw materials and the tailings. These pipelines typically suffer from high wear rates. For example, in Canada's oil sands industry, pipeline wear rates of 1 cm/yr are considered representative. To generate and measure such wear rates at the pilot-scale, significant resources (time and materials) are required; therefore, limited pilot-scale pipeloop investigations have been performed to study erosion in slurry pipelines. The present study is focused on identifying the underlying mechanisms affecting slurry pipeline erosion. The main goal is to relate the parameters affecting pipeline friction loss to erosion rate.

Initially, a lab-scale slurry pot tester was chosen to investigate the effects of slurry properties on erosion rate. In this phase, the effects of carrier fluid viscosity, impact angle and particle properties on erosion rate were studied. It was observed that particle density and shape strongly affect the erosion rate. Slurry-specimen impact angle also significantly changes the erosion rate. Finally, specimen erosion rates were measured at various carrier fluid viscosities. It was observed that carrier fluid viscosity has an indirect effect on the erosion rate. Using Bagnold's methodology, the normal and shear stresses on the specimen surface were calculated. The

magnitude of the normal and shear stresses on the surface were identified as the key parameters affecting the erosion rate.

In the next phase of the study, a purpose-built pipeloop was utilized to study the effect of slurry hydrodynamics on erosion rate using silica sand and Al_2O_3 slurries. Two pipe diameters (75 and 63 mm) were utilized in this study. It was observed that independent of particle type and pipe diameter, the erosion rate increases with increasing velocity. However, the erosion data from the two pipe diameters revealed that velocity cannot be used to model erosion data. After examining the evidence available in the literature, solids shear stress was introduced as an alternative to velocity for the purpose of erosion rate prediction. It was observed that the pipe erosion rate increases logarithmically with increasing solids shear stress.

In general, specimen surface stresses were identified as the key parameter affecting the erosion rate. Using solids stresses, a new model was proposed to predict the effect of flow parameters on erosion rate. The model proposed is capable of predicting the effect of flow parameters such as solids concentration and carrier fluid viscosity on erosion rate, which represents an important new tool for scale-up purposes. The results of this study can directly be applied to predict erosion rates in slurry

pipelines in the mining industry and specifically in Canada's oil sands industry.

Acknowledgment

I consider myself lucky for being class mates with my best friend and life partner for the last 12 years of my education. She helped me in every step of this Ph.D. and most probably this is the only section of this dissertation that has not gone through her watchful technical review. Therefore, without a doubt my biggest thanks goes to my wife (Leyli Mirmontazeri).

I am also grateful to have Sean Sanders as my Ph.D. supervisor. Being able to keep up with his extremely high standards is a daunting task but the final reward is definitely worth the effort. Beside his unique technical abilities, I always admired him for his ethical values. He thoroughly took the role of educator beyond the technical aspect.

I would like to use this opportunity to thank all of the people who gave me technical advice during the course of this Ph.D. and also apologize to the people who I forgot to include in this list: Reza Hashemi, Reg Eadie, Dongyang Li, Melissa McKibben, Ryan Spelay, Robert Cooke.

Special thanks goes to Tony Yeung. He has always been a great friend and helped me go through different steps of life including the present Ph.D. Beside friendship, his technical guidance has always been a great asset for me.

I thank my mother for being a great support and encouragement in my life. I will never forget all of her sacrifices to improve my life.

I would also like to thank Terry Runyon for her help, especially her efforts in making my graduation as smooth as possible. Also, Lily Laser thoroughly deserves my thanks for helping me all the way through my post graduate studies.

Contents

List of Figures

List of Tables

List of Symbols

Roman characters

A	Area (m^2)
A_1	Upper layer area (m^2)
A_2	Lower layer area (m^2)
A_P	actual particle area (m^2)
C	Volume concentration (%)
C_i	Volumetric concentration of component i (%)
C_{max}	Maximum packing concentration (% by volume)
C_r	In-situ solids concentrations (% by volume)
C_v	Delivered solids concentrations (% by volume)
C_s	Solids concentration
c	Fraction of particles cutting in idealized manner (% by number)
c	Speed of sound (m/s) Equation 1.5
cv	Wall contact particle flux (m/s)
D	Pipe diameter (m)
D_0	Reference pipe diameter (m)
d	Particle diameter (µm)
d^+	Dimensionless particle size
d_{50}	Particles size (µm)
d_A	Nominal particle diameter (m)
$(dP/dz)_s$	Solids pressure gradient inside the pipe (Pa/m)
$(dP/dz)_{s,o}$	Base line solids pressure gradient inside the pipe (Pa/m)
E	Erosion rate (cm/yr)
F	Normal force (N)
F_m	Empirical constant
F_s	Empirical factors for material properties
f_{cf}	Carrier fluid friction factor
f_f	Fanning friction factor
f_s	Particle friction factor
G	Gravity constant (m/s^2)
h	Penetration rate (m/s)
I	Erosion rate ($kg.m^{-2}.s^{-1}$)
J_I	Tangential stress (Pa)
J_{II}	Normal stress (Pa)
K	Empirical constant ($kgm^{-2}Pa^{-1}$)
k	Empirical constant (cm/year)
k_0	Constant
k_1	Constant
L	Spool length (m)
M	Mass of eroding particles (kg)
m	Mass of an individual particle (kg)
N	Measured gamma ray intensity (count/s)

N_0	Baseline intensity (count/s)
N_B	Bagnold Number
n	Empirical constant
P_c	perimeter of the area-equivalent circle (m)
P_p	Actual particle perimeter (m)
p	Pressure (Pa)
Q	Flow rate (L/s)
R	Slurry stratification ratio
r	Average particle radius (m)
S_1	Wetted perimeters of the top layer (m)
S_2	Wetted perimeters of the bottom layer (m)
t	Traverse time (s)
U	Particle velocity (m/s)
V	Velocity (m/s)
V_1	Upper layer velocity (m/s)
V_2	Lower layer velocity (m/s)
V_c	Deposition velocity (m/s)
V_L	characteristic particle impact velocity (m/s)
V_{NWL}	Crossover velocity
V_r	Eroded volume (m^3)
W	sand production rate (kg/s)
W_s	Wear rate (cm/yr)
w_0	Baseline wear rate (cm/year)
x_t'	Horizontal velocity of tip of particle when cutting ceases (m/s)
x	Length of beam through the slurry (cm)
x_w	Length of the beam through pipe wall (cm)

Greek characters

α	Impact angle (º)
β	Angle which defines the bottom layer height (º)
ρ_i	density of component i (kg/m^3)
λ	Linear concentration (% by volume)
η_s	Coefficient of friction between the particles and pipe wall
μ_f	Carrier fluid viscosity (Pa.s)
μ_f	Radiation absorption coefficient of the fluid (cm^{-1})
μ_s	Radiation absorption coefficient of the solids (cm^{-1})
μ_w	Radiation absorption coefficient of the pipe wall (cm^{-1})
$\tau_{1,}$	Upper layer averaged wall shear stress (Pa)
τ_2	Lower layer averaged wall shear stress (Pa)
τ_{12}	Shear stress acting in between these two layers (Pa)
$\tau_{average}$	Average stress (Pa)
τ_c	Coulombic stress (Pa)
τ_{cf}	Carrier fluid wall stress (Pa)

τ_k	Kinematic stress (Pa)
τ_f	Fluid stress (Pa)
τ_s	Inter-particle stress (Pa)
τ_w	Shear stress on the surface (Pa)
v_s	Local particle velocity (m/s)
$\dot{\gamma}$	Shear rate (s^{-1})
ρ_{cf}	Carrier fluid density (kg/m^3)
ρ_f	Carrier fluid density (kg/m^3)
ρ_s	Solids density (kg/m^3)

1. Introduction and Literature Review

Mining operations (and other industries) produce and transport large volumes of slurries (i.e. mixtures of solid particles and liquid). The conventional and most economical means of shipping these slurries is pipeline transportation [3, 4]. The wear life of the pipelines used for slurry transportation is of utmost importance, as any failure may result in significant environmental or economic losses. Part of the issue is that these pipelines operate at high solids concentrations and high velocities and material wear can occur through purely erosive or synergistic erosion-corrosion mechanisms [3]. Pipeline wear resistance and lifecycle are nearly impossible to predict and thus significant financial and human effort is dedicated to the study of wear [3, 5-8].

In commercial applications, wear rates of 1 cm/yr are considered to be on the high side. A wear rate of this magnitude typically limits pipe life to 1 year or less [3]. The time and energy required to reproduce and measure that rate at the lab-scale are prohibitive. Large volumes of mixture are also required. Therefore, limited wear testing using laboratory-scale pipelines has been performed. Instead, the mechanisms behind pipeline wear have been investigated using bench-scale equipment that bears little resemblance to pipe flow. Also, pipeline wear research is traditionally performed by material scientists with limited interest in pipeline

hydrodynamics [9-16] even though it is well understood that pipeline wear is a strong function of the flow past the pipe wall [17-21]. As a result, various attempts to scale up research data from lab tests to the industrial-scale have failed. For example, Parent and Li [3] compared the performance of carbon steel and stainless steel alloys in three (3) different bench-scale tests (jet impingement, slurry pot and ASTM G65, see Section 1.6 for detailed description and examples). In their bench-scale tests, the alloys showed relatively similar wear rates (i.e. maximum 15% difference); in a commercial pipeline, however, they observed that stainless steel will last at least 80% longer than carbon steel.

In the following sections, the importance of erosion damage will be discussed. Field measurement techniques and the current understanding of erosion phenomenon will be explained. Furthermore, current models to predict the erosion of slurries and single particle impacts will be introduced. Various research techniques will be evaluated and compared and finally the research objectives and contributions of this thesis project will be presented.

1.1 Wear costs

There are many examples of extensive wear damage found in the chemical and mining industries. For instance, fluidized bed reactors (e.g. heavy hydrocarbon cracking) face intense wear damage but excellent mass and heat transfer properties make them a good candidate for certain applications [22, 23]. Another good example is tailings transportation. Most mining operations use pipelines as the main method of tailings transportation. These pipelines face severe wear damage especially in the presence of coarse particles [24-27]. One can conclude that wear damage will directly affect the economics and operating efficiency of a plant.

To give an idea of the magnitude of the costs associated with wear damage, the annual costs for just one major producer in the Canadian oil sands industry is about $450 million annually [4], and, according to Fuhr et al. [28], $1 billion for the Alberta oil sands in general. Much of this cost is related to pipeline wear and can be categorized into three main areas [29]: a) operational costs; b) underproduction costs; and c) service costs.

To avoid unscheduled shutdowns and accidents, most plant owners utilize online monitoring for equipment that is exposed to abrasive conditions, such as slurry pipelines and pumps. Regular monitoring, especially in

remote areas, increases operating costs significantly [30]. In addition to cost impacts, harsh or hazardous environmental conditions may expose the plant staff responsible for the online monitoring to dangerous situations (e.g. underwater pipelines).

Wear damage will also decrease equipment efficiency. For instance, the efficiency of a centrifugal slurry pump will deteriorate substantially as the casing and impeller are exposed to the abrasive mixture. The rate of pump performance degradation is a strong function of the slurry abrasivity. For example, Gandhi et al. [31] showed that pump wear will increase significantly as the slurry solids concentration increases. Additionally, Wu et al. [32] studied wear on impellers in solid/liquid/gas mixed tanks. They observed significant wear damage on the impeller, which will decrease the mixing efficiency inside the tank. In addition to efficiency loss, wear damage can also cause equipment failure. Both of these phenomena will result in an overall decrease of efficiency and operating time; hence, an increase in production costs.

1.2 The importance of wear in pipeline design

Almost all attempts to predict and/or mitigate wear during pipeline design are based on knowledge gained through experience, with little fundamental understanding of erosion available to design engineers. Initially, choosing the proper pipe material plays a significant role in the overall performance of a slurry pipeline. For example, in the presence of corrosive material (e.g. water or acidic solutions) it is critical to choose a corrosion-resistant alloy (e.g. stainless steel) [33, 34]. Prediction of pipe wear behaviour is of importance in the case of justifying the use of high cost, novel alloys. Currently, most alloy developers and pipe manufacturers are only able to provide information on alloy ranking and qualitative comparison of different materials, which provides insufficient information to predict the exact life of a pipe in operation. For example, Tian and Addie [35] used a coriolis tester (see Section 1.6.3 for details) to study the effectiveness of 2 type of alloys (i.e. aluminum and high-Cr white iron). They used silica sand slurries with various particle sizes (d_{50} = 50 to 1400 μm) as the abrasive. They observed that the aluminum alloy shows a significantly higher wear rate than the high-Cr alloy. For both types of alloys, the wear rate increases as the particle size increases. The use of a coriolis tester in their study to some extent neglects the complexities of wear in an actual pipeline. For example, in a slurry pipeline, increasing the particle size may create a moving particle bed at

5

the bottom of the pipe and change the nature of the particle-pipe wall interaction (see Section 2.2.1 for details).

Pipeline sections should be replaced regularly as a result of wear damage. For example, in the oil sands industry, the average pipeline life is approximately one year [3]. As a result, pipe maintenance is a frequent activity in the plant, which strongly influences the life cycle analysis. Current knowledge of slurry pipe wear shows that it is a strong function of slurry properties such as velocity, particle size, density, shape and concentration[18-21]. To calculate the effect of these pipeline parameters on the overall pipe life, a clear understanding of the science of pipeline wear is required. For example, it is shown that the pipeline wear rate increases exponentially by increasing the velocity (see Section 1.4.1 for details). To minimize the wear, designers have the tendency to maximize the pipe diameter to operate near the deposition velocity[1] (V_c). Unfortunately, at this stage, most wear research is mainly focused on alloy ranking and the effects of slurry flow on wear behavior are not well understood [12, 36-38].

---

[1] Deposition velocity is defined as the minimum velocity which there is no stationary deposit in the slurry pipeline [36]. Operating below deposition velocity is highly not recommended.

1.3 Pipeline wear in the oil sands industry

On average, an oil sands open pit operation will have 90 km of slurry pipelines [39]. These pipelines transport various types of slurries, although all typically contain of sand, clays, bitumen and water. Process components exposed to a slurry are subject to an abrasive environment. The integrity of these transport systems is of utmost importance in the process and any failure will cause significant financial loss. As a result, plant owners have the tendency to employ very conservative wear prevention/monitoring strategies [39].

Currently, oil sands operators attempt to address erosion-related issues through regular monitoring [5]. All sections of each pipeline are regularly monitored to check the intensity of wear damage. The main test performed to check the integrity of the pipe is measurement of wall thickness by ultrasound probe [5]. There are several challenges in obtaining wall thickness measurements. Crews must be sent to remote areas with harsh environmental conditions which is costly and raises safety concerns. Even with recent improvements, ultrasonic measurements are still relatively inaccurate [40]. Kesana et al. [41] observed up to 300% difference in erosion rate simply by using different ultrasound techniques (i.e. Anglehead vs UT Maximum). This difference can be translated into a safety factor of at least 300% while determining the pipe thickness.

The current state of erosion handling relies on detecting and repairing wear damage. Without question, a more thorough and mechanistic study is a very valuable contribution to this field and by understanding the science behind slurry erosion, more proactive approaches can be employed. For example, by understanding the effect of solids concentration on pipe wear rate, an optimal flow condition can be chosen for the pipeline to minimize the wear damage. Good examples of such studies are presented by Parent and Li [3], Neville et al. [42], Schaan et al. [5] and Liang et al. [43].

Parent and Li [3] evaluated various pipe materials for application in the oil sands industry and provided recommendations regarding the appropriate type of alloy for different sections of the oil sands extraction process. These recommendations are based on the performance of these alloys in different bench-scale tests (jet impingement, slurry pot and ASTM G65, see Section 1.6 for a detailed description and examples). Carbon steel is recommended for low corrosion environments. Urethane-lined pipe had a poor wear resistance when exposed to impinging wear (e.g. elbows) but it was found to be suitable for all other operation conditions. Stainless steel is suggested for high corrosion environments with low slurry velocity. They observed that high slurry velocity will damage the protective layer of stainless steel and significantly reduce its wear resistance.

Neville et al. [42] studied the erosion-corrosion resistance of tungsten carbide metal matrix composite coatings. This is a popular coating for equipment used in highly abrasive environments in the oil sands industry. They used the jet impingement technique to expose four different types of coatings to a 5% (by mass) sand slurry. They found that erosion-corrosion (degradation) of such coatings is strongly affected by the surface structure (i.e. grain size). Studies of this type assist the plant operator in choosing the appropriate coating for specific slurry handling equipment.

Schaan et al. [5] analyzed Syncrude's Aurora mine hydrotransport and tailings pipelines. Pipe wall thickness at 600 different locations was tracked using a B-Scan ultrasound device (details described in Section 1.5.2). The results showed a significant increase in pipe wear at the 6 o'clock position of the pipe (i.e. pipe invert) compared to other locations on the pipe circumference. They attributed this wear to the presence of a sliding bed of coarse particles. Because of inconsistencies in slurry properties during the course of data collection, this study was not able to explain the magnitude of the pipeline wear that was observed.

Liang et al. [43] studied the corrosion-erosion of X65 steel in oil sands pipeline conditions. In their study, a jet impingement tester (see Section 1.6.2 for details) was used to bombard the specimen with oil sands slurry (i.e. oil sands process water + silica sand with an average size of 600 µm;

30% by mass). The slurry velocity was set at 3 m/s. They observed that the maximum wear occurred at an impact angle of 45°. Using CFD analysis, they calculated the stress distribution on the surface of the specimen. At low impact angles (e.g. 30°), the fluid shear stress was reported as the dominant wear mechanism. At higher impact angles (e.g. 90°), the particle impact stress was more dominant in determining the wear rate.

Pipeline wear is a well pronounced issue in the oil sands industry. Any investigation focusing on the mechanisms of wear in such pipeline will be a great asset for mine operators. Although oil sands pipeline wear is a combination of erosion and corrosion, the present Ph.D. study focuses only on pipeline erosion mechanisms.

1.4 Current understanding of erosion

In general, erosion can be defined as the removal of material from a slurry pipeline because of the impact between the dispersed solid particles and the pipe wall [44]. There have been numerous studies of slurry erosion (see, for example, Parent and Li [3], Gandhi et al. [45] and Shook et al. [8]). These studies can be categorized into three main groups:

1. Hydrodynamic effects
2. Single particle erosion
3. Alloy properties and erosion

Each group will be discussed in detail in the following sections.

1.4.1 Hydrodynamic effect on slurry erosion rate

In this area, the main focus is to understand the effect of hydrodynamic conditions (i.e. slurry flow) on the erosion rate. According to Shook et al. [6, 8, 19], the key parameters affecting slurry erosion rate are solids concentration, solids properties (e.g. density, shape and size), carrier fluid viscosity, impact angle, specimen properties and velocity. McKibben and Shook [46] organized these parameters into 4 main groups:

1. Velocity: They showed that $W_s \propto V^n$, where W_s is the wear rate, V is the velocity and n is the velocity exponent. As will be shown subsequently, the value of n can vary over a wide range depending on the experimental conditions.

2. Particle properties: They show that as the solids concentration increases the magnitude of energy transferred from particles to pipe wall will be affected. This energy is a key parameter determining the pipe wall erosion rate (see Section 1.4.2 for details).

3. Impact angle: It was shown that in pipe flow the impact angle is low (i.e. less than 20°) and does not affect pipe wear but in fittings and pumps this parameter may play an important role in determining the wear rate [47].

4. Fluid viscosity: Limited studies have been performed on this topic. Generally, the fluid viscosity will affect the particle-wall

interactions and consequently the wear rate [46]. It should be noted that this topic is discussed in detail in Chapter 3.

While it is clear that these parameters have a significant effect on wear rate, this list is probably woefully incomplete. The issue is that erosion testing is very time-consuming and expensive and so researchers are forced to focus on factors of primary importance. For example, Goosen and Maglas [48] did an extensive study on the effect of velocity on erosion rate using a pipeloop apparatus (see Section 1.6.5 for details). The tests were conducted at a velocity range of 2-5 m/s using a fly ash-water slurry (concentration range of 20-60% by mass). They reported exponential growth in mass loss as the velocity increases inside the line but limited data are presented to describe the effect of other parameters such as viscosity. Shook et al. [8] also conducted a comprehensive study to examine the effect of slurry hydrodynamics on the pipe erosion rate using a purpose-built pipeloop. They measured the solids flux at various angular positions of the pipe. They also measured wear distribution around the pipe. They observed a strong correlation between the wear distribution pattern and the solids flux. This study covered a wide range of solids size, concentration and slurry velocities but all of the experiments were performed on a 50 mm pipe.

As a result of such studies, various models have been proposed to predict the effect of velocity on erosion rate. For example, Faddick [49] reported that the erosion rate can be described as:

$$W_2 = W_1 \left(\frac{V_2}{V_1} \right)^n \tag{1.1}$$

where W is the absolute wear rate, V is slurry velocity and n is a number between 2 and 3 depending on the slurry properties. These models are empirical; hence, they have major limitations and drawbacks. For example, in contrast with Faddick, Goosen and Maglas [48] have observed that, in the case of PVC pipe and for a given type of slurry, $n = 1.4$. This degree of variation in the exponent 'n' can result in more than 200% difference in erosion rate by increasing, for example, the velocity from 2 m/s to 3 m/s. Wear predictions are commonly based on "models" (really, correlations) that consider only velocity. Figure 1.1 compares exponents of two empirical correlations. The comparison has been made using the same base line for zero velocity erosion rate. The velocity range represents a typical industrial slurry pipeline flow velocity.
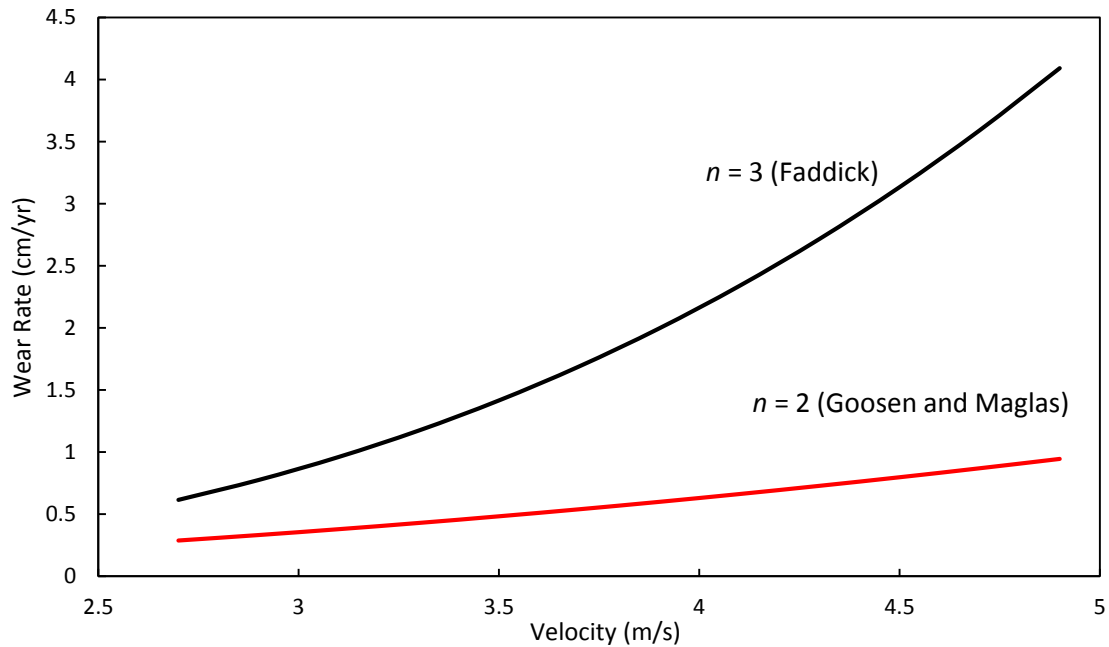
Figure 1.1 Wear rate calculated based on different empirical correlations

Figure 1.1 shows that the power model can only be used to predict the erosion rate in scenarios similar to the original experiments. Any attempt to scale up or extrapolate the data is likely to result in significant error.

Pellegrin and Stachowiak [50] built a sophisticated analytical model to examine the effect of particle shape and size on the abrasivity of the slurry (details available in the original publication). Their model is based on the image analysis of quartz particles. They concluded that particle shape (e.g. presence of sharp tips on the surface) plays an important role on the erosion rate. Their modelling approach depends on the detail analysis of a large number of particle images which makes it impractical for industrial applications. Also, the outcomes of the model are not validated with experimental data.

14

Finnie [51] proposed a well-accepted model to predict the erosion rate:

$$E = \mathrm{m}V^n f(\alpha) \tag{1.2}$$

where V (m/s) is the velocity, n is an empirical coefficient related to the surface material, f is a dimensionless function unique to each material and particle and α is the impact angle. This modelling approach shows strong functionality between erosion rate and impact angle. Figure 1.2 defines the impact angle in slurry-surface erosion studies.
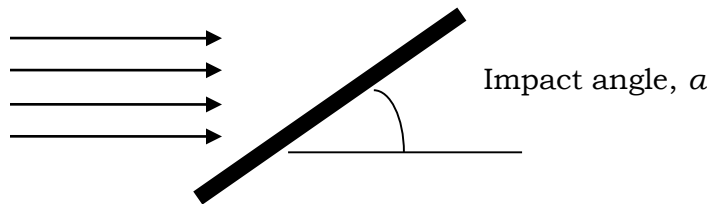
Figure 1.2 Sample-slurry flow orientation

Clark et al. [52] utilized a slurry pot tester to study the effect of impact angle on erosion rate. A carbon steel cylindrical specimen is exposed to a slurry of silica sand and diesel oil (<0.01% by volume). They analyzed the wear pattern and magnitude and reported that the erosion rate is a strong function of impact angle. Gandhi et al. [45] performed a similar study to evaluate the effect of impact angle on erosion of brass specimens in zinc mine tailings. They observed that the maximum wear occurs at an impact angle of 30° (these studies are described in detail in Section 3.2.1). On a much more practical level, Goosen and Maglas [48] utilized a pipeloop to study the erosion rate of pipe fittings and compared the result with erosion rates measured for a straight pipe. Although their study does

not directly investigate the effect of impact angle, it was shown that the overall impact angle will significantly change the magnitude and pattern of the wear. All of the studies show that erosion rate will change significantly when the impact angle changes.

Very few studies have been performed to evaluate the effect of slurry viscosity on erosion rate [46]. For example, Okita et al. [53] studied the effect of viscosity on erosion rate using a jet impingement tester. Huang et al. [20] used a pipeloop apparatus (see Section 1.6.5 for details) to study pipeline erosion. Based on their pipeloop data, they built a model which is capable of predicting the effect of viscosity on erosion rate. Kesana et al. [41] also studied the effect of viscosity on erosion rate in a pipeloop apparatus. They examined the pipe erosion rate at two slurry viscosities (1 mPa.s and 10 mPa.s). These studies are explained in detail in Section 3.2.2.

Limited studies have also been performed to investigate the effect of solids properties. For example, Gupta et al. [54] utilized a slurry pot tester to measure the wear rate of brass and mild steel in various types of copper processing tailings. Data were collected at different solids concentrations, velocities and particle diameters. They have proposed an exponential model to predict the effect of these parameters on erosion rate:

$$E = \mathrm{k}V^m d^n C_s^p \tag{1.3}$$

where d (m) is particle d_{50}, C_s (% by mass) is the solids concentration, V (m/s) is the velocity and m, n and p are empirical exponents. This model is only applicable to the specific system described in their study. Also, limited experimental data (e.g. only two solids concentrations are tested) collected and their non-mechanistic modelling approach significantly limits the application of Equation (1.3).

Fuhr et al. [28] performed a wear study on a pipeloop using a silica sand slurry to investigate the wear pattern and erosion rate on carbon steel piping. They studied the overall dependency of erosion on hydrodynamics by monitoring the effect of flow disturbance (i.e. pump and elbows) on the erosion pattern. Their experiments consisted of two trials: a) velocity = 6.8 m/s, solids concentration = 18% (by volume) and fines concentration = 1.12% (of solids); and b) velocity = 4.1 m/s, solids concentration = 20.5% (by volume) and fines concentration = 0.72% (of solids). They used an ultrasound technique to quantify the wear of the pipe wall (details described in Section 1.5.2). As multiple flow parameters changed in their trials, it is difficult to identify the effect of a single flow parameter on the wear pattern and erosion rate. They observed that elbows and pump disturbance affect the wear pattern. In their experiments, approximately 85 pipe diameters after the pump discharges was required for the flow to reach fully developed condition. The disturbance caused by

17

a 90° elbow required 50 pipe diameters to dissipate. Their findings are generally consistent with the results obtained earlier by Colwell and Shook [55]; however, there is some indication that the flow disturbance caused by a pump can persist farther downstream than was originally believed.

Most erosion studies rely on experimental observations. Computational fluid dynamics (CFD) can also be used to study the effects of slurry hydrodynamics on erosion rate, and is capable of tracking particle-surface impacts. The outcome of these impacts (i.e. surface erosion) cannot be predicted analytically; therefore, CFD models must be very carefully combined with experimental data to ensure that reasonable predictions are obtained. Lester et al. [56], Graham et al. [57], Chen et al. [58], Gnanavelu et al. [59], and Zhang et al. [60] represent good examples of this type of approach.

Lester et al. [56] used experimental data coupled with an empirical model [51]. Simulations provide predictions of particle trajectories and impacts and the empirical model is used to calculate the erosion associated with those impacts. They were able to successfully predict the erosion rates at different impact angles on a cylinder.

Chen et al. [58] utilized CFD modelling to predict the erosion in elbows and plugged T-junctions (i.e. a retrofitted T-junction used as an elbow fitting). The model uses an empirical correlation to predict the wear caused by a particle impact. Model validation revealed orders of magnitude error in the predicted erosion values. The root cause of this error appears to be the erosion correlation. Accurate experimental data can be used to tune the correlations and reduce the prediction error. Chen et al. were able to successfully predict the wear pattern, even though they were not able to predict the erosion rate/amount.

Zhang et al. [60] also used CFD to predict the erosion in elbows. In this study, built-in FLUENT wall functions are used to predict the particle impact behaviour. Using the impact velocity, particle size and wall erosion function, wear is predicted. The model predictions were validated with experimental data. They found that FLUENT accurately predicts the erosion rate for 256 µm particles but predictions for 25 µm particles were very poor. They believe the more chaotic movement of smaller particles (25 µm) results in inaccuracy in their predictions.

Gnanavelu et al. [59] also used CFD to predict erosion rates. They used a jet impingement apparatus (details discussed in Section 1.6.2) to collect experimental data relating particle trajectory to the erosion pattern. Using CFD to predict the jet impingement particle motions and coupling it with

19

the erosion pattern (acquired through experimental work), they were able to successfully predict the erosion pattern. Their approach is limited by the number of particles that can be tracked by the model; therefore, it has limited application in concentrated slurry systems (e.g. industrial pipelines).

Graham et al. [57] have utilized CFD analysis to model the erosion rate on elbows and cylindrical objects. In their study, they used Grant and Tabakoff's [61] model to predict the erosion caused by each particle. They were able to successfully couple the erosion rate to particle impact rate, velocity and impact angle. However, model parameters used in this approach come from experimental data and must be adjusted for each particle and surface type. Even with large quantity of literature available on the topic of CFD wear modelling, all successful models have limited application and any attempt to extrapolate data requires model validation.

In conclusion, the current understanding of slurry pipeline erosion is inadequate. The models proposed by researchers are very limited and are only able to predict the erosion rate in the exact situation of the tests. Any attempt to scale up or extrapolate the data has failed. The effects of other slurry properties (beside velocity) on erosion rate have not been investigated sufficiently. More detailed studies are required to understand

the effect of properties such as solids concentration and carrier fluid viscosity on erosion rate.

1.4.2 Single particle erosion models

A significant portion of the research performed in the area of slurry erosion has focused on single particle behavior. Generally, experimental studies consider the impact of a particle with a flat surface and the resultant damage zone is examined [36, 44, 51, 62, 63]. The goal of these studies is to generate models that can predict erosion according to the main impact parameters, which include:

1. Particle and flat surface hardness
2. Particle impact angle
3. Particle velocity
4. Particle shape and size

Many models of single particle impact include numerous complicated parameters that are not easy to predict or measure, such as particle tip horizontal velocity. A classic example of a single-particle erosion model was introduced by Finnie [36]:

$$V_r = \frac{cMU^2}{4p\left(1+\frac{mr^2}{I}\right)}\left[\cos^2\alpha - \left(\frac{x_t'}{U}\right)^2\right] \tag{1.4}$$

where:

V_r = volume removed from surface (m^3),

M = mass of eroding particles (kg),

m = mass of an individual particle (kg),

r = average particle radius (m),

α = angle of impact,

U = particle velocity (m/s),

p = horizontal component of flow pressure (Pa),

c = fraction of particles cutting in idealized manner (%by number),

x_t' = horizontal velocity of tip of particle when cutting ceases (m/s).

This type of model has very limited direct application and is mainly used to study the science behind particle-surface collisions. There are notable exceptions: for example, Neville et al. [37, 59] were successful in coupling a single particle erosion model with CFD simulations to develop a practical approach for predicting the erosion pattern. The model requires one to track all of the particles and also requires experimental wear data for all of the particle-surface impacts. This approach cannot be used for concentrated slurries or "complicated" geometries, where even a curved pipe surface would be considered to be complicated.

There are various models available to predict erosion rate but they have very limited application. Most models only focus on a single parameter (e.g. velocity) and do not consider the effect of any other variables. These

22

models can only be used to investigate the effect of a given parameter in the specific test situation. For instance, if an equation is proposed to calculate the effect of velocity on erosion rate in a 3 inch pipe, this equation cannot be used for a different pipe diameter. The models that investigate single particle impact are useful in the study of the science behind erosion but measurement complexities and computation limitations restrict their application in concentrated slurries.

1.4.3 Effect of specimen (i.e. alloy) properties on erosion rate

According to McKibben and Shook [64], pipe material plays a key role in determining the overall wear rate. There have been extensive studies comparing various types of alloys with different properties (e.g. hardness). Brown and Heywood [64], Huang et al. [65], Ye et al. [66, 67] Shook et al. [19] are good examples of such studies.

Brown and Heywood [64] used a pin-on-disk (see Section 1.6.3 for details) device to examine the effect of specimen hardness on erosion rate. In their study, a wide range of materials including steel alloys and ceramics were examined. They showed that harder materials provide higher wear resistance.

Huang et al. [65] used a jet impingement apparatus (see Section 1.6.2 for details) to test the wear resistance of copper-nickel alloys. They tested the wear performance of specimens of various compositions of copper and nickel blends. The specimens were bombarded with fine sands (50-70 µm) carried by high velocity air. The particle impact velocity is set at 55 m/s. They observed that the specimen hardness increases as the nickel concentration increases. By increasing the hardness (i.e. higher nickel concentration) the wear resistance of the specimen was improved. However, after a certain hardness, the wear resistance decreases. They associated this behaviour to the presence of oxides on the surface.

Ye et al. [68] investigated the effect of specimen porosity on wear rate. They studied the wear resistance of titanium-nickel (TiNi) alloys. A pin-on-disk device was used for this investigation. It was observed that increasing the surface porosity will significantly reduce the specimen wear resistance. In a related study [66] they heat-treated the TiNi alloy surface and observed that the porosity decreases with heat treatment. It was observed that the heat-treated TiNi alloy has a significantly higher wear resistance which was attributed to its lower surface porosity (compared to the original alloy).

Shook et al. [19] studied the wear resistance of various type of alloys using a 50 mm pipeloop (see Section 1.6.5 for a detailed description of

24

the pipeloop apparatus). Sand-water slurries (with different particle sizes and solids concentrations) were tested. They observed that for fine sand slurries, high density polyethylene has a better wear resistance compared to steel. In contrast, steel has a higher wear resistance than polyethylene when exposed to coarse sand slurries.

In the next section various wear measurement methods will be introduced and the advantages and disadvantages of each will be presented. Reliable wear measurement techniques are essential in any strategy to develop or validate models of wear prediction.

1.5 Wear measurements

To study wear, one must be able measure the wear damage. This measurement includes both the amount and the pattern of the wear. There are several techniques available to track the wear damage on a surface. Each technique has limitations and advantages. However, there are very few methods that can be used on industrial pipelines. In this section, the limitations and benefits of various techniques will be described.

1.5.1 Mass loss

In this technique, the wear of a specimen is calculated by measuring its mass loss during the course of experimentation/operation. Normally, the mass measurement is performed using an accurate scale. However, as the sample overall mass increases (e.g. for a large-scale pipeloop) the accuracy of the weight measurement will decrease.

This technique is very reliable and generates repeatable data. The low cost and low level of complexity make it a good candidate for wear measurement. One drawback is that this method characterizes overall wear of the specimen and provides no information on localized wear. Also, the specimen surface may absorb material (e.g. heavy oil residue). To generate accurate and repeatable data, this residual material should be carefully removed.

1.5.2 Wear rate tracking via specimen thickness measurement

In this method, the thickness of a specimen is measured to calculate the local wear at that specific location. The most common tool selected to perform this measurement is an ultrasound probe [40, 69-74]. Ultrasound waves travel through a metal at a constant velocity. This velocity is unique for each alloy [74]. The ultrasound probe measures the time that

26

the wave travels inside the alloy and using the specific velocity for that alloy, the thickness can be determined:

$$Thickness = \frac{t}{C}$$ (1.5)

where t is the traverse time and C is the speed of sound in that specific alloy. This technique is relatively cheap and simple. Also, the nondestructive nature of ultrasonic thickness measurements make them an excellent candidate for commercial pipe thickness measurement [69-71, 74].

The accuracy of this technique depends on the accuracy of the instrument and the conditions in which it is applied. In an ideal condition, it can measure up to 0.01 mm in thickness change [72]. It should be mentioned that the accuracy will decrease dramatically when the probe is used on a curved surface and exposed to a slurry flow (e.g. slurry pipe wall). The spatial resolution of the test depends on the probe size [73, 75]. The surface on which the ultrasound probe is utilized should be flat and coatings or rust should be removed before the measurements are made [75].

As reported by Schaan et al. [5], Syncrude has used a brightness ultrasound (B-scan) device (Panametrics Epoch 4) to monitor slurry pipeline wall thickness. The B-scan technique assigns unique brightness values for each material in the path of the ultrasound wave. This

brightness information will be translated into an image highlighting each layer on the path of the wave. This image is used to verify the thickness. In their study, the measurements were performed on 2-3 cm intervals along the pipe circumference.

Because of the inconsistencies in readings caused by environmental factors such as the curved pipe surface, the ultrasonic technique is very skill-oriented. For generating repeatable data, the experimental procedure should be followed meticulously and preferably done by the same operator. In general, this technique is not recommended for detecting small changes in thickness. On the other hand, it is a simple, cost-effective technique which makes it valuable for field measurements [40, 69-71]. Recently Kesana et al. [40] manufactured a belt arrangement for the ultrasound probe. This arrangement fixes the location of the probes on the pipe wall which will mitigate the negative effect of pipe curvature on the thickness measurement. In their study, they have installed 16 probes on an elbow to investigate its erosion rate. They noticed that the erosion rate increased by increasing the particles size from 150 μm to 300 μm. The erosion pattern was not affected by the particles size in their study.

A relatively less sophisticated ultrasound device is the Scanimetrics [76] wireless pipe thickness sensor. The sensor is robust and because it is positioned at a fixed location, the accuracy of the sensor is improved. The

wireless data transfer capabilities make it a good candidate for use in remote locations.

Cidra produces a belt sensor under the commercial name of HALO [77]. This instrument has twelve sonar probes spaced equally on the pipe circumference. Using sonar technology, they were able to measure the pipe wall thickness at various angular positions around the pipe. The fixed arrangement (in contrast with a single sensor placed on various locations by the operator) will significantly increase the accuracy and repeatability of data. The details and operating principles of the sensor are not disclosed by the manufacturer.

As a more direct and accurate technique, special micrometers can be used to measure the wall thickness. For example, MITUTOYO Hub micrometers are designed with a small head so the user can fit it inside the pipe for thickness measurements. To perform such measurements, the pipe should be drained and the specimens should be disassembled [78].

1.5.3 Wear damage pattern examination

In addition to wear magnitude measurement, it is often important to examine the wear pattern on a specimen. A common technique for such an examination is to coat the specimen surface with paint. When the specimen is exposed to slurry, the paint layer will be eroded. Wear spots can be detected according to the resulting pattern. Removal of a layer of paint cannot reveal the wear quantity [71]. To overcome this problem, Parslow et al. [7] applied multiple layers of paint, each with a different color and a known thickness; hence, relative local wear magnitude can be calculated by observing the different colors exposed. Wu et al. [32, 79, 80] used the same technique to study impeller erosion in mixing tanks. Recently, Loewen [81] used urethane to coat the specimen. The urethane surface will be eroded at a higher rate compared to the original pipe material which will decrease the experiment time significantly. The disadvantage is that this technique does not consider the effect of material properties on the erosion.

In many erosion studies, more quantitative surface examination techniques are utilized to characterize the wear pattern. The most common devices used for this purpose are the Scanning Electron Microscope (SEM) and the optical microscope [82-85]. These techniques can only give local data regarding the wear pattern on a microscopic-scale. For example Dong et

al. [83] used the block-on-ring apparatus (see Section 1.6.1 for details) to study the wear resistance of Carbon Nano tube reinforced alloys. They used SEM to examine the erosion pattern on the specimen. The area studied was 15 µm × 15 µm.

To evaluate the wear pattern on a more macroscopic scale, one can use a profilometer [86]. This tool works on the principle of laterally moving a stylus on the surface (in contact) and tracking its vertical displacement. This method is not limited to flat surfaces and can also be utilized on curved surfaces (e.g. pipe wall) [87]. Buschinelli et al. [88] replaced the solid stylus with a laser beam to increase the accuracy of the measurements. They investigated the effect of corrosion on the roughness of oil pipelines. Similarly, Graham et al. [57] used a laser scanner to quantify wear on complicated geometries. In their study, the wear pattern on a cylinder exposed to slurry was determined using a 3D laser scanner and coordinate measuring machine.

1.6 Experimental approaches in the study of wear

Many different approaches have been taken to study wear. Each method has been developed for specific applications. In general these techniques can be categorized in six main groups:

1. Dry and wet erosion testers

2. Jet impingement

3. Accelerated slurry flow simulators

4. Toroid wheel

5. Pipeloop

6. Operating pipeline

In the following sections, the principles of operation of each test will be discussed, and the advantages and limitations of each technique will be described.

1.6.1 Dry and wet erosion testers

In general, these techniques work on the principle of sliding two flat surfaces and monitoring the specimen mass loss. The samples should be manufactured with certain specifications and usually the abrasive material cannot be changed. The American Society for Testing and Materials (ASTM) G99 test (i.e. pin-on-disk) and ASTM G77 test (i.e. block-on-ring) are good examples of such techniques [1, 2, 85, 89-91]. Schematic

illustrations of these devices are shown in Figure 1.3. Another popular technique in this group is the ASTM G65 test, which is depicted in Figure 1.4. The main advantage of the G65 tester is the use of solids particles as the abrasive material (in contrast with the abrasive surfaces used in the ASTM G99 and G77 testers).
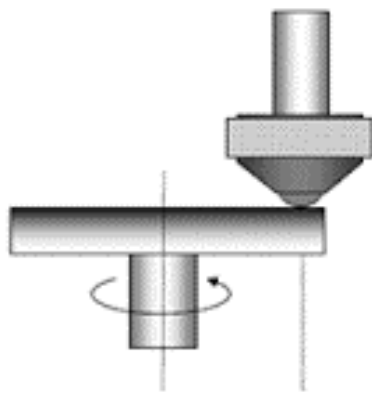
ASTM G99 pin on disk tester   ASTM G77 block on ring tester
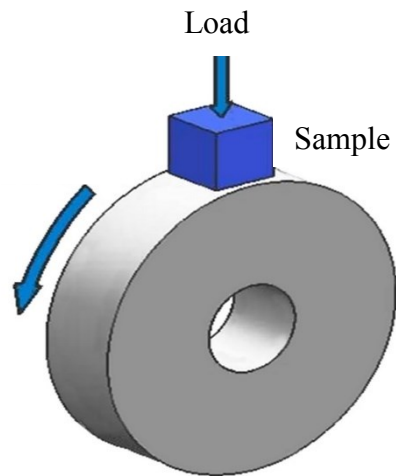
Figure 1.3 ASTM G99 and ASTM G77 schematic [1, 2]
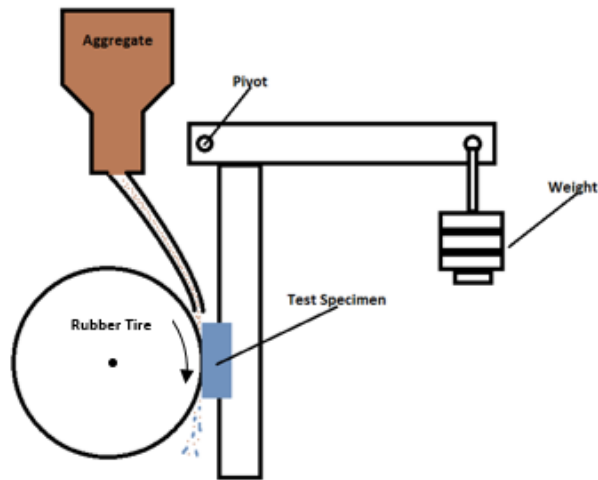
Figure 1.4 ASTM G65 schematic [92]

Because these ASTM tests utilize standardized procedures and well-defined geometries, they produce highly repeatable data, which makes these techniques perfect for alloy ranking. Also, they can be used for the purpose of data comparison between various laboratories and research studies. The test time is relatively short (e.g. 1 hour) and the amount of required sample is small [89, 90]. For example, Guilemany et al. [85, 91] used an ASTM G65 tester to check the wear resistance of novel hard chromium alloy coatings. In their study, the wear resistance of Cr_3C_2-NiCr (CC-TS) and Hard Chromium (HC) steal coatings were compared. The HC coating showed 3 orders of magnitude greater material loss compared to the CC-TS sample.

Gee et al. [90] used these techniques to evaluate the effect of surface hardness on erosion. In this study, an ASTM G65 tester was used on hard metals with hardness values in the range of 800-2200 HV. Three different

34

wheel materials were used: a) dry rubber; b) wet rubber; and c) wet steel. In all cases, the wear rate decreased as the hardness increased. For low hardness materials, steel abrasive shows 2 orders of magnitude higher wear rate compared to rubber. However, for materials with hardness values greater than 1800 HV, all of the abrasive materials produced relatively similar wear rates.

In this group of tests, the specimen and the abrasive material have fixed arrangement (i.e. abrasive sliding on the surface of the specimen) which limits their applicability. Such tests can only rank alloy resistance to sliding wear. The effect of impact velocity, solids concentration and any other slurry properties cannot be studied.

1.6.2 Jet impingement

The jet impingement technique is based on the principle of stagnation point flow, i.e. the particles are "shot" at the specimen. The surface deformation and damage can then be characterized. A general schematic of the experimental setup is displayed in Figure 1.5.
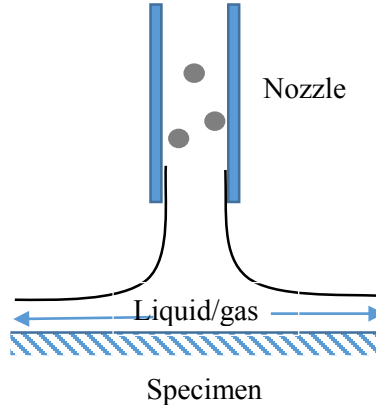
Figure 1.5 Jet impingement schematic

There are numerous variations of this technique. It can operate dry [93, 94] where the particles are carried by gas (e.g. air) or the particles can be suspended in a liquid phase [37, 59, 62]. Also, this equipment can be used to study one particle impact or impacts from a group of particles. The main parameters that can be controlled are particle velocity, impact angle [95], particle size and shape and specimen type [96]. This technique is very good for surface examination studies. A specimen with a specific composition or coating can be tested under conditions where impact angle and particle velocity are held constant. Afterwards, the impacts can be closely examined using SEM or an optical microscope. Surface examination can reveal valuable information, such as the shape of the erosion site and volume of the material removed from the surface [63]. Clearly, this approach is excellent for ranking alloys by comparing the wear damage under identical test conditions.

Because of the well-controlled nature of the system from the perspective of particle-surface impacts, the jet impingement test is the most common technique modelled using CFD studies, or used in combination with CFD studies to predict wear in other geometries. These studies generally combine erosion experiments with single particle erosion models. This technique was originally developed by Zu et al. [94] and later on various researchers combined erosion models with particle impact data obtained from jet impingement tests. For example, Shirazi et al. [97] developed a semi-empirical model to predict the erosion caused by single particle impact using CFD and jet impingement experiments:

$$h = F_m F_s F_p \frac{W V_L^{1.73}}{\left(D/D_0 \right)^2} \tag{1.6}$$

where h is penetration rate, F_m and F_s are empirical factors for material properties and particle sharpness (respectively), F_p is the penetration factor, W is the sand production rate, V_L is the characteristic particle impact velocity, D is the pipe diameter, and D_0 is the reference pipe diameter (25.4 mm). A material parameter (F_m) needs to be acquired experimentally through impingement tests. The particle sharpness factor (F_s) is a function of particle shape and the penetration factor (F_p) is a function of the geometry of the system, which should also be acquired experimentally.

Gnanavelu et al. [59] developed a methodology to predict wear at different velocities and impact angles. Initially, they performed jet impingement tests using 250 µm sand at velocities of 5-10 m.s^{-1}. Afterward, by performing CFD simulations of the jet impingement system, particle velocity and impact angle at each radial position on the specimen are predicted. Combining the CFD simulations and the wear tests, they successfully mapped the erosion to particle impact angle and velocity. Using this erosion map and CFD simulations, they predicted the erosion for other geometries. In their simulations, they have made two key assumptions: a) particles are spherical; and b) particle-particle interactions are negligible. Considering these assumptions, their methodology cannot predict the effect of particle shape. Also, as particle-particle interactions are dominant in concentrated systems, this modeling approach is probably not applicable to most industrial slurry pipelines.

Because of the simplicity and short experiment time, many researchers and plant owners rely heavily on jet impingement tests to evaluate/predict the wear behaviour of commercial equipment. For example, Tang et al. [98] used jet impingement tests to evaluate the erosion/corrosion behaviour of X65 steel which is often used in oil sands applications. In their experiments, they varied impact angles from 30° to 90°; hence, the effect of sliding wear was not examined.

Generally in jet impingement tests, the velocity is much greater than would ever be observed in an operating slurry pipeline. Also, the limitations on the impact angle prevent the user from examining the effects of sliding shear on the surface wear; hence, jet impingement is not recommended for pipe flow simulations and scale up.

1.6.3 Accelerated wear simulators

Process equipment (e.g. pipe and pumps) wear will usually reach measurable levels (i.e. within the accuracy of the measurement technique) in the course of a few months. For example, for oil sands pipelines, a typical wear rate is less than 1 mm/month [5]. As a result, many attempts have been made to simulate pipe wear in an environment that provides accelerated wear. These tests also require small slurry volumes and relatively small specimens, which greatly reduces the costs associated with wear testing. In this section, the slurry pot and coriolis testers will be discussed.

Slurry pot tester

In general, the slurry pot tester works on the principle of exposing the specimen to abrasive slurry (e.g. sand-water slurry) in an enclosed pot. Various arrangements have been studied. For example, Yu et al. [99], Rajahram et al. [100] and Clark [101-103] placed the samples on the rotating shaft to expose them to the slurry and simultaneously suspend the particles (i.e. samples acting as impeller blades). In another arrangement a separate impeller is used to suspend the particles. Samples are exposed to the slurry by mounting them on a sample holder inside the mixed slurry [10, 15, 103-105]. Usually the erosion is measured by weighing the samples before and after each experiment. However, the surface of the sample can also be examined to evaluate the wear pattern. This experimental apparatus is often custom-built (as opposed to purchasing an off-the-shelf unit). It usually consists of an impeller, a tank and an electromotor. The setup should also be equipped with a heating/cooling jacket to control the slurry temperature. Different sizes of slurry pot testers have been used, ranging from 3.8 L [45] to 10 L [99].

In this technique, specimen properties, the rotation velocity, impact angle and slurry properties can be controlled. For example, Clark [103] used a cylindrical aluminum specimen placed inside the slurry pot tester to investigate the effects of impact angle and particle size on the erosion

rate of the specimen. Slurries containing <0.01% (by volume) glass beads (diameters of 10-1000 µm) were used as the abrasive. The results showed that the maximum wear rate occurred at an impact angle of 40°.

Because of the significant difference in hydrodynamic conditions from pipe flow (e.g. particle impact angle), bench-scale slurry pot testers results are generally not suitable for scale up. For example, Madsen [106] performed wear measurements using a slurry pot tester both in the laboratory and in the field (Figure 1.6). Both tests were performed at a temperature of 294 K and a flow rate of 4500 mL/min with 20% (by mass) and 25% (by mass) slurries (clay and chlorite in water, details available in the original publication [106]). In the field, this rate is controlled by the pump and in the laboratory experiments it is controlled by the impeller speed.
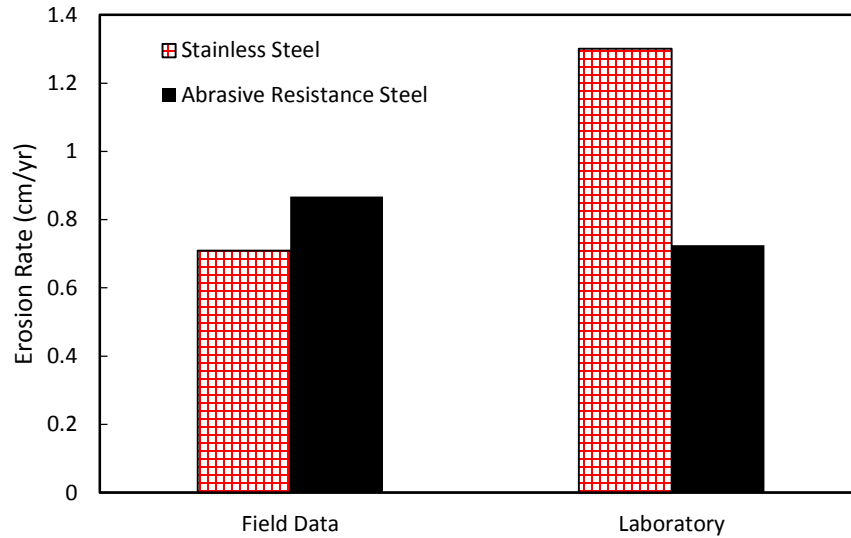
Figure 1.6 Slurry pot measured wear rate for stainless steel and abrasive resistance steel in field and laboratory conditions [106]

It can be observed that the same equipment and type of alloys shows different wear behaviour in field and laboratory conditions. It is possible the field conditions were not identical to the lab tests.

In contrast with Madsen [106], Gupta et al. [54] showed good agreement between slurry pot tester and pipeloop wear results. They used similar slurries in a pipeloop and slurry pot tester and were able to successfully correlate the wear rate data generated from both devices. This study is described in detail in Section 3.2.1. Still, one should be aware of the fundamental differences between the flow pattern inside a slurry pot and in pipe flow. Any scale up attempts should be validated using pilot-scale, pipe loop experiments.

Because of the well-defined geometry of the slurry pot tester, analytical modeling (e.g. using established models to predict the flow behaviour on the specimen surface) are used [103]. The evidence suggests that the slurry pot tester is the best candidate among bench-scale tests for erosion studies that can be directly related to pipe wear studies [54]. For this reason a slurry pot tester has been utilized as a part of the present study to investigate the effect of carrier fluid viscosity and impact angle on the erosion rate.

Coriolis tester

Tuzson et al. [107, 108] developed the original coriolis wear tester in the 1980s. An illustration of their coriolis tester is shown here as Figure 1.7. Coriolis tester work is done on the basis of creating an environment with enhanced slurry-specimen impact [35, 109-112]. This exaggerated impact condition gives the ability to study erosion phenomena in a more time-efficient manner. The slurry is fed through a channel. The feeder rotates, creating centrifugal and coriolis forces. These forces pump the slurry through the outlet channels. The specimen is placed inside the channel and the surface is exposed to the moving slurry.
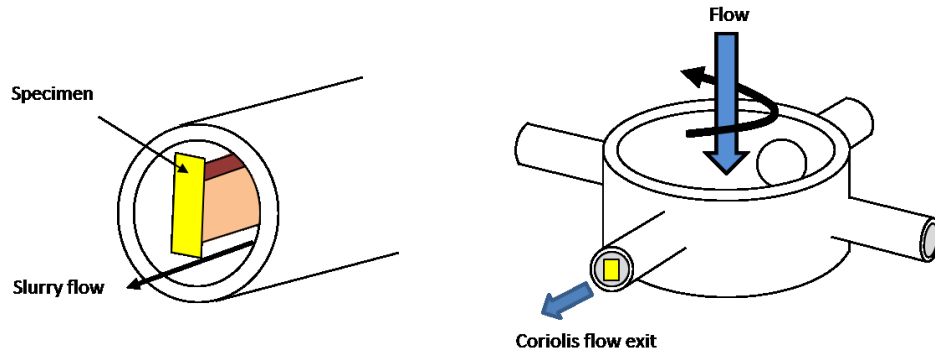
Figure 1.7 Coriolis wear tester [107]

After a certain time the specimen is removed and the wear scars on it are examined. The wear damage area is measured at different radial positions and the results for different materials are typically compared. Clark and Llewellyn [113] used a coriolis tester to investigate silica sand slurry erosion on various types of steels. Their study showed that the wear damage area will increase with radial position. The wear damage area/position behaviour can be correlated to the specific energy of the particles impacting the surface.

The coriolis tester is an inexpensive device that can be easily built and assembled in a lab. Only a small volume of slurry is needed for each test. Moreover, by manipulating the sample holder angle, the impact angle can be changed. However, the flow properties and the impact angle are different from the pipeline condition. In comparison with the slurry pot tester and with industrial pipelines, the typical test velocities are much higher (e.g. 20 m/s [113] compared to 5 m/s [101]). As a result, data from this method cannot be used to predict wear rates in commercial pipelines.

1.6.4 Toroid wheel

The toroid wheel [47] can basically be described as a pipe curved to form a wheel. A portion of the wheel (usually one third) is filled with slurry. The wear specimen is placed inside the curved pipe on the outer circumference, and is held in place with a sample holder [47].The whole system is rotated axially using a motor. Because of gravity, the solids will sit on the bottom of the wheel. Since the specimen is attached to the wheel, it will be exposed to the slurry once each revolution with a relative velocity equal to the linear velocity of outer perimeter of the wheel (i.e. sample location). In principle, this motion is similar to having the specimen at a fixed location and slurry flowing over it. Typically more than one sample holder is provided on each wheel which enables the user to run multiple tests simultaneously using the same slurry. A schematic of this apparatus is presented in Figure 1.8. This apparatus was initially developed by Worster and Denny [114] to study the behaviour of coal particles traveling in a pipe. Later on, Cooke and Johnson [47] developed a toroid wheel based on the same principle to study wear in slurry pipelines.
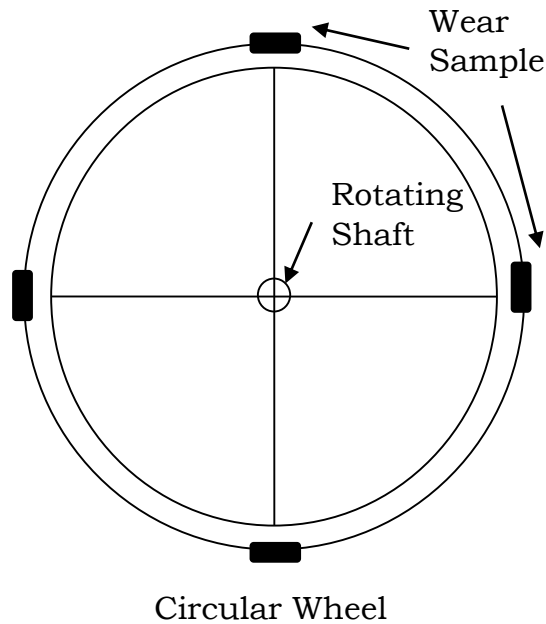
Figure 1.8 Toroid wheel erosion tester

In addition to the circular arrangement described above, Henday [115] has reported a pentagonal wheel which consist of five straight pipes. The bends in the pentagonal wheel will impose an extra disturbance on the flow which may change the wear pattern and the wear rate of the sample. As a result, the circular arrangement is superior to the pentagonal one.

Although the slurry has zero velocity and the pipe wall (i.e. wheel) is rotating, the relative velocity between the slurry and the wall is similar to pipe flow. Also, the effect of curvature on the flow pattern can be minimized by choosing a large wheel diameter/pipe diameter ratio. Considering these facts, toroid wheel tests provide hydrodynamic conditions that are thought to be similar to pipe flow. Cooke and Johnson

[47] used this technique to measure the erosion rate for different solids concentrations (Figure 1.9).
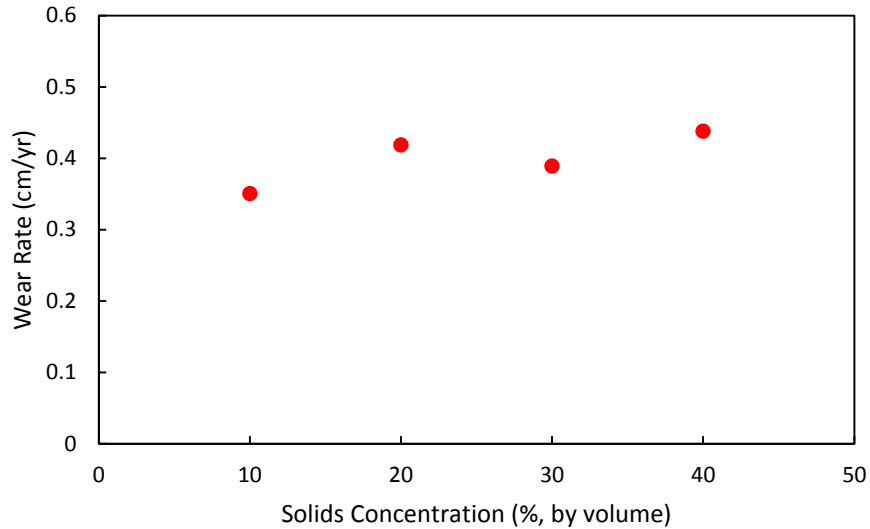
Figure 1.9 Cooke and Johnson study of solids concentration effect on wear rate using a toroid wheel, mild steel wear plate, velocity = 3 m/s, particle d_{50} = 70 μm, particle density = 3640 kg/m^3 [47]

They observed a slight increase in overall wear as the solids concentration increased. However, one can observe that the data do not show a clear pattern.

Slurry abrasivity will decrease as the particles contact each other and the flow boundaries [18, 47]. This phenomenon is usually referred to as particle degradation (additional details are provided in Section 4.3.2). Particle degradation will be more pronounced as the particles are exposed to high velocities and rapid direction changes such as during flow in a centrifugal pump. The slurry inside the toroid wheel does not go through a pump and it is exposed only to the pipe wall. Therefore, particle degradation effects should be lower than they would be in other

47

techniques that recirculate the flow using a pump. Also, the amount of sample required for toroid wheel tests is significantly smaller than that required for pipeloop experiments (see Section 1.6.5).

As the pipe is bent and the cross section is square, the hydrodynamic conditions are almost certainly not identical to pipe flow (e.g. presence of secondary flows). After a certain rotation velocity, the solids will be entrained by the wheel and are no longer stationary on the bottom of the wheel; therefore, higher velocities cannot be tested because of slurry carryover.

1.6.5 Pipeloop

A popular tool to study actual slurry pipeline erosion is the pipeloop [6, 8, 17-21, 48, 116, 117]. This laboratory apparatus consists of a pipeloop and a pump which circulates the slurry (Figure 1.10). The recirculation arrangement will significantly reduce the amount of the slurry required for the experiment. For example, a 3 inch diameter pipe operating at $V = 3$ m/s, requires 10 L/s of slurry if the flow does not recirculate. In a "once through" test enormous slurry volumes would be required, especially considering that a typical erosion experiment may take weeks to produce one data point. In contrast, by recirculating the flow, the user will only need enough sample to fill the volume of the loop (e.g. 200 L volume for

48

an 80 m long, 3 inch pipeloop). Typically this sample can be used for the duration of the test unless the flow properties changes (e.g. particle degradation, as explained in Section 4.3.2).

Test and Instrumentation Section

Test and Instrumentation Section

Feed Tank   Pump
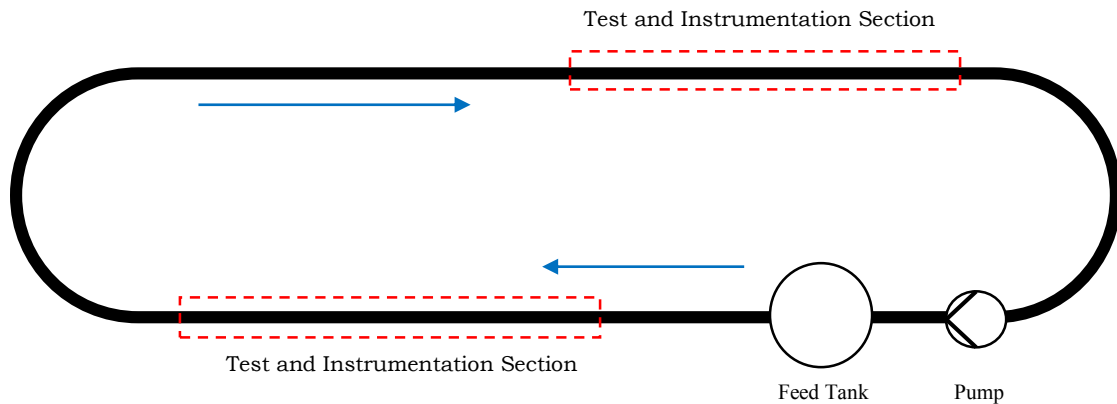
Figure 1.10 Sample pipe loop setup schematic

Different instrumentation and equipment (e.g. pressure gauge, flow meter) can be installed in the loop. The type and location of the sensors can be different for each experiment. For example, to study slurry frictional losses, accurate pressure and flow rate information is required but in a long term erosion study, the flow rate does not need to be monitored as rigorously.

Fittings and loop components (e.g. pump) will cause flow disturbances. To achieve fully developed flow, a single phase flow should travel at least 20 pipe diameters in a straight section [55]. It is critical to install the sensors (e.g. pressure transmitters) and place the test spools (i.e. erosion specimens) in the fully developed sections. For coarse slurries the flow

should travel at least 100 pipe diameters to achieve fully developed conditions [55]. Typical test sections are marked on Figure 1.10. Also, as the slurry properties are a function of temperature, it is important to keep the temperature of the slurry constant; hence, a pipeloop test apparatus should be equipped with a heat exchanger.

Clearly, pipeloop erosion studies can be designed to produce exactly the operating conditions of interest, albeit at a smaller scale. However, pumping of the slurry causes rapid particle degradation (details available in Section 4.3.2). As the wear rate is a strong function of particle properties (see Section 1.4.2), this technique needs to be modified to address the particle degradation issue. Cooke [21] proposed an experimental procedure to back-calculate the particle degradation. They initially ran wear experiments where the slurry was replaced every 80 hours (independent of total experiment time). At the end of the run (e.g. 240 hours and 3 slurry changes) they recorded the wear rate. Afterwards, they repeated the test using shorter slurry change intervals (e.g. 5, 10 and 20 hours). Figure 1.11 shows the erosion rate for each particle replacement interval. The wear rate decreases exponentially with increasing slurry replacement interval.
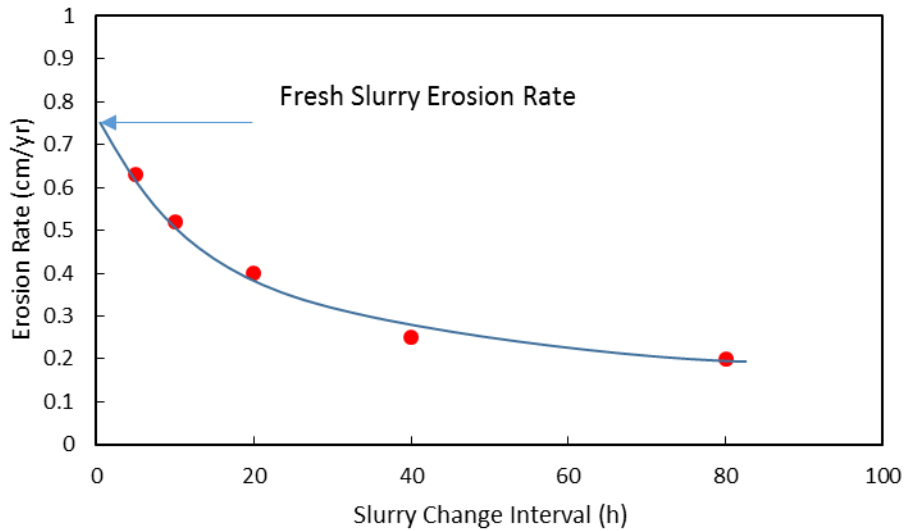
Figure 1.11 Erosion rate vs slurry change interval inside the loop [21]

By extrapolating the exponential graph to time zero, the wear rate for fresh slurry can be calculated. This method is time-consuming and also involves large slurry volumes.

It is clear that there are many drawbacks associated with pipeloop wear testing. As mentioned in the previous paragraphs, these include: a) large volumes of slurry required for each test; b) long experiment time (e.g. 4 weeks); c) particle degradation which increases the demand for abrasive slurry; and d) size of equipment (e.g. large scale pump and tank). The reality is, however, that if one wishes to develop a mechanistic (or semi-mechanistic) model of pipeline wear, high quality pipeloop tests are required, despite all of the challenges associated with them. It is for this reason that pipeloop tests are conducted as part of the present

51

investigation. The experimental details and results will be discussed in Chapter 4.

1.6.6 Operating pipeline

Perhaps the ideal approach for studying pipeline erosion is to investigate directly the industrial slurry pipeline of interest. There are two main strategies for using an operating pipeline as the investigation tool: coupon (or test spool) mass measurement and wall thickness measurement [3, 5].

One can install a coupon or test spool of desired material in the operating pipeline and then calculate the erosion rate by monitoring the mass of the sample. However, to achieve meaningful mass loss, the sample needs to be exposed to the flow for a relatively long time (e.g. 4 weeks for a typical oil sands pipeline with a wear rate of 8 mm/yr). Normally, within this time period, many flow parameters, such as solids concentration and particle diameter will not stay constant; hence, the wear data cannot be directly linked to specific flow rates and conditions. Moreover, installation and removal of the samples requires temporary shutdown of the line, which may not be feasible in many operating scenarios.

The more convenient approach is to measure the erosion rate by monitoring the pipe wall thickness. Pipeline owners regularly measure the

pipe wall thickness as part of their maintenance strategy. Schaan et al. [5] used these data and were able to calculate the local erosion rate for different angular positions of the pipe. During the course of the data collection, flow parameters such as solids concentration and velocity were not constant and the values changed according to process conditions (e.g. feed properties). Consequently, the wear rates observed by Schaan et al. cannot be used to predict the absolute wear rate on different pipelines. However, general wear patterns for slurry pipelines can be predicted using the data presented in their study. For example, if a pipeline operates with a sliding bed at the bottom, one should expect the maximum erosion rate to occur at the 6 o'clock position (i.e. pipe invert).

In conclusion, erosion testing on operating pipelines is not recommended for studying the science and mechanisms controlling erosion. However, field trials are an excellent tool to evaluate the performance of pipe materials. For example, novel materials can be compared to standard alloys by installing spools at problematic locations and monitoring their behaviour. Afterwards, the results can assist in the process of choosing new pipeline materials.

1.7 Experimental techniques: a summary

Although the erosion rate can be high in an operation (e.g. 8 mm/year [5]), this rate is very difficult to measure in laboratory-scale tests. For example, to detect a significant change in pipe thickness (i.e. within the accuracy of the measurement technique) in a pipeloop experiment, a few weeks of circulation may be needed [47]. Required test durations will be very different for various types of slurries and test conditions. Lab-scale wear testers have been developed to significantly reduce the test time and resource consumption.

Dry and wet erosion testers represent the least expensive testing options and provide highly repeatable test conditions [90]. The limitation is that the tests can be used only for alloy ranking. Accelerated flow simulator techniques (e.g. coriolis and slurry pot) reduce the duration of an experiment by about two orders of magnitude. Because of the abnormally high velocity and distorted geometry, coriolis tester results cannot be easily scaled up to pipeline conditions. The slurry pot tester has proven to be the most reliable testing option. The results obtained from a slurry pot tester can be used for scale-up purpose [54]. Also, the slurry pot has a well-defined geometry that can be useful for more quantitative analysis of the system [103].

The jet impingement tester is a suitable technique to examine particle-surface wear damage. The results obtained from this technique have been combined with CFD simulations to develop erosion prediction models [97]. The particle impact angle is in the range of 60°-90° and the velocities are typically higher than 10 m/s [59]; therefore, the results are not suitable for scale-up purpose in slurry pipelines.

In general, lab-scale experimental techniques should be used with caution for scale-up purposes. Even for alloy ranking purposes these techniques can be unreliable. For example, Parent and Li [3] used various techniques to compare carbon steel and dual phase stainless steel wear performance[1]. The results are presented in Table 1.1.

Table 1.1 [2] Comparison of carbon steel and stainless steel performance using various techniques [3]

Test	Material	
	Carbon Steel	Dual Phase Stainless Steel
ASTM G65	300 mm^3	370 mm^3
Jet Impingement	120 mm^3	130 mm^3
Slurry Pot	52 mg	48 mg
Pipeline	4 yr	7 yr

Table 1.1 shows that stainless steel has a higher erosion rate in both the ASTM G65 and jet impingement tests. However, carbon steel erodes more rapidly in the slurry pot tester. Also, comparing these results with

---

[1] The jet impingement tests were performed at an impact angle of 15° and flowrate of 16 L/min. Slurry pot experiments were conducted at 20% (by volume) sand slurry at an impact angle of 15° for 120 minutes.
[2] Because of the nature of the different experimental apparatuses, wear rates are report in various units. For example, the ASTM G65 test results should be reported in terms of the volume of the sample eroded (standard reporting procedure) but for slurry pot tests, typically mass loss is reported. This disparity in wear units reporting does not affect comparisons shown in the Table.

pipeline wear performance, there is no clear relationship between the data obtained at the lab-scale tests and the field performance of an alloy.

The toroid wheel could possibly be considered as the middle step between lab-scale wear testers and pilot-scale wear testers. Because of low particle degradation, the slurry loses its abrasivity less rapidly than would occur in a pipeloop; hence, longer particle change intervals are acceptable. Also, the required volume of slurry is smaller than for a pipeloop experiment (e.g. 20 L vs 200 L). However, the geometry is not identical to a pipeline. Also, there is an upper velocity limit for a toroid wheel which will be amplified as the wheel diameter is reduced.

The ideal solution is to install test spools in an operating pipeline, particularly when the goal is to mitigate a wear-related issue specific to that pipeline. The value of such tests in developing mechanistic models of pipeline wear is questionable, though, as typically a relatively limited range of operating conditions is tested (i.e. velocity and particle diameter). Moreover, the flow conditions will almost certainly change over the duration of the test (i.e. mixture density, carrier fluid viscosity [5]). Plant owners/supervisors must be receptive to the shutdowns required during the test program to install, remove and weigh spools, and the risks associated with premature (and unexpected) failure of a test spool.

Of course, the hydrodynamics for pipeloop testing are provide ideal conditions; therefore, pipeloop testing is best to investigate the science behind the pipeline erosion. A thorough investigation requires large volumes of slurry in addition to long experimental times (e.g. 1 cubic meter of sample and four weeks to acquire each data point in the present study). Looking at the results obtained from the various techniques, and the vast disparity among the data, it is critical to choose an appropriate method for wear measurement based on the goals of the present study. The various techniques and their applicability are summarized in Table 1.2. In the first column, the typical time for each apparatus is presented. For example, a slurry pot experiment can be performed in 1 hour but a typical pipeloop experiment may last as long as 1 month. The next column discusses the amount of slurry and alloy required for each test, each of which directly impacts the cost of the experiments (e.g. 1 m^3 of slurry for each data point in a pipeloop experiment). The column entitled "Hydrodynamic condition study" section illustrates the ability of that tool to investigate the effect of slurry hydrodynamics on the erosion rate. For example, jet impingement can be used to study particle velocity and impact angle effects but it is not suitable for studying wear in pipe flow. The CFD column explains the compatibility of the technique with CFD simulations. The jet impingement tester has a very well-defined flow pattern which makes it relatively straightforward to model. On the other hand, in a slurry pot, the system consists of more moving components

57

(larger number of particles and moving surfaces) and the geometry is more complex. Therefore, CFD simulations of such a system will be more difficult. The last column characterizes the ability of that tool to examine the wear in terms of particle-surface impacts. For example, to investigate the effect of particle impact angle on the erosion rate, a pipeloop cannot be used. In pipeloop tests the particle trajectory is dictated by the hydrodynamics and it is not possible to control. In contrast, the slurry pot technique gives the user some degree of control by manipulating the specimen position against the flow direction.

Table 1.2 Comparison of techniques/tools used to study erosion

	Time order	Sample volume order	Hydrodynamic condition study	CFD Modeling compatibility	Particle-surface impact study
Dry and wet erosion tester	Minutes	grams (specimen) N/A (slurry)	N/A	No slurry	No particle
Jet impingement	Hours	grams (specimen) liters (slurry)	Impact angle Particle velocity	Low particle count, Straightforward to model	Controlled particle trajectory
Slurry pot	Hours	grams (specimen) liters (slurry)	Slurry properties Impact angle	Complicated geometry	Controlled <u>average</u> impact angle and velocity
Coriolis	Minutes	grams (specimen) liters (slurry)	Slurry properties Impact angle	Complicated geometry	Controlled <u>average</u> impact angle and velocity
Toroid wheel	Days	grams (specimen) 10 liters (slurry)	Almost similar to pipe flow	Curved pip, Straightforward to model	Flow direction always parallel to surface
Pipeloop	Weeks	kg (specimen) m^3 (slurry)	Recommended tool	Easy to model, Especially for low solids %	Flow direction always parallel to surface (for straight pipe)
Operating pipeline	Months	kg (specimen) N/A (slurry)	Slurry properties imposed by pipeline feed	Variable properties, Impossible to model	Flow direction always parallel to surface (for straight pipe)

Table 1.2 shows that in general there is no comprehensive tool for all types of wear studies. If small sample volumes and shorter-duraction experiments are desired, the slurry pot tester and toroid wheel are the most promising techniques. However, to understand the effect of flow parameters (e.g. slurry velocity and solids concentration), the pipeloop is the most promising tool. For that reason, pipeloop tests were chosen for the present investigation. The pipeloop test program was augmented by hydrodynamics-related testing conducted using a slurry pot tester.

In the following sections, the research objectives and the contributions of the present study are introduced. Section 1.10 provides an outline of the thesis structure.

1.8 Research objective

The ability to scale-up experimental wear rate data is of the utmost importance to pipeline owners. The majority of research conducted in the field of pipeline wear focuses on limited parameters. For example, Goosen and Maglas [48] examined various solids concentrations and slurry velocities, but performed all of their tests on a constant pipe diameter. Therefore, a new set of experiments should be conducted to predict the effect of any change on other operating conditions. For example, at the

present time, it is not possible to use wear data collected using a 3 inch pipe to predict pipe wear behaviour in a 30 inch pipe.

In order to develop this scale-up capability, it is proposed that the mechanisms that cause friction in slurry pipeline flows—especially those related to friction losses coming from particle-wall contacts—should be exploited to learn more about the relationship between slurry hydrodynamics and pipeline wear. The effects of pipeline properties such as velocity and solids concentration on erosion can be related to their effects on slurry friction losses. To investigate this hypothesis and collect substantial new evidence, this project is divided into three (3) main stages:

1- **Laboratory scale wear investigation**: a bench-scale wear tester (a slurry pot) is used to collect wear data using different slurries.
   - Conventional application of such an apparatus is focused on investigation of specimen properties; therefore, a new experimental procedure is developed for the purpose of investigating the effects of slurry properties on erosion rate.
   - By changing the suspending liquid phase (i.e. carrier fluid), the effect of viscosity on erosion rate is studied.

- The specimen-slurry impact angle is set at various angles, ranging from parallel to the surface to perpendicular. The specimen erosion rate is observed at each angle.

- Using Bagnold's [118] methodology, both normal and tangential stresses on the specimen surface are calculated.

- A clear correlation was observed between the force and the erosion rate.

2- **Pilot-scale wear investigation**: to examine erosional wear under actual pipe flow conditions, a pilot-scale pipeloop is utilized. The following steps are taken during this phase of the research:

- The pipeloop is designed and fabricated.

- An experimental procedure is developed to overcome complications such as particle degradation and the desire to operate uninterrupted for long periods of time.

- The wear rate is measured for two pipe diameters (75 mm and 63 mm) during the same test.

- The effect of average slurry velocity on the erosion rate is observed.

- To examine the effect of density and particle shape, Al_2O_3 and silica sand particles (of the same size) are tested.

- Al_2O_3 particles showed a significantly higher erosion rate, which can be related to the larger particle-wall stress.

- After correlating the erosion rate with slurry velocity, it was revealed that changing the pipe diameter will significantly affect the erosion rate; therefore, pipe wall shear stress was chosen as the correlating parameter.

3- **Analyzing the data collected from both the laboratory and pilot-scale experiments to relate wear rate to underlying mechanisms** (i.e. specimen surface shear).

- By analyzing the data collected from both experiments, it was observed that specimen surface shear has a direct relationship with surface wear.

1.9 Contributions of the present study

Solids-related shear as the key parameter affecting pipeline erosion

By analyzing erosion data collected from pipeloop experiments and slurry pot experiments, surface solids shear (see Chapter 4 for details) was identified as the key parameter affecting the erosion rate.

A new modeling approach to predict the erosion rate

By relating solids shear stress to the erosion rate, a new modeling approach has been proposed to predict the erosion rate in coarse slurry pipelines. Using shear stress prediction models for slurry pipelines (e.g., the SRC two layer model), the effect of flow parameters such as solids

concentration on the magnitude of the pipe wall shear stress can be predicted. The proposed relationship between pipe wall shear stress and the erosion rate can then be used to predict the erosion rate (see Section 4.5 for details).

Robust experimental procedure to perform pipeloop erosion measurements

Pipeloop erosion experiments are inherently associated with particle degradation. A method to overcome this problem is introduced (see Section 4.3.2 for details). Corrosion elimination and pipe alignment methods are also presented (see Section 4.3.1 and 4.4.1 for details).

Slurry pot tests of the effect of carrier fluid viscosity on erosion rate

The slurry pot tester is introduced as a bench-scale technique to investigate the effect of carrier fluid viscosity on the specimen erosion rate. Traditionally, the slurry pot tester is used to evaluate the wear resistance of various alloys using constant slurry properties for. However, in this study, the viscosity of the suspending liquid was altered and the effect on the erosion rate was investigated (see Chapter 3 for details).

1.10 Thesis outline

This thesis is organized as follows:

Chapter 2 covers the current understanding of slurry pipeline friction loss predictions using a well-known two-layer approach. This information provides the foundation for the proposed modeling approach for erosion prediction.

Chapter 3 is focused on laboratory-scale tests. The findings from the slurry pot tests are presented in this chapter. The effect of multiple parameters, such as carrier fluid viscosity and particle density on the erosion rate are discussed. Furthermore, the force on the sample surface has been calculated and the erosion rate has been correlated to both normal and tangential forces on the sample surface.

Chapter 4 is dedicated to pilot-scale tests performed at the Saskatchewan Research Council. In these tests, pipe diameter, slurry velocity and particle type are the controlled parameters and the erosion rate has been quantified using mass loss measurements. Pipe friction loss (i.e. wall shear stress) is used as the correlating parameter to study the behaviour of the wall erosion rate under different hydrodynamic conditions. Furthermore, micron-scale particle properties are tracked during the

experiments. To further the connection between hydrodynamics and erosion, pipeloop tests have been utilized to measure the pipe solids concentration gradient and speculate on the effect of near-wall lift on slurry pipeline erosion.

In the conclusion (Chapter 5), evidence from the lab-scale and pilot-scale tests is combined and the original hypothesis of this study is examined. Recommendations for future investigations in this field are also presented in this chapter.

The slurry pot experiments were performed using the custom made apparatus at Dr. Dongyang Li (University of Alberta, Chemical and Materials Engineering Department) Laboratory. The author proposed and investigated the idea of relating the specimen wear rate to the surface stresses.

The pilot experiments of the present study were conducted in collaboration with the Saskatchewan Research Council's (SRC) Pipe Flow Technology Centre^{TM}. Specifically, the pipeloop slurry replacement and wear spool mass measurements were conducted by SRC staff. The original idea of using various spool sizes to validate the data (see Section 4.4.1 for details) was proposed by Dr. Melissa McKibben. The relationship between

the erosion rate and solids shear stress was developed by the author himself.

Dr. Sean Sanders (University of Alberta, Chemical and Materials Engineering Department) proposed and developed the idea of relating the pipeline near wall solids concentration to the wear rate. The author collected the near wall solids concentrations at various pipeline conditions during the pump calibration phase (see Section 4.3.3 for details) of the experiments.

2. Modelling Friction Losses in Slurry Pipeline Flows

This research is based on the hypothesis that slurry pipe wear has a direct relationship with pipe wall stress; therefore, to study and model the wear, a clear understanding of pipeline frictional losses is required. This Chapter introduces the Saskatchewan Research Council (SRC) two-layer model [119], which will be used in this investigation to characterize or predict wall stresses. Slurry physical properties and characterization terms used in this model are described in this Chapter.

The two-layer model described here was developed at the Saskatchewan Research Council's Pipe Flow Technology Centre^{TM} in Saskatoon. Correlations and modeling details are based on years of pipe flow experiments at the SRC laboratory [117, 120-125]. In this model, the effects of the solids on friction loss are captured through three main mechanisms: a) particle dispersive friction; b) near-wall lift; and c) Coulombic stress. The details of these mechanisms will be explained in Section 2.2. As a result of this mechanistic approach, this model is capable of accurately predicting slurry pipeline friction losses over a wide range of operating conditions.

Since the development of the original model by Gillies et al. [119] various researchers [124, 125] have contributed to further improve the accuracy

68

of the model. For example, Wilson et al. [126] advanced the model by including the near-wall lift as a mechanism affecting slurry pipeline friction losses (see Section 4.6 for a detailed description of this phenomenon).

In the next section, slurry properties required for model calculations are introduced.

2.1 Slurry physical properties

To characterize a slurry, physical properties of both phases (solids and liquid) are used. Slurry (mixture bulk) density is calculated using the from:

$$\rho_m = \sum_i \rho_i C_i \qquad (2.1)$$

where:

C_i = volumetric concentration of component i

ρ_i = density of component i

Researchers in the field of slurry transport, specifically slurry pipe flows, necessarily define two types of solids concentrations: a) in-situ (C_r); and b) delivered (C_v) [117]. The in-situ solids concentration is defined as the spatial average of solids concentration over the pipe cross section. This parameter is the actual solids concentration in a pipe at any given time. The delivered solids concentration is the velocity average of solids at pipe cross section. In other words, it is defined as the concentration of solids

delivered by the flow. Quantitatively these parameters can be described as:

$$C_r = \frac{1}{A} \int_A c\,dA \qquad (2.2)$$

$$C_v = \frac{1}{AV} \int_A c v_s\,dA \qquad (2.3)$$

where:

v_s = local particle velocity (m/s)

c = local particle volume concentration (%)

In most coarse slurries (e.g. sand + water), the solids have a relatively smaller velocity compared to the suspending liquid (e.g. water) [117]. As a result, the delivered concentration is usually smaller than the in-situ concentration. The difference between the two concentrations increases as the settling tendency of the particles increases (e.g. as the particle diameter or density increases).

In the next section, the underlying principles of the SRC two layer model will be described, and the calculation tools and governing equations required to predict the frictional losses will be introduced.

2.2 The SRC two-layer model

To understand the effect of flow parameters such as velocity on pipe erosion, it is critical to understand their effect on pipe wall stress. The SRC two-layer model has been chosen as the suitable tool for describing this effect.

In general, this model divides coarse solids into two groups [127]: a) coarse particles suspended by the surrounding fluid turbulence; b) coarse particles that transmit a portion of their immersed weight to the pipe wall. To mechanistically model the effect of these particles on friction loss, the two-layer model divides these friction losses into 2 groups:

a) **Kinematic friction**: The velocity-dependent friction caused by the fluid phase and the particle stress [117]. Near-wall lift is also included in this group. Kinematic friction is a strong function of velocity and suspending liquid viscosity (details available in Section 2.2).

b) **Sliding bed friction (Coulombic):** The non-suspended particles will form a moving bed at the bottom of the pipe. The weight of the bed is partially transmitted to the pipe wall (i.e. a normal stress). The shear stress required to move this bed is calculated through Coulomb's law [124].

In the next section, the force balance equations used in the two-layer model are introduced. The effect of each aforementioned solids-related mechanism on the pipe friction loss will be presented. The correlations and equations used to calculate the wall stress will be defined.

2.2.1 Two-layer force and mass balances

In the SRC two-layer model, it is assumed that the pipe is divided into two sections. Each section has a constant solids concentration and velocity, as illustrated in Figure 2.1.

(a)   (b)
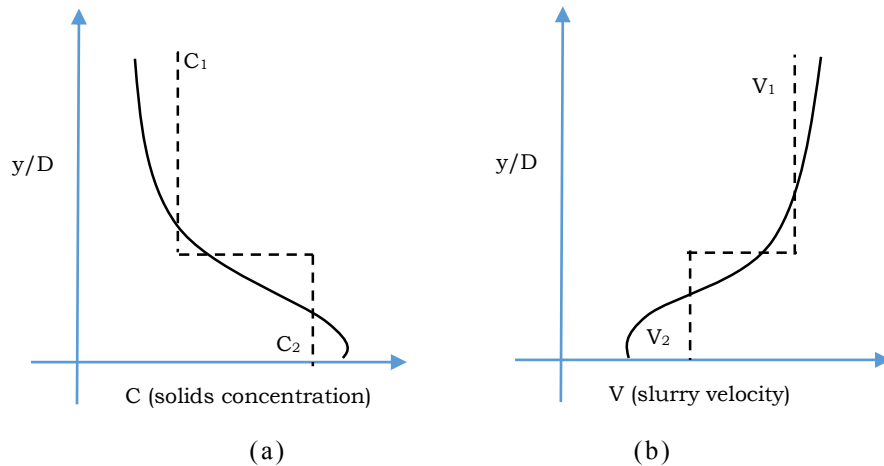
Figure 2.1 (a) Concentration and, (b) velocity vs normalized height from the bottom of the pipe. Solid line represents the actual distributions, while the dashed line represents the simplified, model values [119].

In the model, τ_1 and τ_2 are the averaged wall shear stresses acting on the wetted perimeters of the top (S_1) and bottom (S_2) layers, respectively.

Figure 2.2 describes the two layer model slurry-wall interaction. Beta (β) is an angle which defines the bottom layer height.
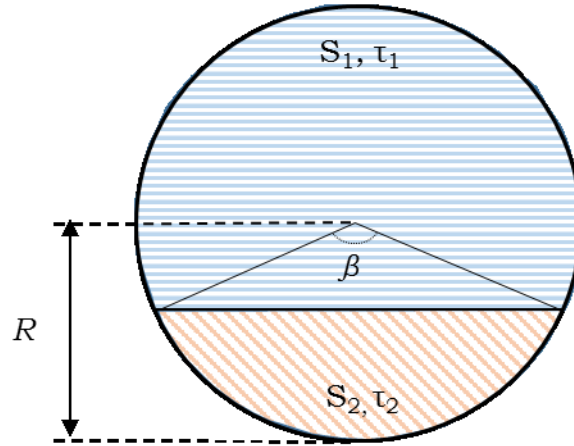
Figure 2.2 SRC two layer model slurry-pipe wall interaction

As the model assumes different velocities for the upper and lower layers, there will be a shear stress acting in between them. This parameter is shown as τ_{12} on Figure 2.2. The stress between the layers (τ_{12}) mainly affects the pressure gradient inside the pipe and does not have a direct impact on pipe wall stresses; therefore, it is not particularly important for the present study. The details of the calculations are explained elsewhere [117].

The model uses force balances for both the upper and lower layers:

Upper layer:

$$-\frac{dP}{dz} = \frac{\tau_{1k}S_1 + \tau_{12}S_{12}}{A_1} \tag{2.4}$$

where dP/dz is the pressure gradient, τ_{1k} is the upper layer kinematic stress and A_1 is the upper layer area; and

Lower layer:

$$-\frac{dP}{dz} = \frac{\tau_{2k}S_2 - \tau_{12}S_{12} + \tau_c S_2}{A_2} \qquad (2.5)$$

where dP/dz is the pressure gradient, A_2 is the lower layer area, τ_{2k} is the lower layer kinematic stress and τ_c is the stress caused by the sliding bed of solids in lower layer (i.e. Coulombic stress). Combining Equations (2.4) and (2.5), τ_{12} can be eliminated:

$$-\frac{dP}{dz} = \frac{\tau_{2k}S_2 + \tau_{1k}S_{1k} + \tau_c S_2}{A} \qquad (2.6)$$

Equation (2.6) presents the effect of wall stresses on the slurry pipe friction loss. The correlations and equations used to calculate these stresses are described in the next section.

2.2.2 Pipe wall stress calculations

In the SRC two-layer model, τ_1 is described using [119]:

$$\tau_1 = \tau_{1k} = 0.5 \left[f_f \rho_f + f_{s1} \rho_s \right] V_1^2 \qquad (2.7)$$

where f_f is the Fanning friction factor calculated from Reynolds number and pipe roughness, ρ_f is the carrier fluid density, ρ_s is the solids density,

V_1 is the upper layer velocity, and f_{s1} is the solids friction factor, calculated using the correlation proposed by Gillies [120]:

$$f_{s1} = \lambda^{1.25}(k_0 \ln d^+ + k_1)$$ (2.8)

In Equation (2.8) λ is the linear concentration, d^+ is the dimensionless particle size and k_0 and k_1 are constants. The dimensionless particle size (d^+) is given by:

$$d^+ = \frac{dV_1(f_f/2)^{0.5}\rho_f}{\mu_f}$$ (2.9)

where d is the particle diameter and μ_f is the carrier fluid viscosity. Based on numerous experiments, Gillies [120] suggested the following values for the constants:

$d^+ < 21$: $k_0 = -1.1\times10^{-4}$; $k_1 = 4.2\times10^{-4}$

$21 < d^+ < 100$: $k_0 = -5.6\times10^{-5}$; $k_1 = 2.6\times10^{-4}$

$100 < d^+$: $k_0 = k_1 = 0$

Linear concentration (λ) is defined as the ratio of particle diameter to the average distance between neighboring particles and can be written as [117]:

$$\lambda = \left[\left(\frac{C_{max}}{C_r} \right)^{\frac{1}{3}} - 1 \right]^{-1}$$ (2.10)

where C_r is the in-situ solids volume concentration and C_{max} is the maximum packing concentration. The maximum packing concentration

(C_{max}) is a parameter used to describe the settled bed volume

concentration of particles when they are randomly packed. Its value

depends on particle size distribution and shape and should be measured

experimentally. In the absence of experimental measurements, for

rounded, relatively isometric particles with a narrow size distribution,

C_{max} is approximately 0.63 [117]. A detailed calculation procedure for

these parameters can be found in [117].

Stress on the pipe wall from the bottom layer (τ_2) has two main

components: the kinematic stress (τ_{2k}), which can be calculated using

Equations (2.8) to (2.10) (substituting V_1 and C_1 with V_2 and C_2), and the

Coulombic stress τ_c:

$$\tau_2 = \tau_{2k} + \tau_c \tag{2.11}$$

As mentioned previously, the Coulombic stress is produced by a moving

bed of coarse solids can be calculated using:

$$\tau_c = \frac{0.5gD^2(\rho_s - \rho_1)(C_2 - C_1)(sin\beta - \beta cos\beta)\eta_s}{s_2} \tag{2.12}$$

where D is the pipe diameter, g is the acceleration of gravity, β is the

angle describing the bed height (described in Figure 2.2), and η_s is the

coefficient of friction between the particles and the pipe wall. It is a

function of particle type and pipe wall material. For sand particles and steel pipe, $\eta_s=0.5$ is a good estimate [128].

The present study aims to examine the effect of solids pipe wall stress on the erosion rate. Both upper layer (τ_1) and lower layer (τ_2) stresses will be evaluated. Using the equations described above, the fluid portion of the stress will be eliminated from the total wall stresses; therefore, the effect of solids stresses (i.e. upper and lower layer solids kinematic stress and lower layer Coulombic stress) on the erosion rate can be examined. The details of these calculations will be presented in Chapters 3 and 4.

3. An investigation of carrier fluid viscosity and impact angle on erosion rate

This Chapter is dedicated to the investigation of carrier fluid viscosity and solids impact angle on erosion rate. A slurry pot tester is chosen for this study.

3.1 Introduction

In general wear studies can be separated into two major categories: a) studies focused on alloy structure and material science; and b) studies focused on slurry properties such as solids concentration and velocity. Various types of alloys have been studied extensively under abrasive conditions; hence, there are relatively well-established experimental procedures to study the effect of alloy properties on erosion rate [9, 12-16, 38, 109, 129].

A good example of an investigation focusing primarily on alloy properties is that of Clark and Llewellyn [113], who conducted an extensive study on various alloys. In their tests, 4 different types of steel were utilized with a hardness range of 220-536 HV. To achieve rapid erosion, the alloys were tested using a coriolis tester and slurry velocities of 14-24 m/s. They

observed a clear correlation between specimen surface hardness and wear rate. All of their tests used a 250 μm silica sand and water slurry (10% by mass) as the abrasive material.

Despite strong evidence of dependency of wear on slurry hydrodynamics (examples and details available in Section 1.4.1), limited studies have been performed to investigate this phenomenon. The next section will review good examples of such studies and will provide the main focus of each.

3.2 Studies of the effects of slurry hydrodynamics on erosive wear

Only a very limited number of studies have been dedicated to the interaction between slurry hydrodynamics and the pipe wall [6, 19, 47, 63, 95, 96]. They are mainly focused on the effect of particle properties and transport velocity, while other parameters, including carrier fluid properties and solids concentration, are not the main topic of discussion [46]. These studies can be categorized in two major groups:

a) Laboratory-scale erosion tests. In this group, studies that utilize equipment traditionally associated with alloys testing (e.g. slurry pot and

jet impingement tests) to instead relate the hydrodynamics of solid-liquid flow to wear.

b) Pilot-scale tests (i.e. pipeloop).

3.2.1 Lab-scale wear studies on the effects of slurry hydrodynamics

As an excellent example of this group, Clark et al. [52, 103] studied the effects of particle diameter, impact angle and impact energy on erosion rate using a slurry pot tester. Their tests were performed using a dilute slurry of silica sand in diesel oil (<1% by volume). The test specimen was cylindrical in shape, and mounted on the slurry pot tester with the impeller edge velocity of 18.7 ms^{-1}. A strong correlation between the particle kinetic energy and erosion rate was observed. Gupta et al. [54] also studied the effects of slurry properties (slurry solids concentration, velocity and particle diameter) on the erosion rate using a slurry pot tester. In their study, they used copper mine tailings (15-45% by mass) and three impeller velocities (3.92, 5.49 and 8.06 ms^{-1}). They showed that the erosion rate increases rapidly with increasing velocity, which is in agreement with similar experiments reported in the literature [47]. Only small changes in wear rate were observed with increasing solids concentration.

Zu et al. [94] originally designed the jet impingement tester as an alternative to other techniques to produce a more controlled erosion environment. Their design gave them the ability to control the impact velocity and angle in addition to slurry concentration. Lu et al. [130] also used a jet impingement tester to study the attack by silica sand and water mixtures on stainless steel surfaces. In their study the effects of velocity (5-10 ms^{-1}) and impact angle (10°-90°) were investigated. They observed that the maximum erosion rate occurred at an impact angle of 60° and the erosion rate increased exponentially with increasing impingement velocity.

Neville and Hodgkiess [38] tested various alloys using a jet impingement tester. In their tests, various alloys were bombarded with a very dilute slurry (<0.01% by volume) flowing at 25 m/s and an impact angle of 90°. Even then, the solids concentrations they tested were at least 3 orders of magnitude lower than the actual pipeline conditions, which makes it impossible to directly utilize their data for pipeline wear predictions. Their study did not directly focus on the hydrodynamics, but it highlighted the importance of solid-surface impact (by comparing the results with a particle-free test).

3.2.2 Pilot-scale wear studies on effect of slurry hydrodynamics

It is obvious that to study pipeline erosion, pipe loop testing is ideal (see Section 1.6.5 for additional details). This technique requires a pilot-scale pipe loop and a relatively large volume of slurry (e.g. 300 L). A single test must be run for weeks and the slurry must be replaced regularly. Despite these disadvantages, there have been some notable pipeloop erosion studies. For example, Shook et al. [19] performed an extensive study of pipeline erosion. In their study, each test took at least 500 hours and the slurry was replaced every 120 hours. They conducted a unique comprehensive study in which both wear rate and particle flux [8] at different angular positions were measured. They were able to successfully demonstrate a strong correlation between the local wear and the local particle flux.

Wood et al. [17, 18, 116] used a pipeloop to study slurry flow-induced erosion in bends and straight pipe sections. They showed that because of different flow hydrodynamics, the erosion rates in bends are significantly higher than those measured in the straight pipe sections. Goosen and Maglas [48] also utilized a pipeloop to study the erosion of PVC pipelines carrying suspensions of boiler ash and water. They showed that by increasing the slurry velocity the erosion rate will increase exponentially.

82

In general, the majority of erosion/hydrodynamics studies are mainly focused on particle concentration, slurry velocity, particle impact angle and particle size. Very few investigations of the effect of carrier fluid viscosity can be found in the literature [46]. For example, Okita et al. [53] studied the effect of viscosity on erosion rate but they used a jet impingement tester. In pipe flow, particle motion is strongly affected by the carrier fluid viscosity, but in the jet impingement tester the particle trajectory and velocity are independently controlled. Huang et al. [20] modeled the effect of carrier fluid viscosity (over a very limited range) on the erosion rate in a pipeline. They suggested that by increasing the viscosity from 1 mPa.s to approximately 2 mPa.s the erosion rate will decrease by 10%. Kesana et al. [41] also studied the effect of solids concentration and viscosity on erosion rate; however, they examined only two viscosities (1 mPa.s and 10 mPa.s). Also, in their experiments the maximum solids concentration was 1% (by mass), which is vastly different from operating slurry transport systems (e.g. 50% by mass sand). Their results showed no clear relationship between wear and viscosity. Depending on the flow regime the wear can increase or decrease by increasing the viscosity. This inconsistency emphasizes the need to examine the underlying mechanisms through which carrier fluid viscosity can affect surface erosion.

The objective of the present study is to investigate the effect of carrier fluid viscosity on surface erosion. In the following section, the influence of carrier fluid on slurry flow hydrodynamics and on wall stresses is described, as this information provides the foundation for the analysis of the slurry pot test results.

3.3 Carrier fluid impact on slurry-wall erosion

In a pipeline, slurry-wall interaction is a strong function of carrier fluid viscosity. This interaction is expected to affect the erosion rate; therefore, the functionality of fluid viscosity on surface stresses should be examined. This functionality is mainly presented through: a) particle friction factor (f_s); b) liquid friction factor (f); and c) flow pattern (i.e. spatial distribution of solids within the flow domain). The following section explains the importance of these parameters and describes the effects that carrier fluid viscosity changes will have (see Chapter 2 for additional details).

Equations (2.7) to (2.9) show that by increasing the carrier fluid viscosity the particle friction factor will increase, which will result in larger kinematic shear stresses (τ_{1k} and τ_{2k}). Coulombic stress (i.e. stress caused by the immersed weight of the sliding particle bed on the pipe wall, τ_c), however, has an indirect relationship with carrier fluid viscosity. Carrier

84

fluid viscosity will affect the height of the bottom layer in the pipe which will consequently change β (Figure 2.2, page 73). As the height of the bed changes, the magnitude of the Coulombic friction will change significantly. The effect of carrier fluid viscosity on wall stress for a specific set of conditions (e.g. D = 0.087 m, C = 30% by volume, V = 3.7 m/s, d_{50} = 450 μm, ρ_s = 2650 kg/m^3, ρ_l = 1000 kg/m^3) pipe is illustrated in Figure 3.1.
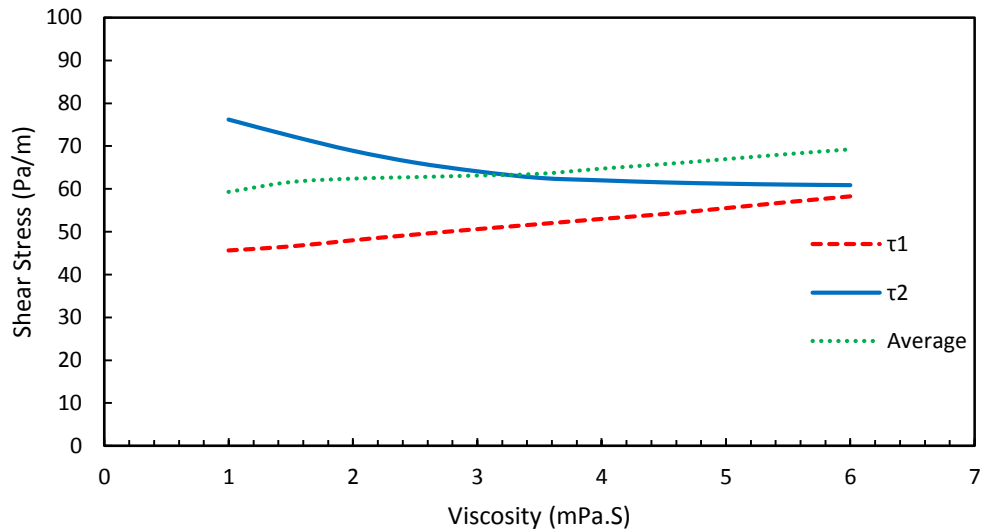
Figure 3.1 Effect of carrier fluid viscosity on τ_1 and τ_2, Pipe ID= 0.087 m, C_v= 0.3, ρ_s= 2650 kg.m^{-3}, d_{50}=450 μm, V = 3.7 m/s ρ_f= 1000 kg.m^{-3}

Figure 3.1 shows that by increasing the viscosity the top layer stress (τ_1) increases but the bottom layer stress (τ_2) decreases. The decrease in τ_2 can be attributed to an increase in the suspending power of the carrier fluid, which results in a lower solids concentration in the bottom layer. The average stress is calculated as:

$$\tau_{\text{average}} = \frac{\tau_1 S_1 + \tau_2 S_2}{S} \tag{3.1}$$

where S_1 and S_2 are the upper and lower layer perimeter. As expected the average stress increases with increasing carrier fluid viscosity.

3.4 Application of slurry pot testers in evaluating the effects of slurry properties on erosive wear

The slurry pot tester is a popular tool in wear investigations [9, 11, 16, 45, 54, 95, 99, 101-104, 129]. As mentioned previously, the main application of this device is for ranking alloys exposed to an abrasive slurry (see Section 1.6.3 for details and examples of such applications). In this section, the focus is on the use of the slurry pot tester to evaluate the relationship between slurry hydrodynamics and erosion.

Gupta et al. [54] used a slurry pot tester to evaluate the wear behaviour of brass and steel at different solids concentrations. In their experiments, the solids concentration was changed in the range of 15 to 45 % (by mass). At each solids concentration, various particle sizes (38 to 450 µm) and impeller velocities (4 to 8 m/s) were examined. They proposed two correlations (derived from their slurry pot data) to predict erosion rates in brass and steel pipes:

$$E_{brass} = 0.0178V^{2.4882}d^{0.291}C_s^{0.516} \qquad (3.2)$$

$$E_{steel} = 0.0223V^{2.148}d^{0.344}C_s^{0.556} \qquad (3.3)$$

where E (cm/yr) is the wear rate, d (m) is the particle d_{50}, C_s (% by mass) is the solids concentration, V (m/s) is the slurry velocity. Table 3.1 compares predicted wear rates to measured values.

Table 3.1 Comparison of predictions of the model of Gupta et al. [54] with experimental values.

Measured wear rate (cm/yr)	Predicted wear rate (cm/yr)	Error (%)
Brass		
0.016	0.014	12.5
0.015	0.016	6.7
0.032	0.031	3.1
0.035	0.041	17.1
0.051	0.050	2.0
Steel		
0.012	0.011	8.3
0.016	0.020	25.0
0.026	0.022	15.4
0.031	0.030	3.2
0.048	0.051	6.2

The original publication did not report the conditions used to validate the model and only the final results are presented. Although the correlations were derived from slurry pot data, the pipeline predictions were in good agreement with experimental observations.

Lin and Shao [95] modified the slurry pot tester to accurately control the impact angle and impeller velocity. They showed that the wear rate increased exponentially with increasing velocity. The velocity exponent increased (i.e. n in Equation 1.1) with increasing impact angle, and

decreased as the specimen hardness increased. The tests were performed at impact angles of 30° and 90°.

Clark [103] used the slurry pot tester to evaluate the effect of impact angle on a cylindrical specimen exposed to abrasive slurry. He observed that the maximum wear rate occurred at an impact angle of 40°. Desale et al. [105] conducted a similar investigation on the effect of impact angle. They observed that the maximum erosion rate occurred at an impact angle of 15°. The results were nearly independent of solids concentration (glass beads in water slurry) over the range tested (1 to 3 % by volume). The inconsistency in the results shows that the impact angle indirectly affects the wear rate. Perhaps a more direct investigation into underlying mechanisms may reveal a more suitable parameter for wear prediction.

Based on the previous studies where slurry pot testers were used to connect slurry hydrodynamics to wear rate, this technique was chosen to study slurry-surface erosion for a range of carrier fluid viscosities. By changing the viscosity, the slurry-wall forces (shear and normal) will change. By relating the erosion rate to these stresses, it is possible to predict the effects of other system parameters such as particle diameter and solids concentration, on erosion.

3.5 Experimental Method

3.5.1 Equipment

The slurry pot apparatus used in this investigation was custom-made and consists of an impeller, a tank and a motor as shown in the simple illustration provided here as Figure 3.2. The setup is also equipped with a heating/cooling jacket to control the slurry temperature.
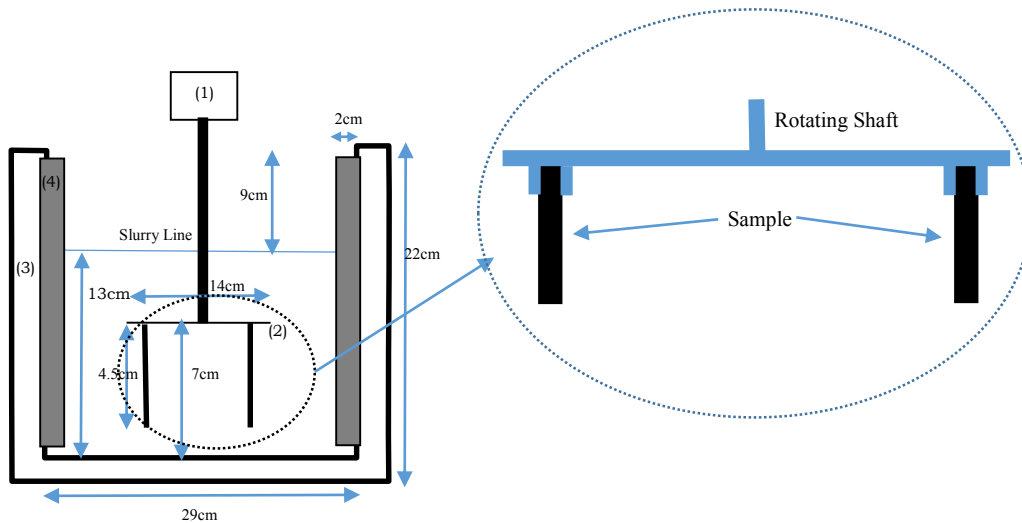
Figure 3.2 Slurry pot schematic (1) electromotor, (2) sample holder diameter, (3) temperature control jacket, (4) baffles

The cylindrical container is 29 cm in diameter and 22 cm in height. The vessel has a total volume of 14.5 L. The sample holder is installed on the rotating shaft of the motor. Four full length baffles are installed at equal spacing in the tank to enhance the mixing. There is no additional mixer in the tank and the samples (i.e. the sample holder) act as the mixer (see the inset of Figure 3.2). There are a total of 4 samples placed on the rotating

disc with 90° separation (i.e. 12, 3, 6 and 9 o'clock positions). The top 0.5 cm of the sample is covered by the sample holder. As a result, the area covered by the sample holder is deducted from total area in subsequent erosion rate calculations.

3.5.2 Materials

Samples are prepared from cutting a sheet of commercial pipe steel (ASTM A53 X65) into the desired coupon sizes (5 cm × 1 cm × 0.5 cm). Each sample is then polished using 1200 grit sandpaper and washed with toluene and distilled water to remove any residual surface material.

The carrier fluid is a mixture of deionized (DI) water and ethylene glycol (HPLC grade, Fischer Scientific) or, for higher viscosity tests, a mixture of DI water and glycerol (HPLC grade, Fischer Scientific). The viscosity of the carrier fluid is altered by manipulating the concentration of glycerol or ethylene glycol.

Carrier fluid viscosities of 0.8 mPa.s (DI water) to 5.7 mPa.s were used. Table 3.2 provides the properties of the carrier fluids utilized in this study. All tests were performed at 25°C and the viscosity and density are reported for that temperature [131]. Addition of glycerol or ethylene glycol will also change the density of carrier fluid mixture by as much as

12.5%; however, the density increase is negligible compared to the dramatic increase in viscosity (~600%).

Table 3.2 Carrier fluid properties

Carrier fluid composition	Viscosity (mPa.s)	Density (kg/m^3)
DI water	0.8	997
20.0% Ethylene Glycol + DI water	1.1	1004
30.0% Ethylene Glycol + DI water	1.4	1009
34.5% Glycerol + DI water	2.7	1082
44.2% Glycerol + DI water	4.2	1107
50.0% Glycerol + DI water	5.7	1121

By manipulating the carrier fluid viscosity over a wide range, both normal shear and shear stresses on the surface will change considerably. Therefore, as discussed in Section 3.4, the erosion rate should change with carrier fluid viscosity.

The particles used in this study are silica sand (Sil Commercial, Sil 4) and Al$_2$O$_3$ (Sil Commercial, Abrasive particle). The particle size distribution for each type of solids was measured using the dry sieve technique and the results are presented in Figure 3.3.
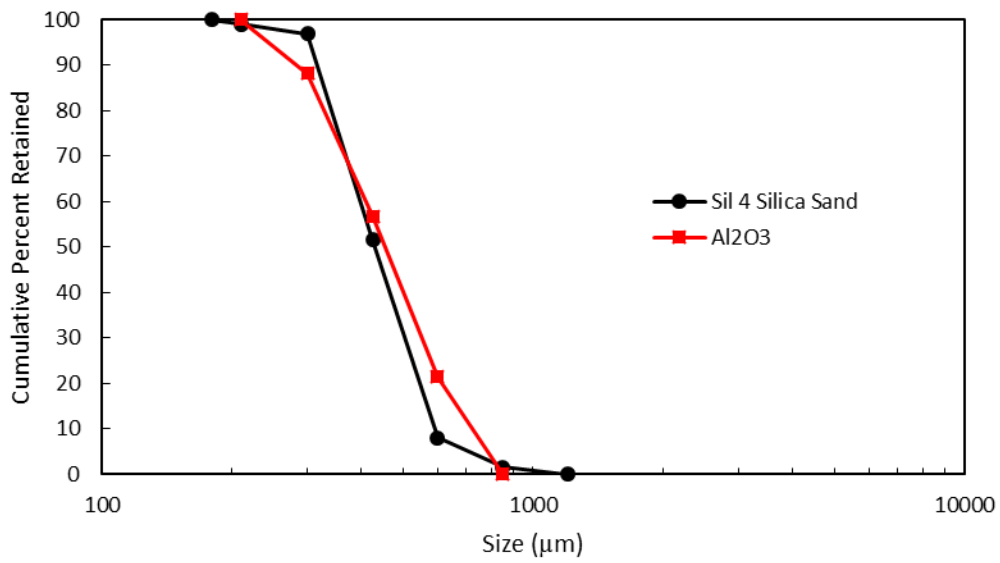
Figure 3.3 Particle size distribution of the particles used in the present study

Figure 3.3 shows that the particle types are nearly identical in size. However, they have significantly different density and shape. Aluminum oxide is much more angular. A light microscope (Carl Zeiss Canada: Axiovert 200) is used to observe and compare the particle shapes. Particle images are presented in Figure 3.4.
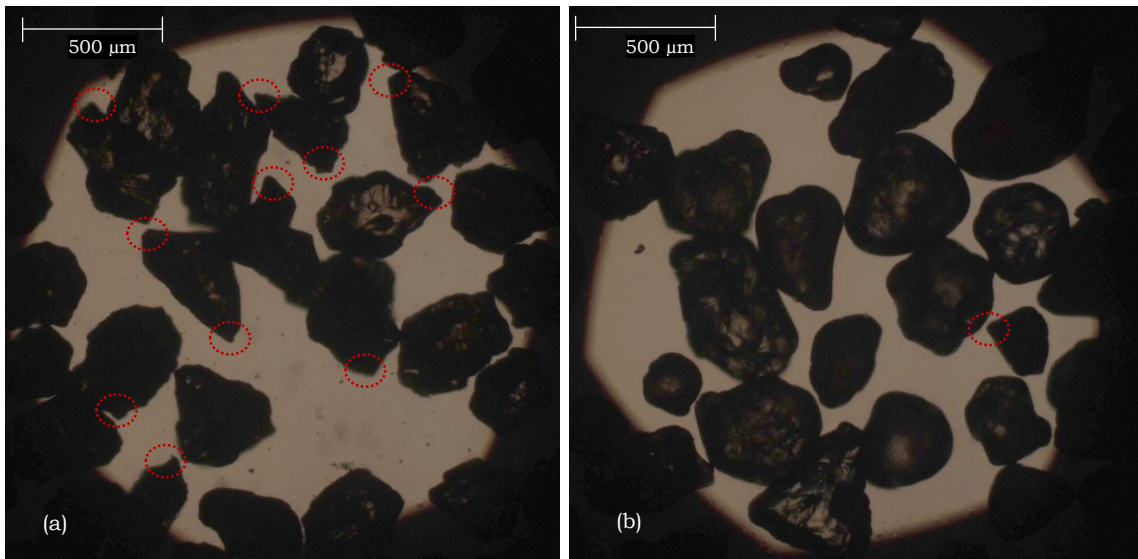
Figure 3.4 Light microscope images of (a) Al_2O_3 and, (b) silica sand. Sharp tips are highlighted

Particle circularity (C) is defined as the ratio of the perimeter of the area-equivalent circle (P_c) to the actual particle perimeter (P_p):

$$C = \frac{P_c}{P_p} = \frac{\pi d_A}{P_p} \qquad (3.4)$$

where

$$d_A = \left(\frac{4A_P}{\pi}\right)^{1/2} \qquad (3.5)$$

Note that A_P and P_p come from analysis of 2-D images of the particles. Aluminum oxide particles used in this study have a circularity of 0.68 which is significantly smaller than the silica particle circularity of 0.80. The lower circularity for Al_2O_3 represents their more angular nature and can be associated with the sharp tips found on those particles. The abundance of these sharp tips will decrease the particle-surface impact area; therefore, the impact stress (i.e. force/area) will be larger for an angular particle.

In addition to Al_2O_3 and silica sand, rounded sand is also used for slurry pot experiments. Rounded sanded is prepared by recirculating the new sand inside a pipeloop (see Section 4.2.1 for details) for 4 weeks at approximately 3 m/s velocity. Sieve analysis is used to measure the particle size distribution for the rounded sand particles. Figure 3.5 presents the results.
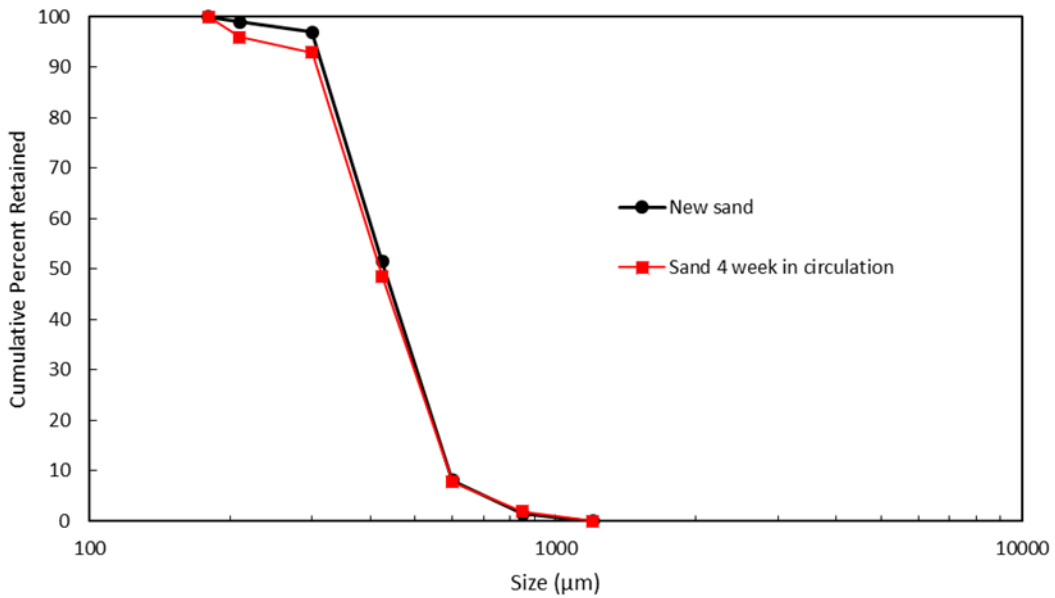
Figure 3.5 Particle size distribution of new sand and sand 4 week in circulation

Figure 3.5 shows that the rounded sand has a higher percentage of particles below 210 µm compared to the new sand. However, the overall d_{50} is similar. Microscopic images are used to examine the shape of the rounded sand particles. Figure 3.6 presents microscopic images of the fresh sand and rounded sand.
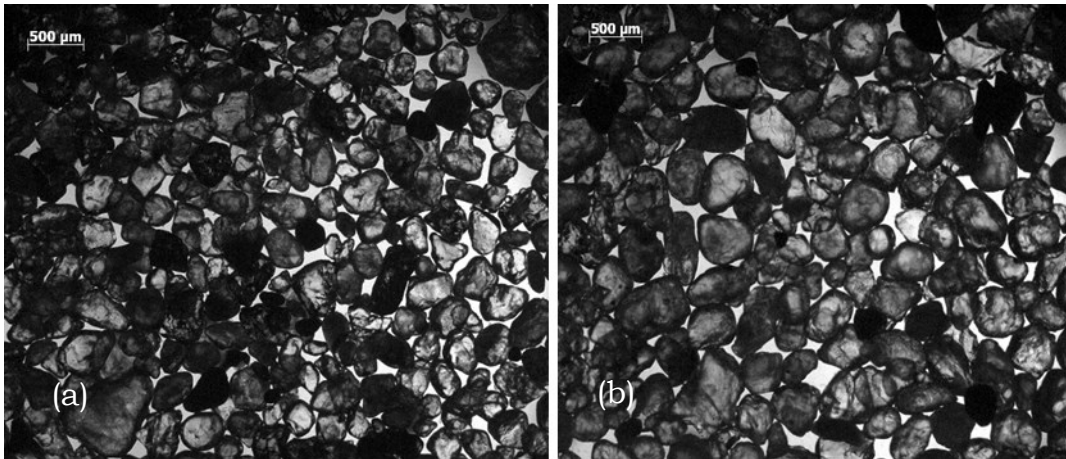
Figure 3.6 Microscopic image of (a) new sand and (b) rounded sand

Analysis of the images presented in Figure 3.6 shows no distinct difference between the circularities of the new and rounded sand. Rounded sand particles appear to have smoother surfaces. Figure 3.7 presents particle surface images taken at a higher magnification.
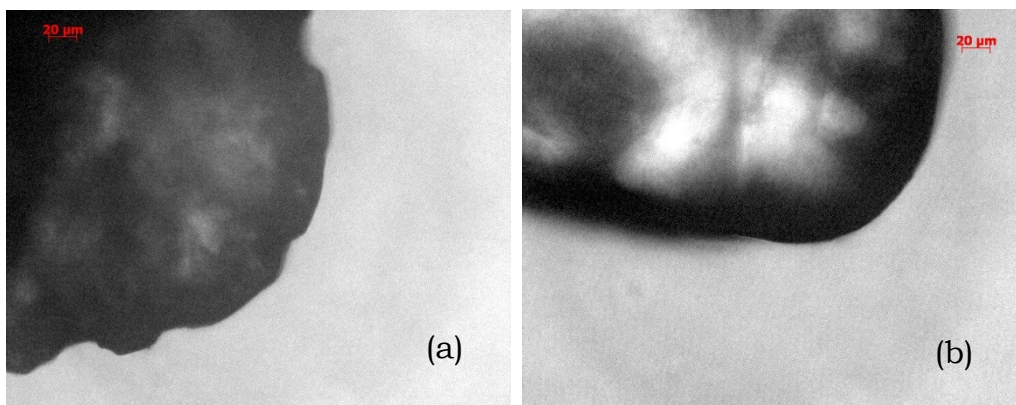
Figure 3.7 surface examination of the particles (a) new sand and (b) rounded sand

Figure 3.7 shows that as the particles recirculate inside the pipeloop, particle surfaces become smooth. In the following sections, to examine the effect of particle surface topography, the erosion rate of rounded and new sand will be compared.

The particle properties have been summarized in Table 3.3. The values of particle density reported here are obtained from the manufacturer and the maximum packing concentration (C_{max}) is measured in the lab. In this study, it is measured using a graduated cylinder. Initially, a known mass of solids (e.g. 100 g) is poured into the cylinder. The cylinder is tapped on the table at least 10 times to achieve maximum packing. The total bed volume is recorded based on the graduations on the cylinder. The volume of the solids is calculated by dividing the known solids mass by the particle density. The maximum packing concentration is calculated by dividing the solids volume by the bed volume.

Table 3.3 Particle properties

	d_{50} (mm)	Density (kg/m^3)	C_{max} (% by volume)	Particle Circularity
Silica Sand	0.420	2650	64	0.80
Rounded Sand	0.410	2650	66	0.80
Al_2O_3	0.425	3950	58	0.68

3.5.3 Procedures

The mass of each sample is measured using an analytical balance (Mettler Toledo, ML204, 0.1 mg accuracy). Afterward, coupons are placed in the sample holders at the desired impact angle. A corrosion inhibitor (VCI-1 Corrosion Inhibitor Powder, KPR ADCOR INC) is also added to the system to minimize mass loss caused by corrosion (see Section 4.3.1 for details of corrosion inhibitor performance test). The specimens travel

96

inside the tester at 660 RPM (approximately 5.5 m/s). Each experiment is run for 45 minutes, after which the samples are removed, washed with water and toluene, dried and weighed. Sample mass loss is determined by comparing the final and initial mass of each specimen. The erosion rate is calculated by dividing the mass loss by the duration of the experiment (i.e. 45 minutes) and the area of the specimen exposed to the slurry.

The surfaces of selected samples were examined using a Scanning Electron Microscope. The SEM used in this study is a Hitachi S-2700 equipped with a PGT (Princeton Gamma-Tech) IMIX digital imaging system and a PGT PRISM IG (Intrinsic Germanium) detector for energy dispersive X-Ray analysis (EDX). Table 3.4 provides a summary of the experimental conditions tested during the course of this study.

Table 3.4 Test conditions	
Mixer speed	660 RPM
Temperature	25° C
Particle type	Al_2O_3 or silica sand
Carrier fluid viscosity	0.8 – 5.7 mPa.s
Mixing time	2700 s
Solids concentration	19% by volume
Sample orientation	0°, 30°, 60°, 90° impact angle

The solids concentration is chosen to resemble a typical slurry pipeline. By choosing a wide range of carrier fluid viscosities, the erosion rate can be studied in various flow regimes (see Section 3.7 for details). Silica sand and Al_2O_3 particles have similar sizes (but significantly different densities and shapes; hence, the effect of density and shape can be studied

97

by examining the erosion rate of these particles at otherwise similar conditions.

3.6 Results

Three parameters were studied during the course of this investigation: particle properties (shape and density), impact angle and carrier fluid viscosity. In this section, the effect on erosion of each of these parameters is presented.

3.6.1 Effect of particle properties

To investigate the effect of particle shape and density, three different types of solids were chosen:

1- New silica sand

2- Rounded silica sand

3- Al_2O_3 abrasive particle

The new silica sand and the Al_2O_3 particles were described in the previous section and their specific shapes can be seen in Figure 3.4. The rounded sand was prepared by circulating a sample of the new silica sand in a pipe loop for 4 weeks. As presented in Figure 3.6, rounded and new sand have relatively similar macroscopic properties. The main difference between them is the surface roughness (described in Figure 3.7). These particles have almost identical diameters. Figure 3.8 shows the measured erosion

rates for the different types of particles at two viscosities. This section of the present investigation focuses on the effect of particle properties; therefore, only two viscosities are tested. In the following sections, a more comprehensive study of the effect of carrier fluid on wear rate is presented.
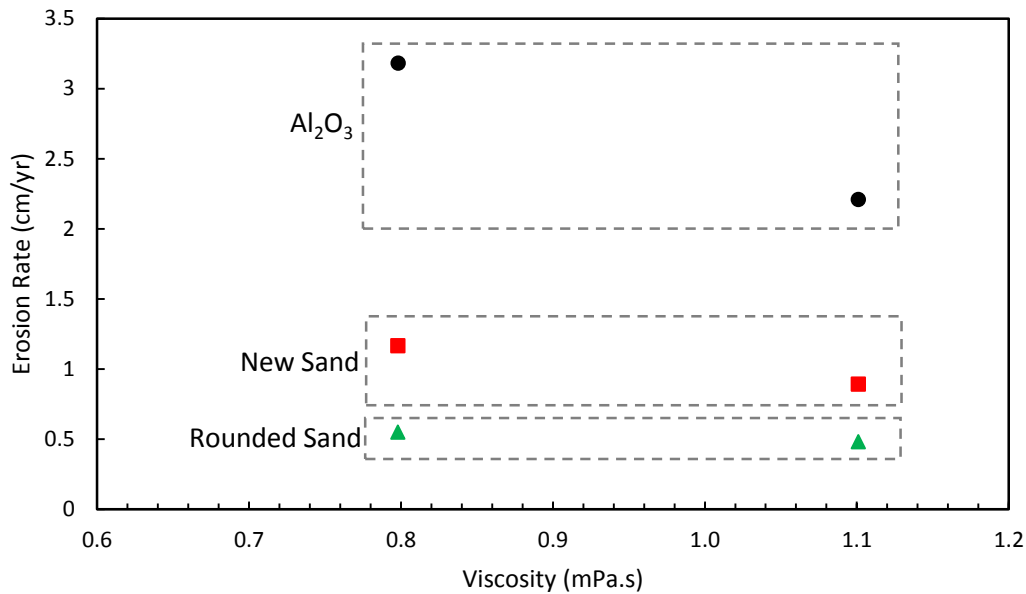
Figure 3.8 Erosion rate for different types of particles

It can be seen that the erosion rate increases dramatically for tests done with the Al_2O_3 particles, and the tests conducted with the rounded sand show much lower erosion rates compared to the new sand. As presented in Section 3.5, the circularity of Al_2O_3 is 0.68, while the value for the new silica sand is 0.80.

Pellegrin and Stachowiak [50] proposed a sophisticated model to relate particle shape to the abrasivity of the slurry. In their model, impact area

is defined as the surface area in which the particle and specimen are in contact through an impact incident. They proposed that abrasivity is a function of impact energy per unit of the impact area. This parameter has the same nature as surface stress. Particles with higher density (i.e. Al_2O_3) transfer greater stresses (i.e. energy/impact area) to the surface; therefore, they result in higher erosion rates. Angular (i.e. Al_2O_3 particles) and/or rough particles (i.e. new silica sand) contribute in reducing the impact area; thus, the particle impact has a higher stress and the particles are said to be more abrasive.

3.6.2 Effect of impact angle

The erosion rate on the surface was measured at 4 different impact angles 0° (parallel to the surface), 30°, 60° and 90° (normal to the surface). Figure 3.9 shows the erosion rate at different viscosities and impact angles.
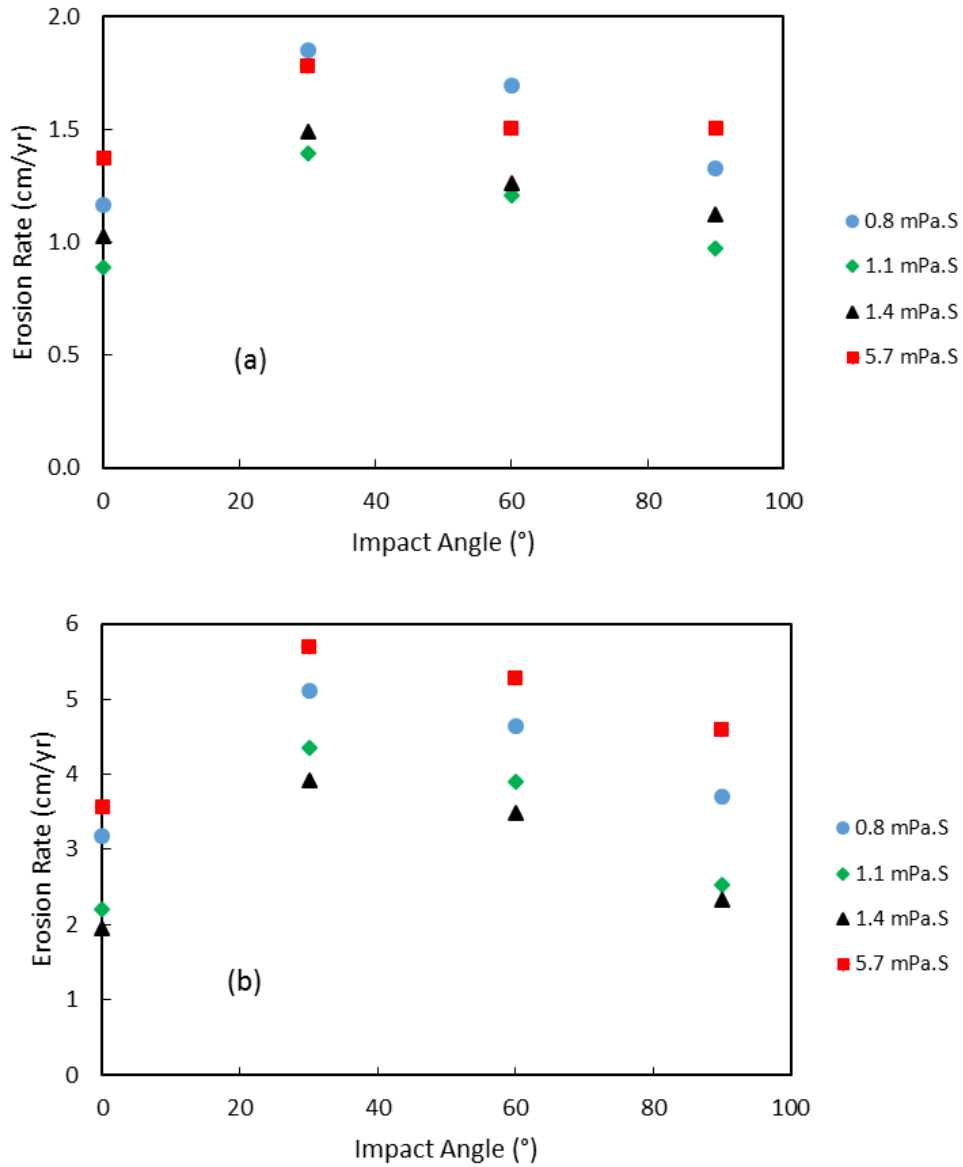
Figure 3.9 Erosion rate at different impact angles, *d*= 420 mm, *N*= 660 RPM, 30°C

(a) 19% new silica sand, (b) 19% Al_2O_3

It was observed that the erosion rate initially increases with increasing impact angle but once α > 30°, the erosion rate decreases. This pattern was consistent for all carrier fluid viscosities tested. The same trends were also observed for Al_2O_3 particles but the erosion rates were significantly higher. Gandhi and Neville et al. [45, 132] observed similar

trends in both jet impingement and slurry pot tests. In their tests, the lowest erosion rate occurred with α=90° (i.e. with stagnation point flow).

3.6.3 Effect of carrier fluid viscosity

Figure 3.10 shows the erosion rates measured for different carrier fluid viscosities.
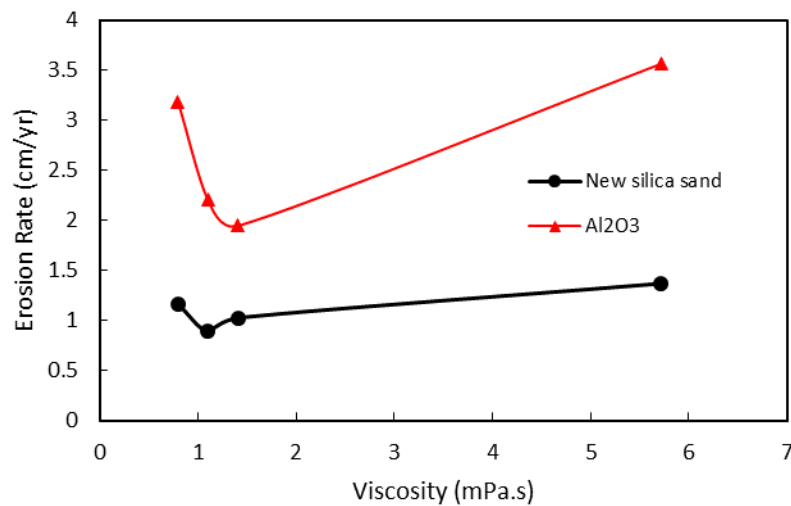
Figure 3.10 Variation of erosion rate with carrier fluid viscosity for slurry pot wear tests (C= 19%, d= 420 µm, N= 660 RPM, α = 30°)

As noted in Section 3.2.2, limited studies have been performed to examine the effect of carrier fluid viscosity on erosion rate. Huang et al.'s [20] model predicts pipeline erosion at different Reynolds numbers (details available in the original publication). Their model predicts that pipeline erosion rate decreases with increasing viscosity. The results of Figure 3.10 follow this trend up to a certain viscosity (1.1 mPa.s for new silica sand and 1.4 mPa.s for Al_2O_3). However, at higher viscosities, the erosion

rate increases with increasing viscosity. Kesana et al. [40] studied the erosion rate of 90° elbows at various carrier fluid viscosities (see Section 3.2.2 for details). They observed that the erosion rate increases with increasing viscosity (from 1 mPa.s to 10 mPa.s). This pattern is in agreement with the measurements made at high viscosities in the present study (i.e. $\mu > 1.1$ mPa.s for silica sand and $\mu > 1.4$ mPa.s for Al_2O_3). Kesana et al. were not able to explain this behaviour and recommended further investigation into the nature of this phenomenon. The results presented here, in combination with the data available in the literature, reveal the indirect effect of viscosity on erosion rate. The subsequent analysis provides a physics-based explanation of the effect of carrier fluid viscosity on erosion rate, which gives insight into underlying mechanisms affecting erosion.

3.7 Analysis

Traditionally, slurry pot erosion tests are performed at fixed hydrodynamic conditions and the focus is on alloy properties [12]. In contrast, in this study, the carrier fluid viscosity is chosen as the manipulated variable; hence, the forces on the surface of the sample are changing. As a result, to understand the observed behaviour, one should consider both the mechanisms behind the surface erosion and also the mechanisms that dictate the forces acting on the surface of the sample. In

this analysis, existing surface erosion theories and the results obtained during the present study are coupled with the concept of surface forces produced by the flow of the slurry over the sample surface.

It is commonly believed that slurry erosion (for soft alloys) consists of three main stages, as shown in Figure 3.11 [44].
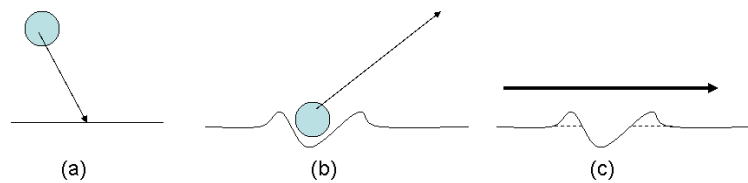
Figure 3.11 Schematic illustration of the generally accepted three-stage surface deformation mechanism for soft alloy slurry erosion (a) initial solids surface impact, (b) surface deformation, (c) material removal[44]

Initially the particle hits the surface. If the impact has enough energy, the surface is plastically deformed. Subsequently, the deformed volume will be removed (eroded) by shear over the surface.

The SEM images collected during the present study support this description of the surface deformation mechanism. Figure 3.12 (a) shows a typical SEM image from an Al_2O_3 test at an impact angle of 30° and Figure 3.12 (b) shows an image for new silica sand tested at similar conditions. These images clearly show that three different topographies exist:

104

1. Smooth surface, which can be the result of no particle impact or a low energy impact.

2. Deformed volcano-shaped surface. This impact site is the result of a high energy particle impact. This is similar to the mechanism described in Figure 3.11.

3. Rough surface, which represents the eroded surface (i.e. Figure 3.11 c).
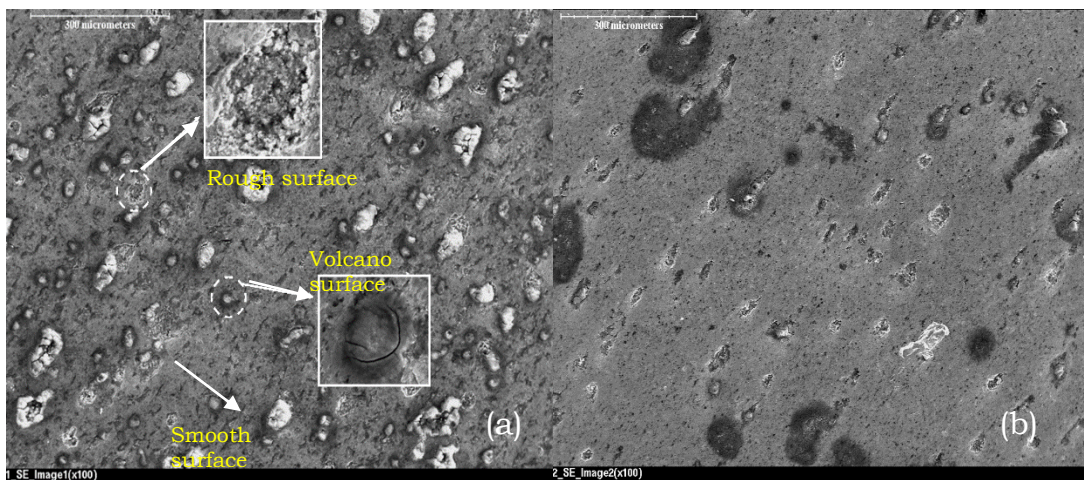
Figure 3.12 SEM images of the sample surface. (a) Aluminum oxide, (b) silica sand, impact positions and erosion positions are highlighted, (C=19%, d=420 µm, N=660 RPM, α=30°, μ=0.8 mPa.s)

The images also show a significant difference between the impact site density on the surface exposed to aluminum oxide particles (Figure 3.12a) and that exposed to new silica sand (Figure 3.12b). The higher density of surface deformations can be related to the greater overall mass loss of the sample, which is in agreement with the data presented in Figure 3.10. By detecting the surface at various stages of erosion and comparing the topography to images available in the literature [133] one can conclude

105

that the three-stage erosion described above is the dominant erosion mechanism for these samples. This mechanism reveals the functionality of the erosion rate on surface stresses which will be the basis of the analysis presented below.

3.7.1 Effect of impingement angle

To relate the aforementioned surface deformation mechanism to the effect of impact angle on erosion rate, SEM images were collected. Figure 3.13 shows surfaces for tests conducted at different impact angles. At $\alpha = 0°$ the surface shows both deformed impact sites and eroded sites. At this orientation, the flow is parallel to the surface. At $\alpha = 30°$ and $\alpha = 60°$, a particle's velocity trajectory has both parallel and normal components; therefore, particles slide on the surface after the initial impact. The impact sites are no longer circular and the sliding effect is visible on the SEM images. At $\alpha = 90°$ particles will not slide on the surface and the impact sites are circular. Also, the number of eroded sites is much smaller compared to other impact angles.
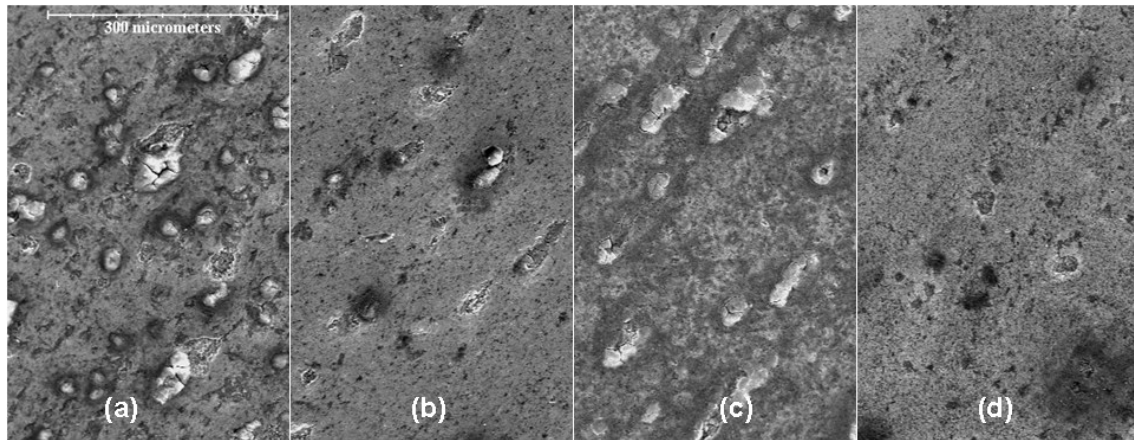
Figure 3.13 SEM image of the erosion surface at different impact angles, (*C*=19%, *d*= 420 µm, *N*=660 RPM, *µ*=0.8 mPa.s, new silica sand), (a) *α* =0°, (b) *α* =30°, (c) *α* =60°, (d) *α* =90°

At *α* =90°, the surface was exposed to a very large number of deforming impacts. However, because of the stagnation flow, the tangential shear is very low. As a result, the total erosion rate will be relatively small compared to *α* =30° and *α* =60°.

Finnie's [51] model of erosion (see Section 1.4.1 for details) shows that erosion rate is a strong function of impact angle. In his analysis, a successful impact requires enough energy to initially dig into the specimen surface (i.e. imposing normal stress on the surface); afterwards, the tangential portion of the impact energy (i.e. shear stress) is required to remove material from the surface. Following his methodology, the low erosion rate at α=90° can be attributed to the absence of shear stress and at α=0°, low normal stresses contribute to the low erosion rate.

3.7.2 Effect of carrier fluid viscosity

Several studies have shown that erosion rate is a strong function of force on the surface [5, 8, 19]. For example, Kleis and Kulu [44] showed that for a single particle, the erosion rate (I, kg.m^{-2}.s^{-1}) is a function of both tangential (shear) and normal stresses. This functionality can be presented as:

$$I = K(J_I + J_{II})$$ (3.6)

where K (kgm^{-2}Pa^{-1}) is a constant (i.e. material resistance to wear) that is a function of particle and surface properties such as particle diameter and surface hardness, J_I (Pa) is the tangential stress and J_{II} (Pa) is the normal stress. Both stresses J_I and J_{II} are functions of velocity, solids concentration and density and carrier fluid properties (viscosity and density). Therefore, to understand the relationship between the carrier fluid viscosity and the surface erosion rate, one should examine the effect of viscosity on the normal and shear stresses acting on the specimen surface.

For highly concentrated coarse particle slurries, the main friction caused by the solids on the surface is caused by inter-particle stress τ_s [123]. This stress was originally observed and defined by Bagnold [118]. Bagnold measured the shear stress on the surface (τ_w) of a specimen exposed to slurry flow by suspending the slurry between two cylinders and measuring

108

the torque required to rotate the outer one. He also recorded the pressure
on the cylinder surface to calculate the normal stress on the surface. He
assumed that the total shear stress on the surface is the sum of the fluid
and particle stresses:

$$\tau_w = \tau_f + \tau_s \tag{3.7}$$

By conducting the experiments at zero solids concentration, Bagnold
obtained τ_f. For the slurry experiments, then τ_s can be obtained by
measuring τ_w. Furthermore, Bagnold defined a parameter (i.e. Bagnold
Number) to predict the relationship between the shear and normal stresses
on the surface caused by a moving slurry:

$$N_B = \frac{\rho_s d^2 \lambda^{\frac{1}{2}} \dot{\gamma}}{\mu_f} \tag{3.8}$$

where ρ_s is the particle density, d is the particle diameter, $\dot{\gamma}$ is the shear
rate, μ_f is the carrier fluid viscosity and λ is the linear concentration
defined as:

$$\lambda = \frac{1}{\left(\frac{C_{max}}{C}\right)^{\frac{1}{3}} - 1} \tag{3.9}$$

where C_{max} is the maximum packing concentration of the solids and C is
the solids volume concentration. Bagnold showed that when $N_B < 40$, the
ratio of shear to normal stress, τ_s/σ, is 0.75 and when $N_B > 450$ this ratio is
0.32. In the transition zone, the ratio decreases monotonically with
increasing N_B, from 0.75 to 0.32.

The nature of the forces in a slurry pot system and Bagnold's Couette experiments are very similar. In both experiments, there is no moving bed of solids; hence, no Coulombic stress exists and the main source of stress is from the interactions of the solids and the carrier fluid with solid surfaces. In the Couette geometry, the particles move parallel to the surface (in reality the particles are stationary and the cylinder surface is moving). Although the specimen in a slurry pot test is not a cylinder, it can be considered as a portion of a hypothetical cylinder moving parallel to the particles. Thus for the tests, the shear and normal stresses on the surface of the sample are calculated using Bagnold's methodology [134]:

$$N_B = \frac{A \rho_s d^2 \lambda^{\frac{1}{2}} U}{\mu_f} \tag{3.10}$$

The Bagnold number (N_B) is originally defined for the Couette geometry as a function of shear rate ($\dot{\gamma}$) (see Equation (3.8)). To account for the differences between the slurry pot tester and Bagnold's experiments, the constant A is used here, which also allows for the use of U instead of $\dot{\gamma}$. This constant is a function of system geometry, such as the impeller distance from the tank wall.

Although Bagnold's approach has never been able to describe quantitatively the wall shear stresses in a flowing mixture, the general functionality and choice of key parameters that he provided has proven to be incredibly useful. For example, Shook and Bartosik [123] used

Bagnold's methodology to calculate friction loses in vertical pipeline slurry flow. For this reason, it is proposed that the normal stress in the slurry pot tester may be calculated based on known (or calculated) shear stress values using Bagnold's functionality. Equations (2.7) to (2.10) are used to predict the solids shear stress on the surface. The following steps and assumptions are required for this calculation:

- In Equation (2.7), the fluid friction factor is eliminated, to calculate the solids shear stress.
- Solids friction factor (f_s) is a function of λ (linear concentration) and d^+ (dimensionless particle size).
- Dimensionless particle size (d^+) is calculated using Equation (2.9) and the carrier fluid properties.
- Linear concentration (λ) is calculated using Equation (2.10) in the in-situ solids concentration (C_r) is assumed to be equal to solids concentration inside the slurry pot tester.

One should note that Equations (2.7) to (2.10) are designed to predict the stress in pipe flow geometry which will limit the application of the results to slurry pot tests. For example, in both geometries the slurry flow is parallel to the flow (for impact angle of 0°) but in a slurry pot the surface is flat (in contrast with curved pipe surface). Considering all of the differences between the two geometries, the goal is not to provide a

111

quantitative analysis of the wear mechanisms in a slurry pot. Rather the objective is to demonstrate qualitatively how surface stresses might affect the erosion rate, and then compare that qualitative analysis with actual experimental data.

Using this methodology and the Bagnold number, the solids normal and shear stresses on the surface are calculated and the results are shown in Figure 3.14. It should be noted that in this analysis, the stresses are calculated based on the assumption that flow will shift from the viscous regime (i.e. $\tau_s/\sigma = 0.75$) to the inertial regime (i.e. $\tau_s/\sigma = 0.32$). In other words, the transitional regime has been neglected in this analysis.
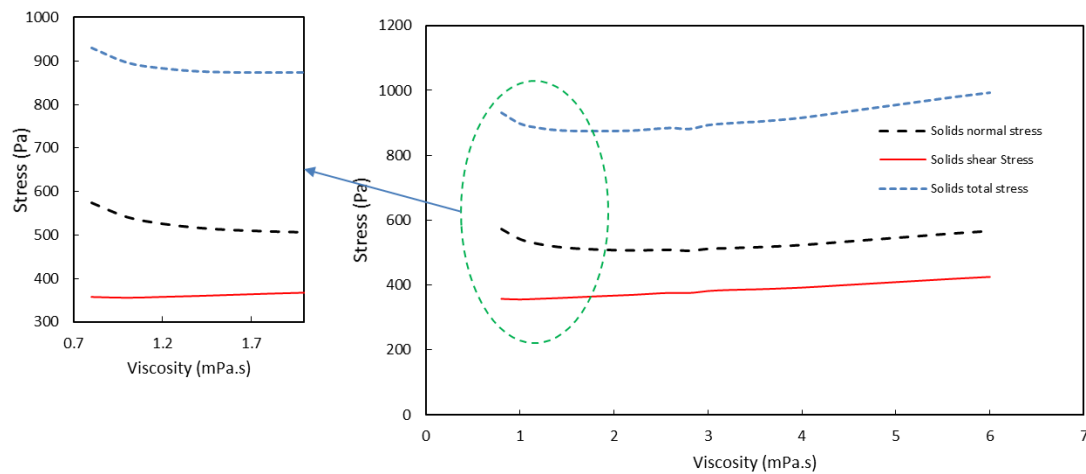
Figure 3.14 Normal and shear stresses on the surface, calculated based on Bagnold's model

According to Kleis and Kulu [44] model, erosion rate is a function of both shear and normal stresses. In their model, these two components are summed to reflect the total stress (see Equation (3.6) for details);

112

therefore, in the present study, the total solids stress is defined as the summation of the normal and shear stresses acting on the surface. The total stress on the surface is predicted based on the ratio of normal to shear stress derived from Bagnold's calculations. As the carrier fluid viscosity increases, the ratio of normal to shear stress will increase significantly; hence, the total stress on the surface will reach a minimum at 2 mPa.s. Recall that the erosion results presented in Figure 3.10 showed a minimum erosion rate at $\approx$ 2 mPa.s.

Carrier fluid viscosity affects the normal and shear stresses on the specimen surface. In the Kleis and Kulu model of erosion [44], the normal and shear stresses are related to erosion rate. As noted in this section, Equations (2.7)-(2.9) are used to calculate the shear stress τ_s on the surface at each viscosity. Afterwards, using the Bagnold approach and Equation (3.10), the normal stress (σ) on the surface is calculated. The total stress on the surface is therefore the sum of $\tau_s + \sigma$. Although this summation has no physical meaning, it includes the effect of both stresses and follows the modeling approach introduced by Equation (3.6). The results are presented in Figure 3.15. A linear relationship between erosion rate and total stress on the surface can be observed. This linear behaviour is in good agreement with the Kleis and Kulu model. The slope of the line

represents K (i.e. material resistance to wear) in their model. The

representative K values are also calculated for each particle[1].
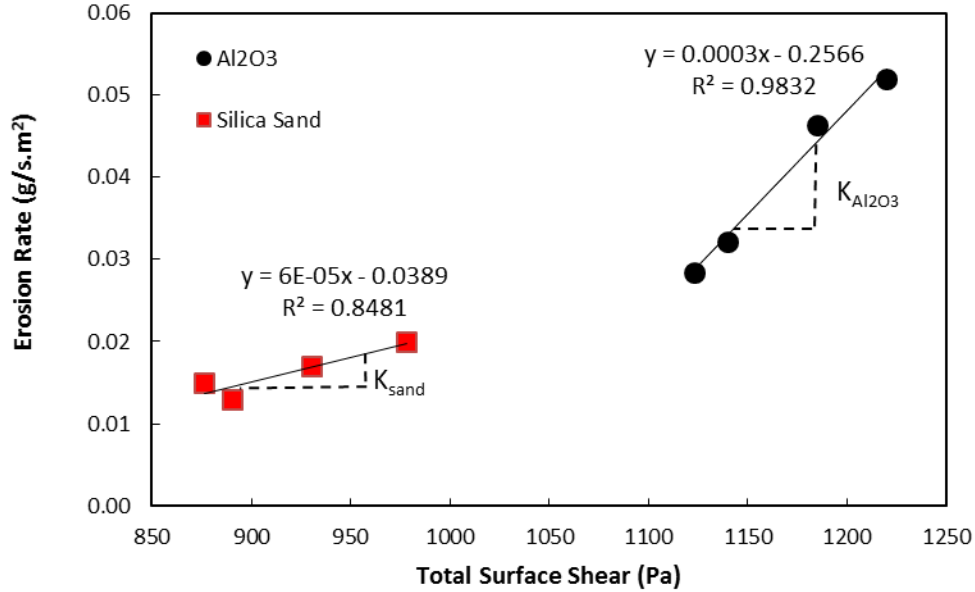
Figure 3.15 Erosion rate vs total shear on the surface for the two particle types tested during the present study

To compare the results obtained here with the Kleis and Kulu model, the

erosion units have been converted from cm/yr to $g/s.m^2$. The K value for

aluminum oxide particles is higher than that for new silica sand. This

phenomenon is related to the more angular shape and higher density of the

Al_2O_3 particles (see Section 3.6.1 for analysis of particle properties on

erosion rate). The results are presented in Table 3.5.

---

[1] According to Kleis and Kulu, K can be calculated using the following parameters: hardness of the particle and specimen, density of particle and specimen and depth of indentation. Depth of indentation is acquired experimentally by observing impact of a single particle on the specimen surface. In the absence of experimental data, present study has used the values reported by Kleis and Kulu. Details of this calculation are available elsewhere [44].

Table 3.5 Values of constant K for this experimental setup

Slurry	Experimental K Value ($kgm^{-2}Pa^{-1}$)	Kleis and Kulu model K Value ($kgm^{-2}Pa^{-1}$)
New silica sand	$6.\times E^{-5}$	$2.\times E^{-6}$
Al_2O_3 particles	$3.\times E^{-4}$	$3.\times E^{-6}$

By replacing the sand particles with higher density and more angular Al_2O_3 particles the slurry abrasivity changes with the same trend in both the slurry pot (i.e. present study) and the single particle approach (i.e. Kleis and Kulu model). However, the absolute values are significantly different. The Kleis and Kulu model is designed for single particle impacts. It does not include the effects of multiple particle impacts or particle shape. As a result the difference between the experimental values and model predictions can be attributed to those effects.

3.8 Conclusions

Here, a slurry pot tester was chosen to investigate the effect of the following parameters on erosion rate: carrier fluid viscosity, impact angle and particle shape and density.

It was observed that carrier fluid viscosity plays an important role in dictating the erosion rate. By manipulating the carrier fluid viscosity, the sample surface stress changes. Based on the surface deformation model of

Kleis and Kulu [44], both tangential and normal stresses are directly related to erosion rate; in other words, any significant change in either of these parameters will drastically change the erosion rate.

In this study, the maximum erosion rate occurred at an impact angle of 30°. This phenomenon was independent of carrier fluid viscosity and particle properties. The low erosion rates observed at impact angles of 0° and 90° are attributed to small normal and shear stresses, respectively.

New silica sand shows higher erosion rates compared to rounded sand. It was observed that these particles have similar shape and size but the rounded sand particles have a smooth surface compared to new sand. The sharp tips on the surface of the new sand particles cause higher impact stresses which consequently increase the erosion rate.

3.9 Novel contribution of this investigation and recommendations

In contrast with the common practice of correlating the erosion rate to mixing parameters such as velocity and impact angle, this study takes the approach that the erosion rate is a function of the shear and normal stresses acting on the surface.

In this study the force on the sample surface is calculated using Bagnold's methodology [118]. Current efforts are ongoing to directly measure both tangential and normal stress on the surface of the sample. For example, Noda et al. [135] and Ayaz et al. [136] have developed sensors which can be manufactured for this purpose. However, as the sensor should be installed inside a slurry pot impeller, special wiring and data transfer methods should be implemented. This will give the ability to correlate the erosion rate to the surface force more accurately.

Based on the comparison of rounded sand and new silica sand erosion rates, a detailed investigation of particle surface properties (e.g. roughness) on the erosion rate is also recommended.

4. Pilot-Scale Investigation of Pipe Wall Erosion Mechanisms

4.1 Introduction

As noted in Section 1.3, one of the main challenges for slurry pipeline owners is the loss of pipe wall material due to particle-surface erosion. This phenomenon is extremely complicated and the underlying mechanisms are not well understood. Laboratory apparatuses, such as the coriolis tester and jet impingement technique, drastically change the slurry flow environment compared to pipeline conditions (see Section 1.6.3 for details). For example, in most lab-scale tests, solid-wall impact angle and impact velocity are altered compared to pipeline conditions. In terms of slurry velocity, this variation can be as dramatic as 7 m/s in a jet impingement tester [38, 59] and 20 m/s in a coriolis tester [113] compared to a value of approximately 3 m/s under pipeline conditions [18, 19]. Furthermore, under slurry pipeline conditions, the particle-wall impact angle can vary from 0-20° [46]; whereas, in jet impingement tests the impact angle is a controlled variable with a different range (e.g. 60°-90°) [59, 63]. As noted in Section 1.6, data obtained from most bench-scale tests are not suitable for scale-up. Considering these factors, one can conclude that the most accurate technique to study this phenomenon is the direct observation of pipeline erosion.

118

Direct observation can be performed on actual industrial pipelines. The time required for these observations is typically on the order of months [3, 5]. During the course of field experiments, flow parameters like solids concentration and particle diameter are likely to change [5]. The combination of these two challenges makes it almost impossible to perform a repeatable experiment on an operating pipeline. Even in the case of constant flow parameters, the flow conditions are dictated by design constraints and operating targets. Therefore, the effects of flow parameters, such as velocity, on erosion rate cannot be studied independently.

Another option for direct observation of pipeline erosion is through the use of a pilot-scale pipeloop (see Section 1.6.5 for details). In pipeloop tests, flow parameters (e.g. velocity and solids concentrations) can be controlled. In theory, the effect of each parameter on erosion can be observed. Careful consideration is required to overcome operational challenges associated with pipeloop experiments. Some of these issues and mitigation strategies are described in Section 4.3.

In this study a purpose-built, pilot-scale pipe loop has been used to conduct an extensive pipe wear measurement campaign. Specifically, the effects of mixture velocity, pipe diameter and particle properties (density and shape) on erosion rate have been investigated.

In this Chapter, the experimental details of the pipeloop testing and experimental results are presented. A new modeling approach to predict the effect of flow parameters on erosion rate will be introduced and described. Finally the idea that one could take advantage of slurry hydrodynamics to reduce erosion rates is discussed.

4.2 Experimental details

In this section, the pipeloop used in this study is described. The materials utilized for wear testing are presented and the procedures for operating the loop and measuring erosion rates are discussed in detail.

4.2.1 Pipeline test facilities

The loop utilized in this study is located at the Saskatchewan Research Council's Pipe Flow Technology Centre^{TM} in Saskatoon, Canada. The pipe loop is 80 m long, meaning it contains two approximately 40 m straight sections connected to each other. The schematic of the experimental setup is presented as Figure 4.1.
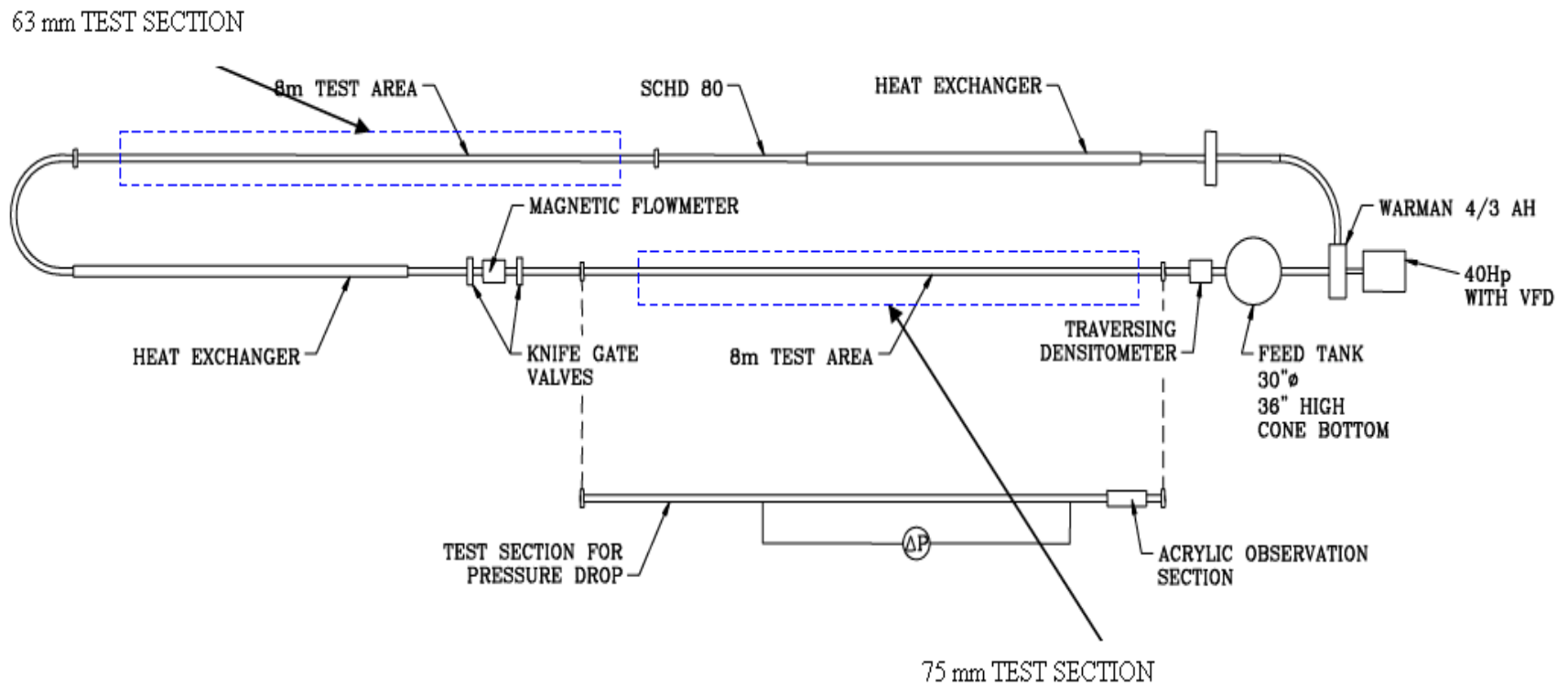
Figure 4.1 Pipe loop layout

The pipe loop is constructed with 3 inch diameter pipe and fittings. It is connected to a feed tank (diameter = 30 inch, height = 36 inch, conical bottom). The two test sections have been built with two different internal diameters (75 mm and 63 mm), which enables the study of two different mixture velocities during each run.

Each wear test section consists of 5 spool pieces held together using flexible clamps. Figure 4.2 presents the test section schematic and a photograph of the clamped test spools. Test spools of different lengths are used to evaluate the relationship between edge effects and wall erosion rate (see Section 4.4.1 for a detailed description). The spools are marked to ensure that they are always reinstalled in the same location and with the same orientation.
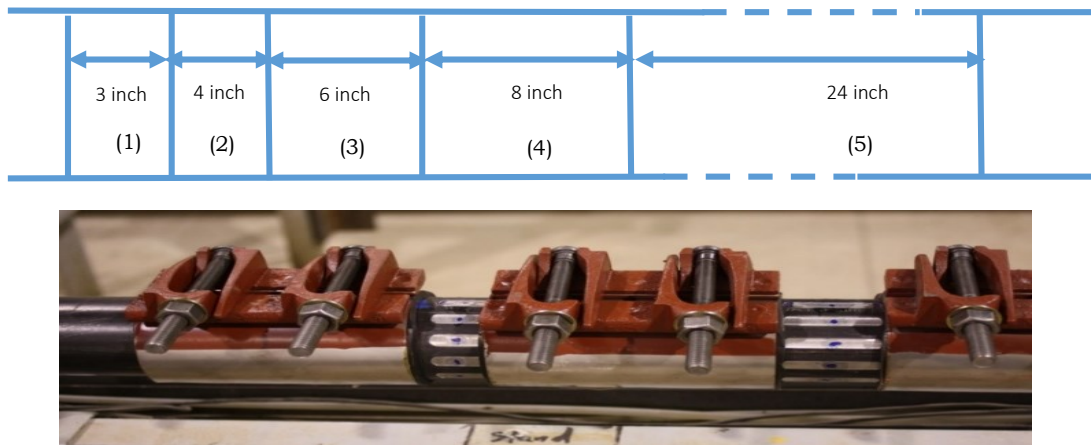
Figure 4.2 Test section assembly

Each test section is located approximately 100 pipe diameters downstream of any fittings or bends, which should be sufficient to obtain fully developed flow [28, 55]. This pipeloop is purpose-built for erosion studies. The connecting pipes and fittings have thick walls (Schedule 80 pipe) and large wear allowance. The test spools are made from carbon steel (ASTM A53) Schedule 5 pipe. Since the experimental procedure involves determination of the erosion rate using the mass measurement technique (see Section 4.2.3 for details) it is advantageous to construct the test spools using Schedule 5 pipe, which has a significantly lower mass per unit of length than thicker pipe (e.g. Schedule 80). In these tests the erosion mass loss is on the order of grams (e.g. 4 g/week). By choosing a light weight spool (e.g. 1 kg instead of 5 kg), the accuracy of mass loss measurement is improved (see Section 1.5.1).

123

The slurry is circulated in the loop using a rubber-lined centrifugal pump (Warman 4/3 WPA 43A01AU). A pump performance curve is available in Appendix A. The pump speed is controlled through a 40 hp 600 V VFD (Benshaw Model RS1040SX6B). The 40 hp pump motor is a Hyundai model HIS 324SR234.

The setup is equipped with a traversing gamma ray densitometer located just upstream of the pump inlet. This sensor is capable of measuring chord-averaged solids concentrations at any vertical position within the pipe, as shown in Figure 4.3 [121].
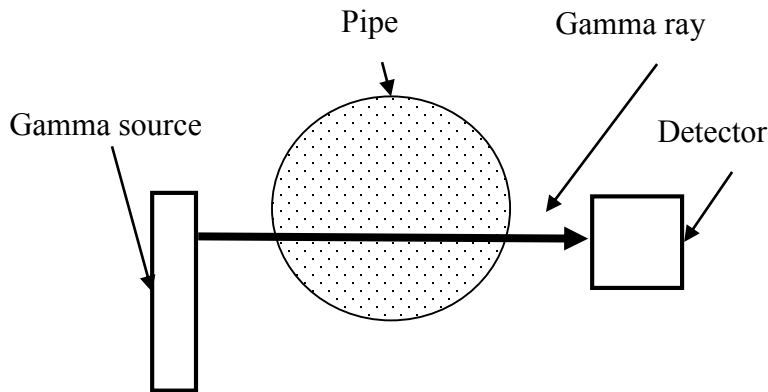
Figure 4.3 Schematic illustration of gamma ray densitometer

A gamma ray densitometer has 4 major components: a) gamma source (Cesium 137, 50 mCi) and source housing; b) shutter; c) collimator (for focusing the beam); and d) detector (Ortec Na-I scintillation radiation

detector). The output of the detector is recorded using the SRC's data acquisition system while interacting with Ortec Maestro Multichannel Analyzer Software. The sensor and the gamma source are mounted on a hydraulic jack to set the height of the densitometer. The height can be set to a precision of 0.01 mm.

As the gamma ray passes through the pipe and slurry, a portion of it is absorbed. The amount of gamma ray absorbed for any mixture can be calculated using the Beer-Lambert law. Equation (4.1) is the interpretation of Beer-Lambert law for a two-phase flow inside the pipe:

$$\frac{N}{N_0} = e^{[-(\mu_w x_w + \mu_f x(1-C) + \mu_s xC)]} \qquad (4.1)$$

where:

N = measured gamma ray intensity (count/s)

N_0 = baseline intensity (count/s)

μ_w, μ_f, μ_s = radiation absorption coefficient of the pipe wall, fluid and solids, respectively (cm^{-1})

x_w = path length of the beam through pipe wall (cm)

x = path length of beam through the slurry (cm)

C = chord-averaged volume concentration of solids (-)

In this study, the sensor is positioned on the lowest height to examine the near-wall lift effect (see Section 4.6 for details). This will enable the user to record the slurry density inside the pipe at y/D=0.05, or 0.05 D from the bottom of the pipe.

The temperature is held constant using two double pipe heat exchangers, with glycol circulated through the annulus of each heat exchanger to ensure isothermal operation. For this study, all tests were conducted at a slurry temperature of 20°C. Pressure drop measurements are taken over the straight section upstream of the pump suction. The loop is equipped with a transparent section to visually determine the deposition velocity and to observe the slurry behavior in the pipe. A magnetic flow meter is installed on the pipe to monitor the slurry flow rate, although this meter is removed during erosion testing, as described in Section 4.3.3.

4.2.2 Materials

The particles used in this study are silica sand (Sil Commercial, Sil 4), Al_2O_3 particles (Sil Commercial, abrasive particle) and zirconium silicate (Quackenbush Co, QBZ-58A). The particle properties have been summarized in Table 3.3 (see Section 3.5 for details). As zirconium

silicate particles were not utilized in the main test program (i.e. erosion testing), their properties are presented only in Section 4.6.1. The suspending liquid is City of Saskatoon municipal water. Also, corrosion inhibitor (VCI-1 Corrosion Inhibitor Powder, KPR ADCOR INC) is added to the slurry at a concentration of 1% (by mass) to eliminate corrosion. The effectiveness of the inhibitor was tested and the results are presented in Section 4.3.1.

4.2.3 Procedures

Loop assembly

Test spools are washed with toluene and DI water to remove residual materials on the surface. They are then placed in an oven at approximately 100°C for 24 hours. The dry spools are weighed and the mass of each is recorded. The spools are assembled using flexible clamps. To generate repeatable data, it is critical to align the pipe spools meticulously (see Section 4.4.1 for details).

Loading the slurry

To achieve precise solids concentration inside the loop, it is critical to accurately measure the total volume of the loop. As a one-time test, the loop is filled and then the feed tank is isolated from the loop and the loop content is drained into a container. The mass of the drained water is recorded and using the water density the volume is calculated. In these experiments, the total volume of the loop is approximately 195 L.

To begin a test run, the loop is filled with water. The following steps should be taken to calculate the mass of solids to be added to the loop: a) determine the desired solids concentration in the loop (e.g. 20% by volume); b) calculate the solids volume by multiplying the total volume of the loop by the desired solids volume concentration (e.g. 195 L × 0.2 = 39 L); and c) calculate the solids mass by multiplying the solids volume by the solids density (e.g. 39 L × 2.650 kg/L ~ 103 kg). To avoid sudden surges of local solids concentration inside the loop, particles are added gradually through the feed tank. It is critical to keep the pump running during this process. The water velocity is approximately set at 4 m/s during the loading process.

Trapped air bubbles attached to particles in the slurry can change the overall density of solids. To avoid this problem, after loading the loop, the slurry is heated to 50° C. By increasing the temperature, the air release process is facilitated. Next the slurry is cooled down to reach the desired experiment temperature (i.e. 20° C in the present study).

Erosion test

After the slurry has been prepared and loaded into the loop, it is circulated in the loop for the desired time (e.g. 4 weeks). The slurry flow rate is controlled by pump RPM (details described in Section 4.3.3). During each test, to reduce the effect of particle degradation, the entire slurry volume is replaced every week. The interval was chosen based on some supplementary experiments performed prior the erosion tests (see Section 4.3.2 for details). After completing the experiment, the loop is drained and the test spools are disassembled.

Erosion rate calculation

After a test is completed, the test spools are disassembled. They are washed with toluene and DI water to remove residual surface material. The cleaned spools are placed in the oven for 24 hours at ~100°C. The mass of the dry spool is measured and recorded. The mass lost is calculated by deducting the final mass from the original mass. The erosion rate is calculated by dividing the eroded mass by the experiment time.

Before any erosion experiments could be conducted, a number of tests were completed. Primarily, these tests were required in order to develop erosion test operating parameters/conditions. These ancillary tests are described in the next section.

4.3 Ancillary testing required in support of the pipeline wear tests

4.3.1 Corrosion testing

In a slurry pipeline, pipe material will be removed by both corrosion (i.e. chemical reaction) and erosion (i.e. physical removal) [3]. The focus of this study is slurry erosion. As mentioned previously, to eliminate possible corrosion damage on the test samples, corrosion inhibitor (VCI-1 Corrosion Inhibitor Powder, KPR ADCOR INC) is added to the slurry. To check the effectiveness of the inhibitor, lab-scale investigations were performed.

Slurry with similar composition to the pilot-scale tests (e.g. 20% by volume sand) was prepared in a 2 L beaker. The solids are suspended with use of an impeller set to a low RPM. Slurry pot test coupons (5cm×1cm×0.5cm pipe steel) are placed in the slurry. The sample is left inside the slurry for 3 weeks (similar to pipeloop tests). The sample is taken out and washed with DI water and toluene to remove any residual surface material. As the slurry is mixed at very low impeller speeds, the erosion damage is negligible and therefore the measured sample mass loss

is an indicator of corrosion damage. The results are presented in Figure 4.4.
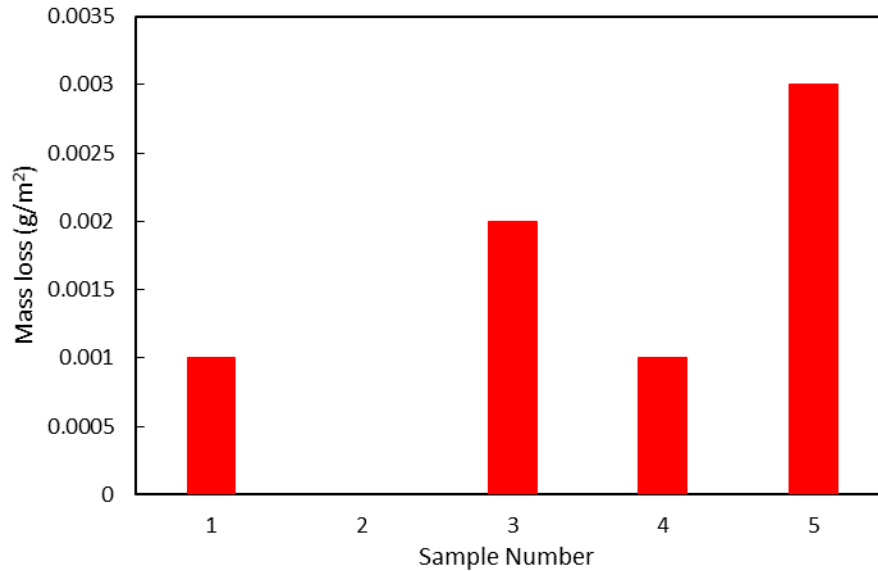
Figure 4.4 Corrosion damage in presence of corrosion inhibitor

Figure 4.4 shows the corrosion damage for 5 different samples. Sample number 2 mass loss is below the measurement accuracy. Comparing the corrosion mass loss (maximum of 0.003 g/m^2) to overall mass loss of pipe section in the pilot-scale experiments (approximately 10 g/m^2), it can be concluded that during the course of the pipeloop experiments, corrosion damage can be neglected and the overall mass loss in the pipeloop tests can be attributed to slurry erosion alone.

4.3.2 Particle degradation

As the particles circulate inside the loop, they are exposed to harsh conditions, especially when they pass through centrifugal pumps and pipe fittings. The particle-wall and the particle-particle impacts will alter the shape and size of the particles. This phenomenon is usually referred to as particle degradation [47]. As a result of particle degradation, the slurry will display different abrasive characteristics with time while circulating in the loop. To avoid this problem and also to be able to produce repeatable data, particles should be replaced regularly with new ones. To find the appropriate particle replacement interval, particle shape and size are monitored by taking samples while the slurry is recirculating. An optical microscope (Carl Zeiss Canada: Axiovert 200) is used for particle shape determination while sieve analysis was used for particle size distribution measurements. Figure 4.5 examines the effect of particle circulation on the particle shape (i.e. roundness) and Figure 4.6 presents particle size distribution for fresh and circulated sand after 1 and 4 weeks of experimental time. This experiment is performed using a 20% (by volume) silica sand slurry at 4 m/s velocity.

133
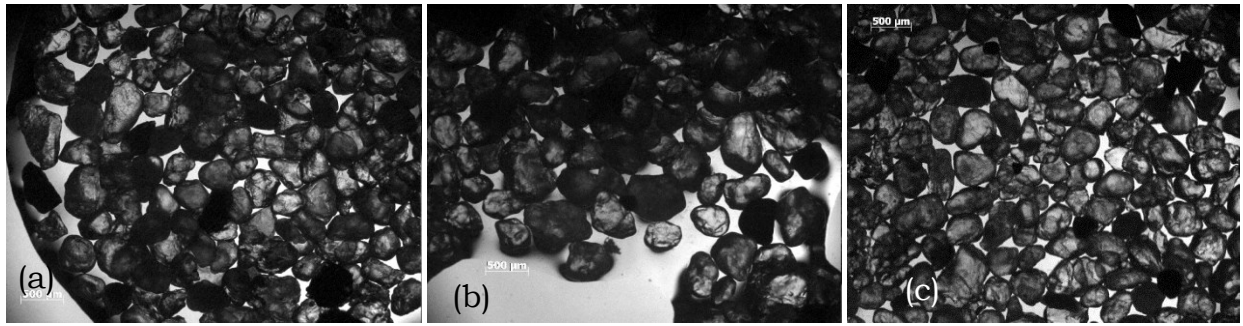
Figure 4.5 Particles shape examined under an optical microscope: (a) fresh sand; (b) 1 week in circulation and (c) 4 weeks in circulation
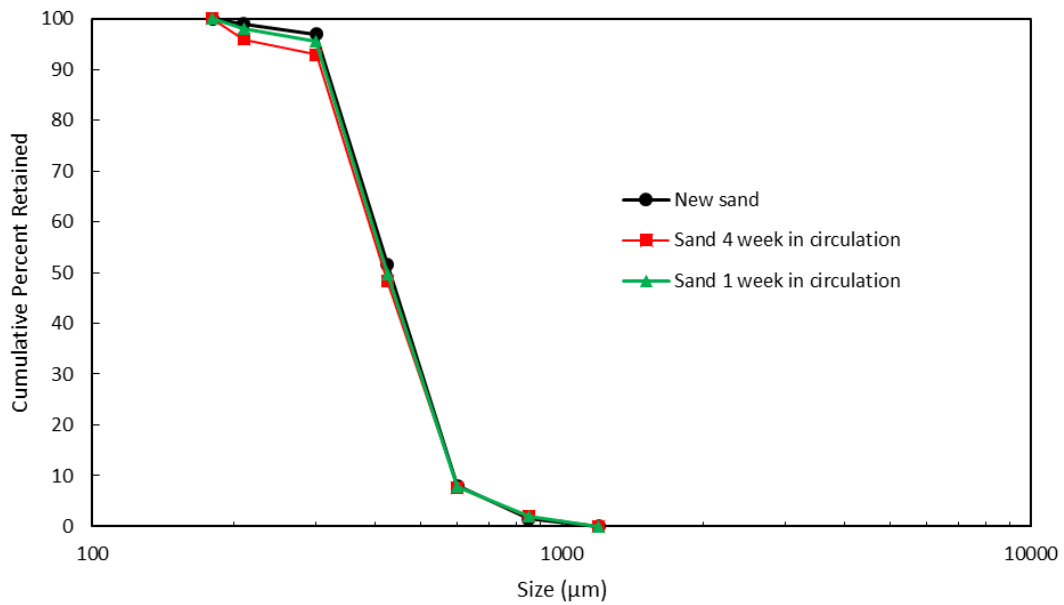
Figure 4.6 Particle size analysis using dry sieving method

It was observed that the particle shape and size do not measurably change after 1 week of circulation. After 4 weeks, the percentage of particles smaller than 210 µm increases and the d_{50} decreases slightly. The properties of these particles are reported in Table 4.1.

134

Table 4.1 Properties of new silica sand, and sand circulated 1 week and 4 weeks

	d_{50} (µm)	<210 µm fraction (% by mass)	Particle Circularity
New silica sand	420	1.1	0.80
1 week circulation	420	2.0	0.80
4 weeks circulation	410	4.1	0.80

Circulation of the slurry seems to "chip away" at the particles, rather than breaking them. This process is known to generate "fines" (< 75 µm particles). These fine particles can be considered to be part of the slurry carrier fluid [117]. As noted in Section 4.3.2, particles with similar shape and size may have different abrasivity. It is necessary to monitor the fines concentration in the carrier fluid in addition to shape and size as a measure of particle degradation inside the loop. To do so, slurry samples were taken at various intervals from the loop. The carrier fluid is separated from the coarse particles using a 75 micron sieve. The carrier fluid is then weighed and placed inside an oven for 24 hours at ~100°C. The dried sample mass is measured. The fine solids concentration is calculated by dividing the dry mass by the original mass. The results are presented in Figure 4.7.
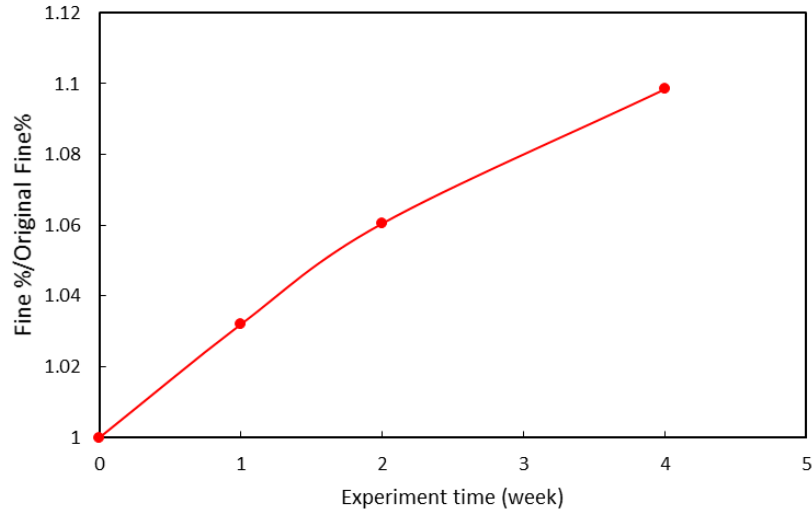
Figure 4.7 Normalized (divided by the original) carrier fluid fines concentration at different sand circulation time, solids concentration = 20% (by volume) silica sand, velocity = 4 m/s

Figure 4.7 shows that after 1 week of circulation, the fines concentration increases only by 3%. The rate of particle degradation inside the loop should be balanced with the cost (time and materials) of slurry replacement. Considering the size monitoring and carrier fluid fines concentration evidence, it was determined that a slurry replacement interval of 1 week provided the best balance between minimizing particle degradation effects and overall test costs.

4.3.3 Pump RPM–flow curve development

Recall that the pipeloop used in the present study has a magnetic flow meter installed in the loop. In order to avoid accelerated wear and consequent regular replacement of an expensive instrument, flow curves were developed so that the pump RPM could be used as a flow indicator and then the flowmeter could be removed from service during the wear tests. Since centrifugal pump speed does not on its own provide an indication of flow rate (or velocity), calibration tests were done with each type of slurry to develop pump RPM-flow rate curves. The results are presented in Figure 4.8.
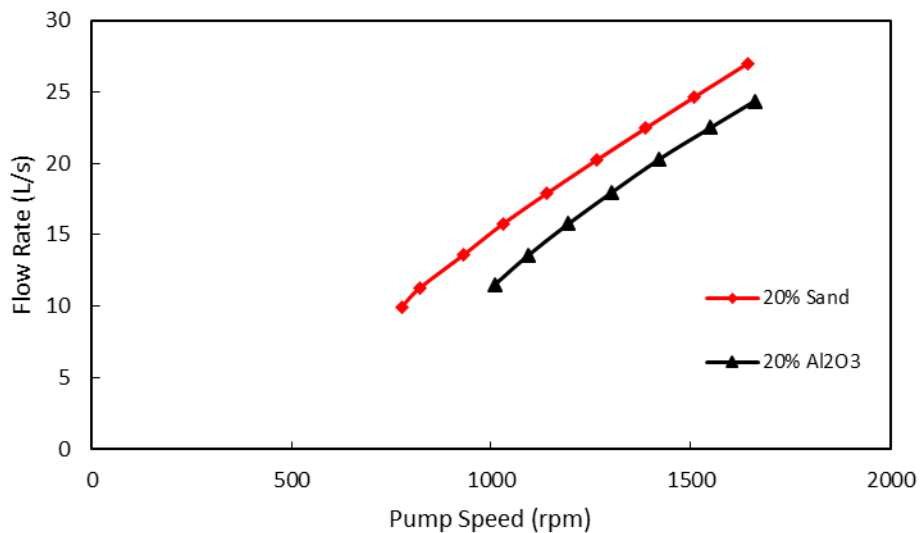
Figure 4.8 Development of pump RPM-flow rate curves for Al_2O_3 and silica sand at experiment concentration.

After the data were collected, the magnetic flow meter is removed from the loop and the flow rate is controlled by selecting the pump RPM to achieve the desired flow rate. The following equation is used to calculate the pump RPM for each flow rate:

$$Q = aR - b$$

<div align="right">(4.2)</div>

where:

Q = flow rate (L/s)

R = pump RPM

a and b = constants acquired experimentally for each slurry

Table 4.2 shows the constant (a and b) values for slurries used in this study:

Table 4.2 Constant values for pump RPM-flow rate correlations

	a	b
20% Sand	0.0194	4.6
20% Al$_2$O$_3$	0.0196	7.9

These correlations are applicable for this specific experimental apparatus only, and any alteration such as pump replacement, or pipeloop changes would require recalibration.

4.4 Experimental results

This section presents the results acquired during the pipeloop experiments. The results are categorized into 3 groups: test spool length effect on erosion rate; velocity effect on erosion rate; and ultrasound thickness measurements.

4.4.1 Effect of test section length/position on erosion rate

As mentioned in Section 4.2.1, the pipe spools are installed adjacent to one another and held together with flexible clamps. The test spools have 5 different lengths (3", 4", 6", 8" and 24"). All the spools have pipe ID of 75 mm and wall thickness of 2.1 mm. Figure 4.2 (Section 4.2.1) presents the schematic and image of this arrangement. This section describes the test performed to check for existence of edge effects.

The loop is loaded with 20% sand (Sil 4) slurry and circulated for 3 weeks. At the end of each week, however, the loop is emptied so that fresh (new) slurry can be used. At that time, the test spools are disassembled, cleaned and weighed (see Section 4.2.3 for details of experimental procedure). The results are presented in Table 4.3.

139

Table 4.3 Mass loss of each test spool

Circulation Time		0 h	128 h	272 h	1088 h
Part #	Length (in)	Mass (kg)	Mass (kg)	Mass (kg)	Mass (kg)
1	3	0.539	0.536	0.533	0.523
2	4	0.596	0.593	0.590	0.578
3	6	0.696	0.692	0.690	0.675
4	8	0.941	0.936	0.930	0.911
5	24	1.430	1.422	1.414	1.384

The erosion rate is calculated by subtracting the final mass of the spool piece from the original mass and dividing it by the experiment time. To compare the results from the different test spools, the total mass loss for each is normalized using the original pipe weight. The results are presented in Figure 4.9.
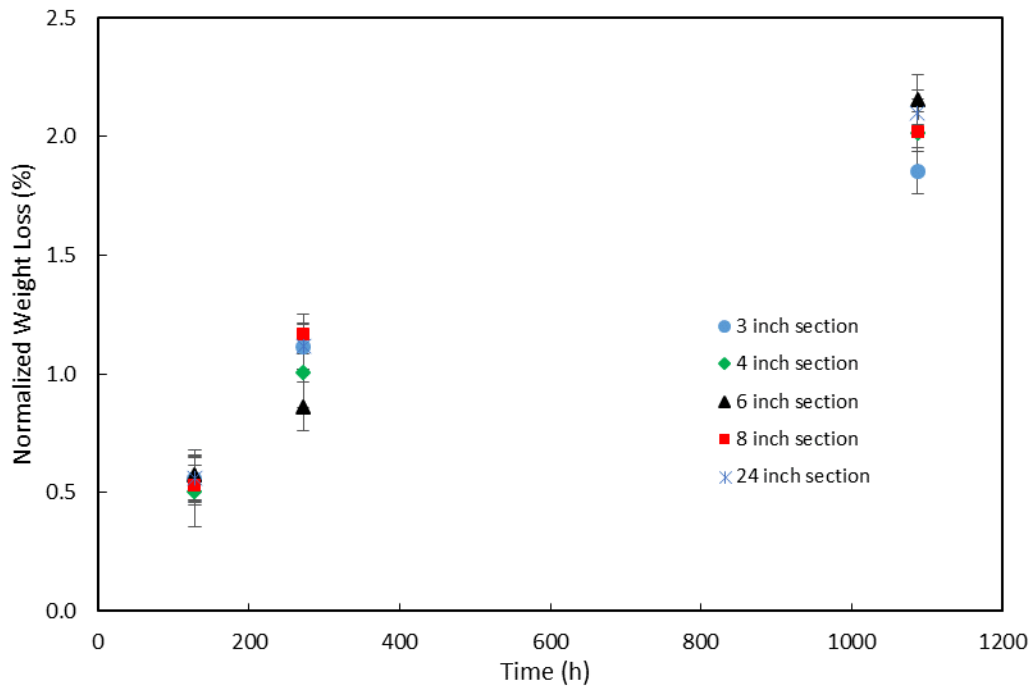
Figure 4.9 Normalized weight loss of test sections after different experiment times

Figure 4.9 shows that at each time interval, the test spools experienced relatively similar mass losses. Table 4.4 summarizes the normalized mass loss measurements and also provides the "coefficient of variation" of each time interval. The coefficient of variation is calculated by dividing the standard deviation by the average value of the data points at each time interval. It represents the dispersion of the data and typically it is used to show the precision and repeatability of the data. When the coefficient of variation is less than one, data can be considered repeatable and reliable [137].

141

Table 4.4 Error values for pipe alignment test

Circulation Time	128 h	272 h	1088 h
Part #	Mass Loss (%)	Mass Loss (%)	Mass Loss (%)
1	0.557	1.113	1.855
2	0.503	1.007	2.013
3	0.575	0.862	2.155
4	0.531	1.169	2.019
5	0.559	1.119	2.098
Coefficient of Variation	0.051	0.116	0.055

It can be observed that at each circulation time, the coefficient of variation is significantly smaller than 1; therefore, the data can be considered repeatable. In other words, statistically, all the test spools have similar normalized mass loss at each circulation time.

If the test spools are not aligned, the edge of each spool will cause a flow disturbance; therefore, the spool edges erode at a different rate compared to the middle of the spool. Figure 4.10 presents a schematic of this phenomenon.
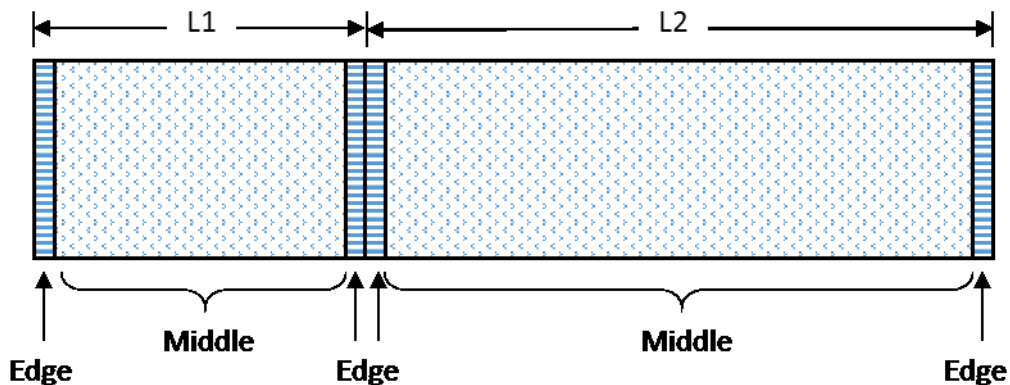
Figure 4.10 Test spool erosion schematic.

142

The total spool erosion rate can be calculated as:

$$E_i = E_{ei} + E_m \times L_i \qquad (4.3)$$

where E_i (kg/s) is the erosion rate of the spool number i, E_{ei} (kg/s) is the edge erosion rate, E_m (kg/s.m) is the middle erosion rate per unit length and L_i is the spool length. As the spools cross sections are similar, E_m is assumed to be independent of the spool length. By normalizing the erosion rate using the spool length, Equation (4.3) can be rearranged into:

$$\frac{E_i}{L_i} = \frac{E_{ei}}{L_i} + E_m \qquad (4.4)$$

If the magnitude of edge erosion (E_{ei}/L_i) can be neglected compared to middle erosion rate (E_m), the total normalized erosion rate (E_i/L_i) will be independent of the spool length (L_i). Otherwise, the total normalized erosion rate should change with changing the spool length. The data introduced in Table 4.4 represents E_i/L_i ratio. As mentioned previously in this section, the normalized erosion rate (E_i/L_i) can be considered independent of spool length for the data presented in this section; therefore, the edge erosion can be neglected for the spool alignment used in the present study.

143

This observation indicates that the pipes are aligned and there is no edge effect disturbing the flow inside the pipe. The implication is that with careful spool arrangement, short test spools can be used and will provide repeatable data. Therefore, in the future, shorter test spools can be installed in the loop which will allow for simultaneous testing of different metal alloys and different flow velocities.

4.4.2 Effect of slurry velocity on wear rate

Pipe erosion rates were measured for two slurries: 20% (by volume) silica sand and water and 20% (by volume) Al_2O_3 and water. The tests were conducted at velocities of 2-3.5 m/s in the 75 mm pipe (3.5-5 m/s in the 63 mm pipe). Each test took approximately 4 weeks with the slurry replaced weekly to minimize the effect of particle degradation (see Section 4.3.2).

Figure 4.11 displays the measured wear rate at different velocities for the sand and Al_2O_3 slurries. It is apparent from the data of Figure 4.11 that the erosion rate increases with increasing slurry velocity. Similar trends were observed for the larger (75 mm) and smaller (63 mm) pipes and for

144

both the sand and Al_2O_3 slurries. This behavior is in agreement with related literature [47-49] (see Section 1.4.1 for details and examples).
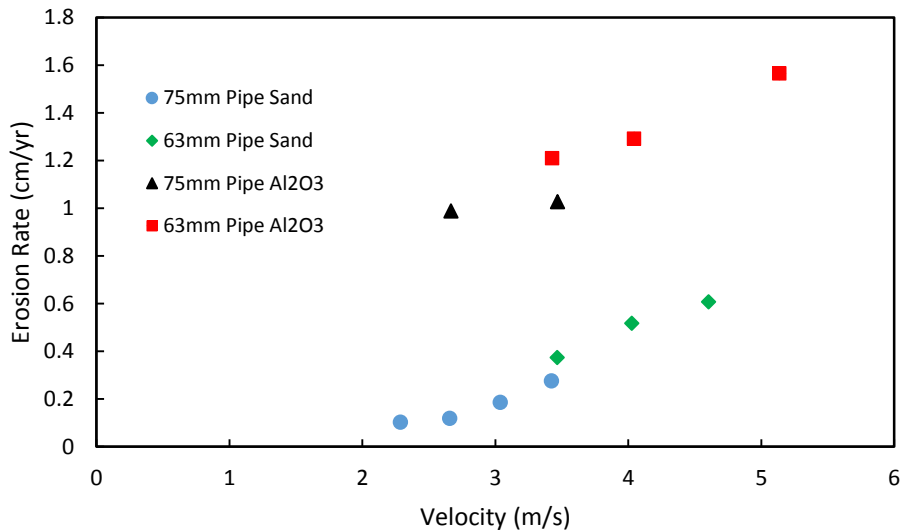
Figure 4.11 Measured wear rates from pipe loop tests

Comparison of data from the 63 mm line with those from the 75 mm line reveals that the velocity has an indirect effect on erosion rate and does not reveal the effect of other flow parameters such pipe diameter. For example, note that at a velocity of 3.5 m/s, the erosion rate is different for each pipe diameter and the difference is significantly larger than measurement error. As a result, correlating the erosion rate with slurry velocity is not sufficient and additional parameters such as pipe diameter should be included in the modelling approach.

4.4.3 Ultrasound wall thickness measurements

In an attempt to measure the local erosion rate on each angular position of the pipe, an ultrasound thickness measurement (UTM) probe is utilized. Ultrasound thickness measurement is a non-destructive technique commonly used to measure the thickness of metals. This technique works on the principle of measuring the ultrasound travel time inside a metal (see Chapter 1.5.2 for details).

Specific locations on the outer pipe surface have been flattened (10 mm width) to minimize the error associated with pipe curvature effects. Twelve measurement sites were created on pipe perimeter. To make the measurements, the probe is placed on the pipe at a given measurement location. The operator scans the test site and records the minimum reading. Figure 4.12 presents a schematic of the pipe cross section and a photograph of a measurement site on the pipe.
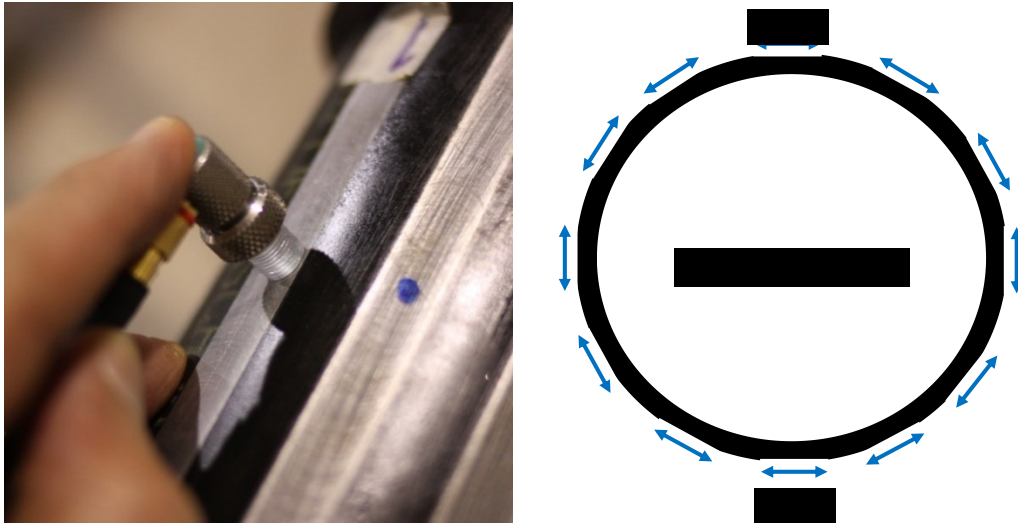
Figure 4.12 Pipe cross section schematic; ultrasound thickness measurement sites highlighted

For each angular location on the pipe, the pipe wall thickness is recorded as the experiments progressed. The frequency of measurement was not constant. Initially the measurements were performed with a time interval of 8 hours and as the experiments progressed it was increased to 240 hours. As an example, the results for a 20% sand slurry are presented in Figure 4.13. Other data sets (available in Appendix B) are qualitatively similar to the results presented here.
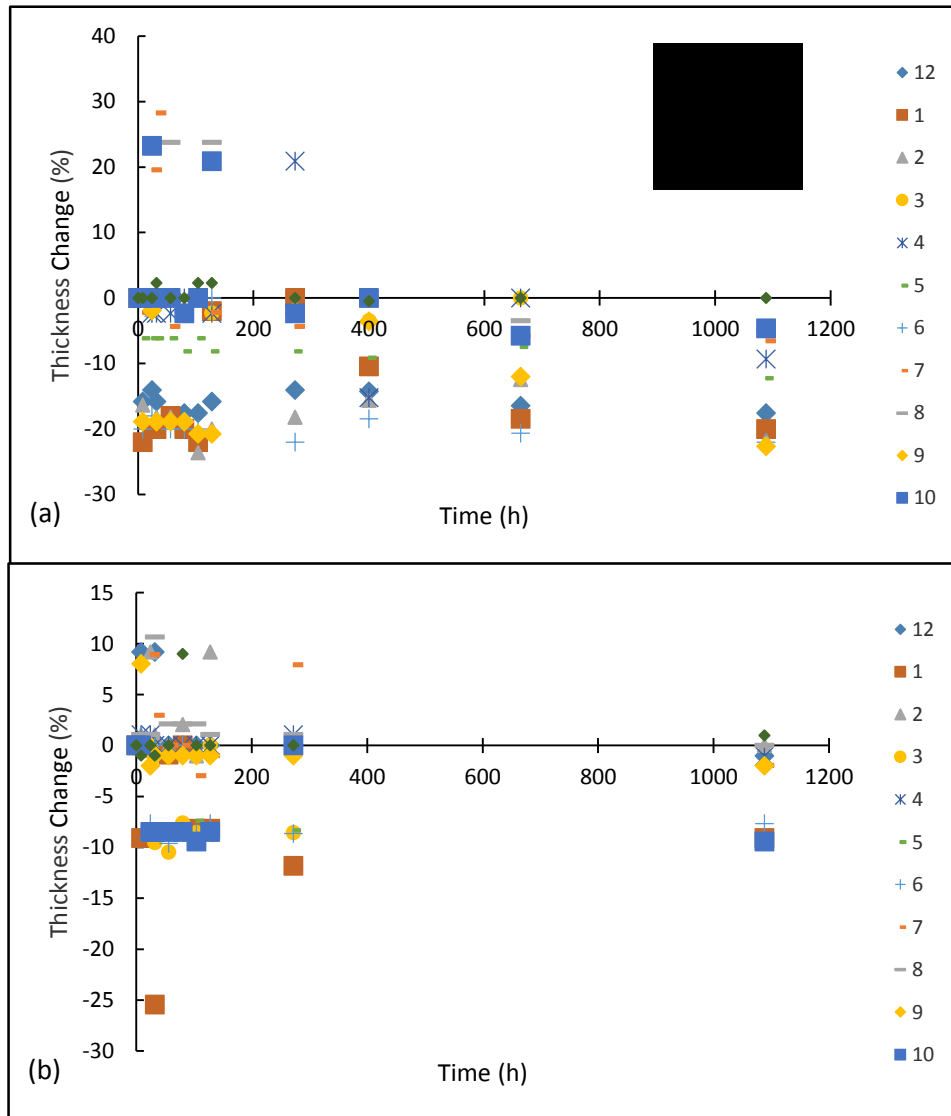
Figure 4.13 Ultrasound thickness measurements on 12 angular positions, 20% Sand, (a) pipe ID = 63 mm, velocity = 4.60 m/s (b) pipe ID = 75 mm, velocity = 3 m/s

Figure 4.13 shows no clear trend in the wall pipe wall thickness as the experiments progress. Surprisingly, at some times the wall thickness increases as the slurry is recirculating. This phenomenon can be attributed

148

to measurement error, pipe curvature or surface residual material (see Section 1.5.2).

To further examine the data, the ratio of the pipe invert thickness change (i.e. 6 o'clock position) to that measured at the top of the pipe (i.e. 12 o'clock position) is calculated. At the pipe invert, the moving bed of particles will increase the stress on the pipe (i.e. Coulombic stress effect, see Section 2.2.1). The bottom-to-top ratio reveals the possible effect of this stress on the thickness change (i.e. pipe wall erosion). For each velocity, this ratio is calculated at various experiment times. To reduce the noise level, the average value of this ratio at each velocity is used for the analysis. The results are presented in Figure 4.14.
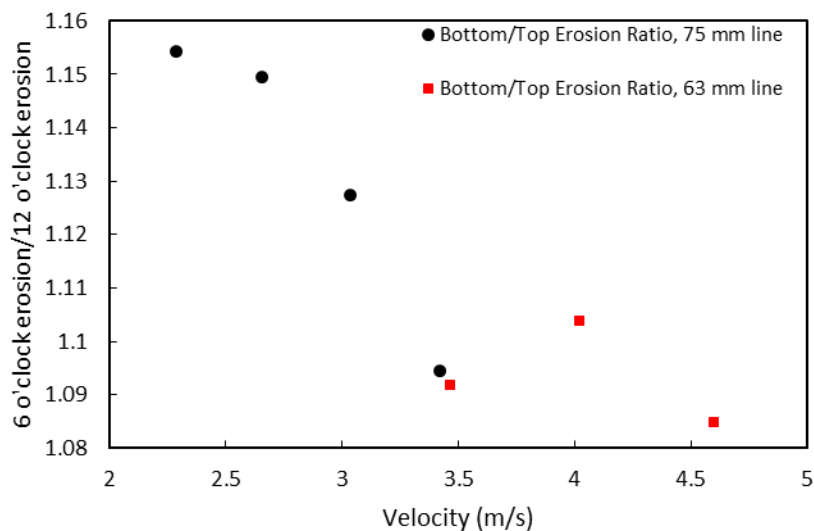
Figure 4.14 Bottom/Top thickness change at various velocities. 20% Sand

149

Figure 4.14 shows that the erosion rate at 6 o'clock is higher than that measurement at the 12 o'clock position. The difference in erosion rate at the two positions decreases as the slurry velocity increases. This phenomenon was independent of pipe diameter. As mentioned in Section 4.2.1, the traversing gamma ray densitometer is capable of measuring the chord-averaged density of the slurry at bottom 5% of the pipe (i.e. $y/D =$ 0.05). Using the chord-averaged density and slurry components (i.e. sand and water) densities, the solids volume concentration at bottom 5% of the pipe can be calculated:

$$C_s = \frac{\rho_m - \rho_f}{\rho_s - \rho_f} \qquad (4.5)$$

where C_s is the solids volume concentration, ρ_s is the solids density, ρ_f is the fluid density and ρ_m is the mixture density. The bottom solids concentration at each test velocity is compared to the thickness change ratio in Figure 4.15.
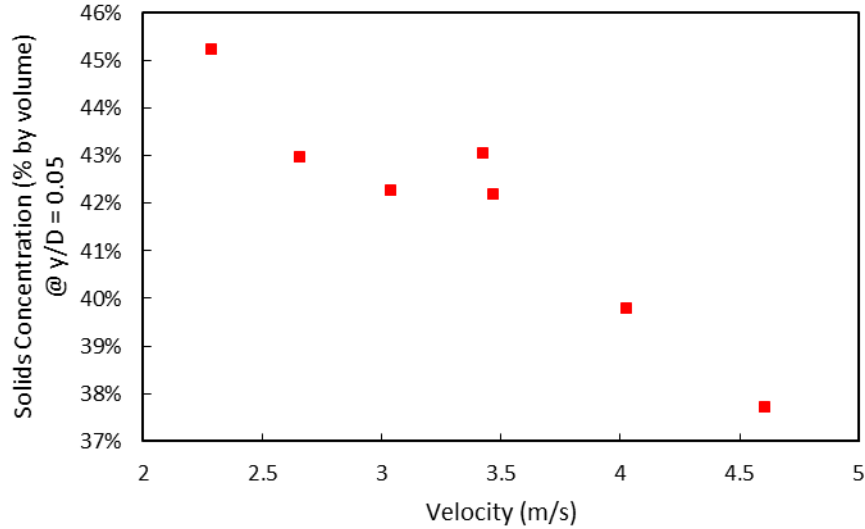
Figure 4.15 Bottom 5% (@ *y/D* = 0.05) solids concentration at various velocities; C_s = 20% sand

Figure 4.15 shows that with increasing the velocity, the bottom 5% solids concentration decreases. The bottom 5% solids concentration and the bottom-to-top thickness ratio (see Figure 4.14) follow the same trend with increasing velocity. This trend highlights the importance of solids concentration as an underlying parameter affecting erosion mechanisms. The mechanisms of solids-pipe wall interactions will be discussed in Section 4.5.

Ideally, ultrasound measurement site should be flat to increase the measurement accuracy. Here, pipe sections are only flat on the outer wall. Also, any residual material deposited on the inner surface of the pipe will interfere with the measurements. These factors have contributed to the relatively poor accuracy of the ultrasound measurements in the present

study. Although various researchers were able to use this technique with more success, for experiments operated at less abrasive conditions (e.g. lower velocities) the results are not reliable for absolute wear rate measurements. Despite the inconsistency in the ultrasound data presented here, still the ratio of bottom-to-top thickness loss revealed valuable information regarding pipe wall erosion mechanisms. In conclusion, ultrasound thickness measurement is not recommended for detection of small changes in the pipe wall thickness. To be able to perform such measurements, the experiments should run for significantly longer times to observe greater pipe wall mass loss. It was revealed that near-wall solids concentration strongly affects the pipe wall erosion rate.

Although further analysis of the ultrasound measurement data revealed some insight into erosion mechanisms, considering the time-consuming nature of these tests and the limited information gained, the ultrasound measurements were not performed during the Al_2O_3 erosion tests.

4.5 Development of an erosion model based on particle shear stress

As described in Section 1.4.1, typically the erosion rate in slurry pipelines is correlated with slurry velocity. The erosion results obtained here, for two different pipe diameters, revealed that considering only the slurry velocity is not sufficient to predict the erosion rate. Additional parameters such as pipe diameter and solids concentration should be included in the modeling approach. In this section, a new parameter will be introduced based on the underlying mechanisms of slurry pipe-wall erosion to replace velocity as the correlating variable.

Nesic [138] studied the wear behaviour of slurries in two different pipe diameters (solids concentration = 2% by volume, pipe ID = 21 and 42 mm). In his experiments, the local stress on the pipe was predicted using CFD analysis. He was able to observe a strong correlation between the surface stresses and wear rate of the pipes. Schaan et al. [5] studied wear in an oil sands hydrotransport pipeline. They observed higher erosion rates in the bottom section of the pipeline compared to the top. They associated the difference to the presence of a moving bed of solids at the pipe invert. Shook et al. [8] performed a unique study in which they measured both solids flux and erosion rate at various angular positions

during slurry pipeline flow. The results revealed a strong correlation between the solids flux and the local erosion rate. Various other studies have observed that the erosion caused by particle impact is a strong function of the surface stress [5, 44, 45, 101, 139]. For example, Kleis and Kulu [44] showed that for a single particle, the erosion rate is a function of both normal and shear surface stresses. Clark [101] showed that erosion rate on a cylinder exposed to slurry is a function of the impact energy transfer (see Section 1.4.1 for more examples and details of the experiments). Based on the evidence available in the literature and the original hypothesis of the present study, solids particle-pipe wall stress has been chosen as the correlating parameter for erosion predictions in slurry flow. The SRC two-layer friction loss model was chosen to calculate the slurry pipe wall solids stress.

The SRC two-layer model categorizes the wall stress in a slurry pipeline into solids and carrier fluid stresses (Equation (2.7)). As discussed in Section 2.2, solids stress inside the pipeline has two components (Equation (2.11)):

1) Solids kinematic stress
2) Coulombic stress

Each of these components is the summation of the stresses imposed on the pipe wall from each interacting particle; hence, the total solids stress on the wall calculated using the SRC two layer model is a good quantitative indicator of solids particle-pipe wall interaction. Equations (2.7) to (2.9) are used to calculate the average wall stress (see Chapter 2 for a detailed procedure). The wall stress is calculated by combining the effect of the upper layer (τ_1) and the lower layer (τ_2 and τ_c):

$$\tau_w S = \tau_1 S_1 + \tau_2 S_2 + \tau_c S_2 = -\frac{dP}{dz} \times A \qquad (4.6)$$

where τ_w is the total wall stress, S is the wetted perimeter, S_1 and S_2 are the upper and lower layer perimeters respectively (see Figure 2.2), A is the pipe cross sectional area and dp/dz is the pipe frictional gradient. To isolate the solids-wall stresses, the carrier fluid stress should be subtracted from the average stress. A modified form of the Equation (2.7) is used to calculate the carrier fluid wall stress. In this modified form, the solids portion is eliminated:

$$\tau_{cf} = 0.5 \left[f_{cf} \, \rho_{cf} \right] V^2 \qquad (4.7)$$

where τ_{cf} is the carrier fluid wall stress, f_{cf} is the carrier fluid Fanning friction factor, ρ_{cf} is the carrier fluid density and V is the velocity. Carrier fluid friction factor (f_{cf}) is calculated using the carrier fluid properties

155

(e.g. density and viscosity) and the Churchill equation [140]. The solids wall stress is calculated by subtracting the carrier fluid stress from the total stress and is converted into solids pressure gradient by normalizing it with the pipe cross section:

$$\left(\frac{dP}{dz}\right)_s = \left(\frac{dP}{dz}\right)_m - \left(\frac{dP}{dz}\right)_f \tag{4.8}$$

where $(dP/dz)_s$ is the solids pressure gradient, $(dP/dz)_m$ is the mixture pressure gradient and $(dP/dz)_f$ is the carrier fluid pressure gradient. The calculated values are used as the correlating parameters to predict the erosion rate behaviour of both pipe diameters. Figure 4.16 shows the erosion rate as a function of the solids pressure gradient.
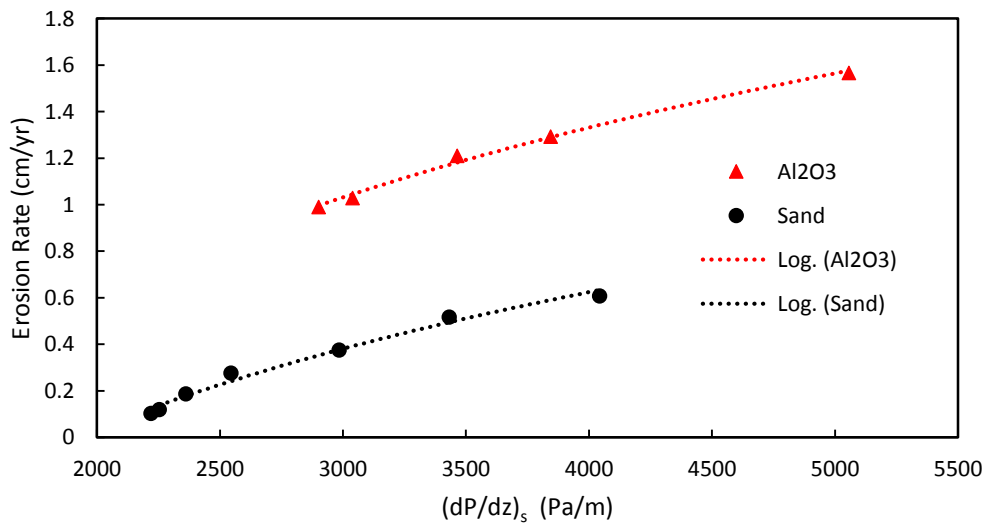
Figure 4.16 Correlation of measured erosive wear rates with solids pressure gradient

156

Figure 4.16 shows that by replacing slurry velocity with solids pressure gradient as the correlating parameter, the two data sets for the 75 mm pipe and the 63 mm pipe collapse. Also the erosion will increase logarithmically with increasing pressure gradient. Using the proposed model, the wear rate can be predicted by the following equation:

$$w = w_0 + k \ln\left(\frac{(dP/dz)_s}{(dP/dz)_{s,o}}\right) \qquad (4.9)$$

where

w^1 = wear rate (cm/year)
w_0 = baseline wear rate (acquired experimentally, cm/year)
$(dP/dz)_{s,o}$ = base line solids pressure gradient inside the pipe (Pa/m)
k = constant (cm/year)
$(dP/dz)_s$ = solids pressure gradient inside the pipe (Pa/m)

Fitting the experimental data presented in Figure 4.16 to Equation (4.9), values for k and w_0 are calculated. For these calculations the first data point (i.e. smallest pressure gradient) is chosen as the baseline

---

[1] The wear rate (w) is not exclusively associated with top or bottom of the pipe erosion rate and is calculated by dividing the mass lost by the experiment time; therefore, it represents the total pipe erosion rate.

measurement. Any arbitrary point will also serve this purpose. Figure 4.17 presents the results of this calculation.
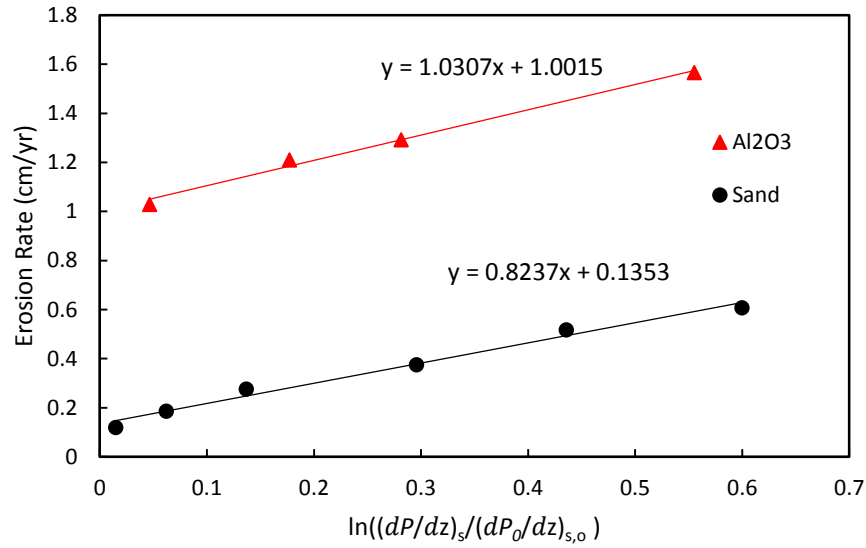
Figure 4.17 Wear rate data fitted to the logarithmic model

The experimental data show that the wear rate will grow at a relatively similar rate for both aluminium oxide and sand slurries, but the base line wear rate is much higher for aluminium oxide. Table 4.5 displays the results for aluminium oxide and sand slurries.

Table 4.5 k and w_0 values

	w_0	k
Aluminium oxide	0.13	1.05
Sand	0.82	3.26

4.5.1 Industrial pipeline wear prediction

The proposed modelling approach can be used to predict the effect of flow parameters on the wear rate of an industrial slurry pipeline. Consider the following example: Plant A has a tailings pipeline operated at the following conditions: solids concentration of 20% (by volume) and velocity of 4 m/s. This pipeline is facing 0.8 cm/yr wear rate. The plant owner decides to recover water from the tailings line before feeding it to the pipeline. As a result, the new operating conditions are: solids concentration of 30% (by volume) and velocity of 3.8 m/s. The higher solids content may have negative consequences on the pipeline wear but with the models available in the literature it is not possible to predict what they might be. The proposed modelling approach can be used to predict the new wear rates. The following steps should be taken for reliable prediction of the wear:

1. Build the model for a specific pipe material.
2. Obtain accurate pressure gradient measurements for the pipeline under current (baseline) operating conditions.
3. Obtain wear rate measurements for the pipeline under current (baseline) conditions.

4. Predict the pressure gradient for the new (proposed) operating conditions.

5. Use the proposed model to predict the ratio of the new wear rate to the current wear rate.

Initially, a set of pipeloop wear experiments should be performed, using the desired pipe material (e.g. carbon steel) and a representative slurry. The wear data obtained from these tests will be used to build the logarithmic growth model (similar to the analysis described in Section 4.5). As an alternative, comparable wear data from the literature can also be used. The following model will be the outcome of this investigation:

$$\text{w} = w_0 + k \ln\left(\frac{(dP/dz)_s}{(dP/dz)_{s,o}}\right) \qquad (4.10)$$

where

w = wear rate (cm/yr)
w_0 = baseline wear rate (acquired experimentally, cm/yr)
$(dP/dz)_{s,o}$ = base line solids pressure gradient inside the pipe (Pa/m)
k = constant (cm/yr)
$(dP/dz)_s$ = solids pressure gradient inside the pipe (Pa/m)

The ideal approach is to obtain pressure gradient data by direct measurement. It is critical to perform such measurements on a section of

160

the pipe where the flow is fully developed. For most industrial slurries, fully developed flow will be achieved in approximately 100 pipe diameters downstream of a disturbance [55].

The next step is to assess the current wear rate. Most pipeline owners monitor the pipe wall thickness regularly. The average pipe wall thickness (i.e. radial average on one pipe location) is a good indicator of pipe wear. The wear rate can be measured by dividing the pipe wall thickness by the measurement interval (e.g. 8 mm/yr). These data are readily available for most slurry pipelines. It is important to choose a time interval over which the slurry properties are relatively constant (e.g. constant flow rate). The study of Schaan et al. [5] is a good example of such an analysis.

The pressure gradient associated with the new operating conditions can be predicted using a model. A good example is the SRC two-layer model [128]. This model is capable of predicting the pressure gradient for typical industrial slurries with a high degree of accuracy.

As presented earlier, the wear rate will increase logarithmically as the solids pressure gradient increases. Based on the model built in Step 1 the following equation can be used to predict the new wear rate:

$$New\ wear\ rate = \ Curren\ wear\ rate + k \ln \left(\frac{New\ pressure\ gradient}{Current\ pressure\ gradient}\right) \quad (4.11)$$

The k value used in this equation is specific to a chosen pipe material and particle properties. Any change in any of these properties (e.g. particle density) requires repetition of Step 1 in the modelling approach. This modelling approach is limited by the experimental data. Specifically, the model application is limited to the following conditions:

1. Straight pipe sections (e.g. not suitable for fittings).

2. Ductile pipe materials (e.g. carbon steel).

3. Similar particle structure to experimental data. For example, the model developed for sand particles cannot be utilized for large lumps.

4. Relatively similar particle size distribution shape between the experimental data and the target condition (i.e. narrow vs broad size distribution).

5. Similar flow regime to experiment conditions (i.e. contract load fractions $C_c/C_r \leq 0.1$)

An example of the application of the model to an industrial

pipeline erosion case study is presented in Appendix F.

4.5.2 Model validation

In this section, the validity of the proposed modelling approach is

examined by testing it with pipe erosion data available in the literature.

The solids pressure gradient is calculated using the method explained in

Section 4.5. Note that in the absence of necessary experimental conditions

for such calculations, reasonable assumptions have been made. These

assumptions will change the absolute value of the results but the trend

will not be affected. Generating accurate pipeline erosion data is very

challenging (see Chapter 1.6.5 for examples of difficulties associated with

these experiments). Therefore, limited data are available for this analysis.

The model inputs used for the calculation of solids shear stress are

presented in Appendix C.

McKibben [6] performed erosion testing for acrylic pipe in a vertical

loop. Figure 4.18 presents the erosion rate in McKibben's experiments for

silica sand at 3 different solids concentrations (20, 30 and 40%).

163
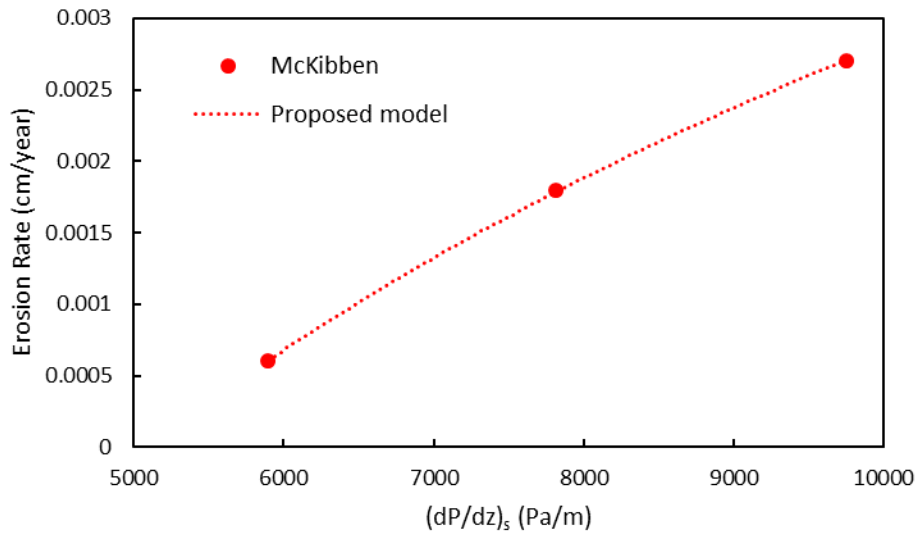
Figure 4.18 McKibben [6] erosion rate data as a function of solids pressure gradient, acrylic pipe, vertical loop, 10, 20 and 30% solids concentration (from left to right), details of the experiments available in Appendix C.

One can observe that even though their experimental conditions are drastically different from those of the present study, the erosion data still follow the logarithmic trend when correlated against the solids pressure gradient.

Moreover, Shook et al. [19] performed wear studies in a horizontal pipe. Their experiments were performed for various pipe materials and particle sizes at different velocities and their results are shown in Figure 4.19.

164
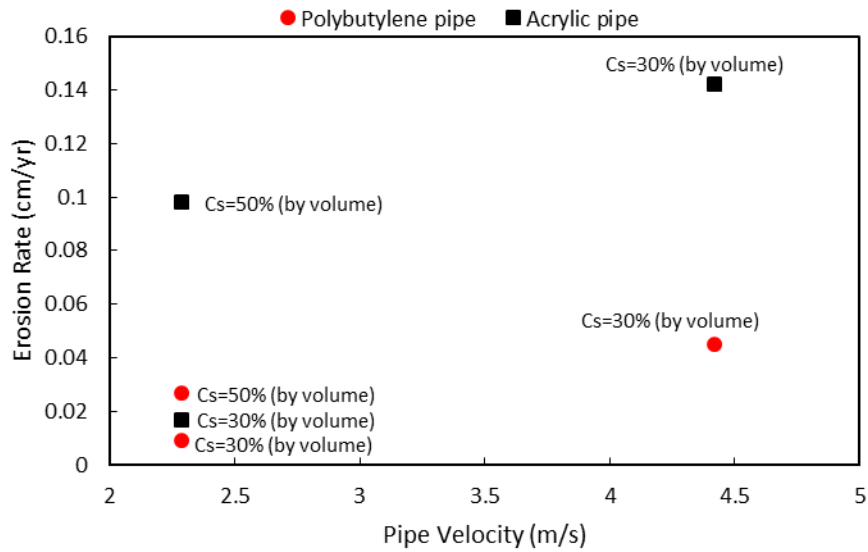
Figure 4.19 Shook et al. [19] pipe erosion as a function of pipe velocity for various solids concentrations, details of the experiments available in Appendix C

The main goal of the Shook et al. [19] study was to evaluate the wear resistance of various pipe materials under pipe flow conditions. Considering the analysis presented in Section 4.4.1, test spools as short as 3 inch can also produce repeatable data; therefore, these tests could have been performed on various pipe materials simultaneously. To check the validity of the proposed model, the Shook et al. [19] data are also correlated as a function of the solids shear stress and the results are presented in Figure 4.20. The model inputs used to calculate the solids shear stress is presented in Appendix 3.

165
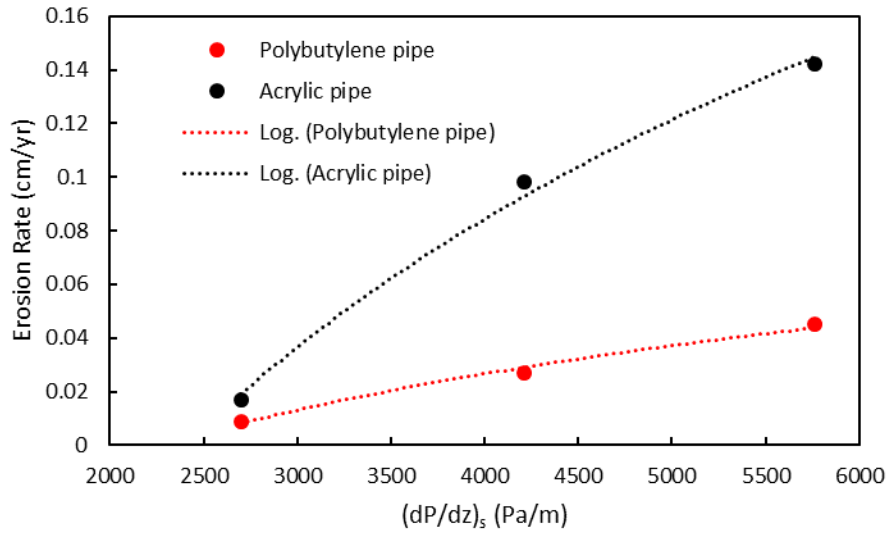
Figure 4.20 Shook et al. [19] erosion rate data as a function of solids pressure gradient, details of the experiments available in Appendix C

One can observe that both types of pipe materials show a logarithmic growth in erosion rate with increasing solids pressure gradient, which is in complete agreement with current study. Using this new approach the effect of both pipe velocity and particle size can be predicted. Table 4.6 shows values of w_0 and k calculated for the literature data analyzed above.

Table 4.6 w_0 and k values for various experimental data

		w_0	k
McKibben [6]	Pipe Steel, Sand	0.0169	0.7242
Shook et al. [19]	Acrylic pipe[1]	0.0356	0.1403
	Polybutylene pipe[1]	0.0015	0.0574

[1]The data in study covered a wide range of velocities and sand concentrations

166

One can observe that w_0 and k values are strong functions of the system properties (e.g. pipe material and solids type). This again highlights the fact that a baseline experimental value is essential for this modeling approach to accurately predict the effect of slurry properties (e.g. solids concentration and velocity) on erosion rate.

Wear data from Goosen and Maglas [48] are chosen to further examine the proposed modeling approach. In their experiments, bottom ash slurry, which has very different properties compared to sand slurries (e.g. 30% density difference), is tested. The flow rate was constant during the course of these experiments. Various pipe diameters were examined during their experiments. As the flow rate is constant, changing the pipe diameter will result in different pipe velocities. Table 4.7 summarizes their test conditions.

Table 4.7 Goosen and Maglas [48] test conditions

Pipe material	PVC
Slurry	40% Bottom ash + water
Flow rate	0.015 m^3/s
Steel pipe IDs (m)	0.091, 0.078, 0.063

Their erosion data are presented in Figure 4.21 as a function of slurry velocity. To reveal the complexities of the data, Figure 4.21 also provides the pipe diameter for each data point.

167
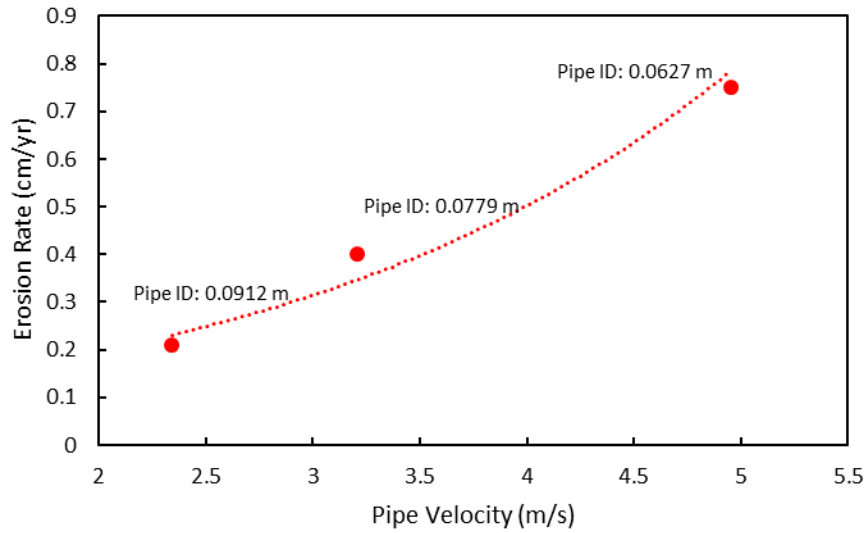
Figure 4.21 Goosen and Maglas [48] wear data , details of the experiments available in Appendix C

Goosen and Maglas observed exponential growth in wear rate as the velocity increases (i.e. reduction in pipe diameter). To check the validity of the proposed modeling approach, the solids pressure gradient for each data point was calculated. The wear rate is presented as a function of solids shear stress in Figure 4.22.
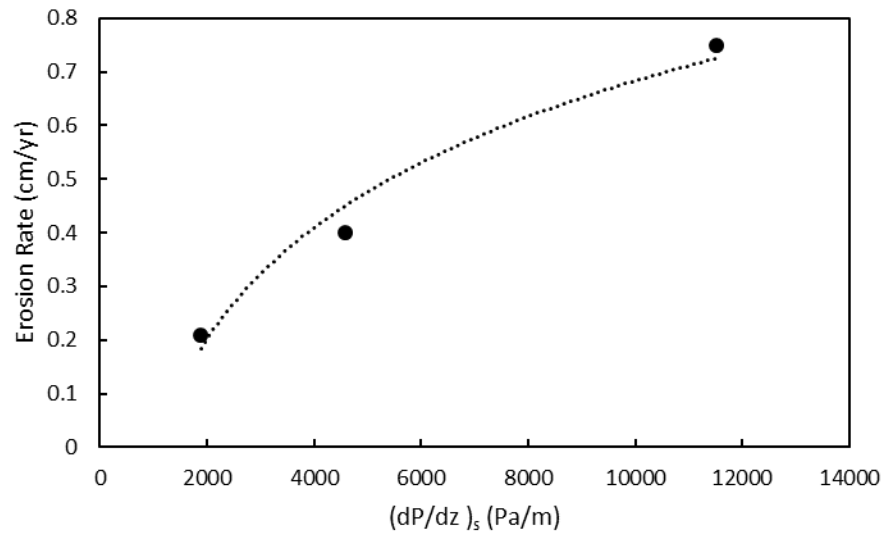
Figure 4.22 Goosen and Maglas [48] erosion rate data as a function of solids pressure gradient, 20% bottom ash, details of the experiments available in Appendix C

Presented wear rates show logarithmic growth as the solids pressure gradient increases, which is in agreement with the proposed modeling approach.

In conclusion, a wide range of wear data has been examined to examine the validity of the proposed model. It was observed that the new approach successfully predicts the wear behaviour of slurry pipelines in various scenarios. The diversity of the magnitude of the w_0 and k values shows the importance of baseline measurement to successfully predict the wear behaviour of a slurry pipeline.

169

4.6 Possible implications of the near-wall lift force n erosive pipe wear[1]

As described in Section 4.2.1, the pipeloop apparatus is equipped with a gamma ray densitometer. The off-bottom (y/D=0.05) solids concentrations data obtained for various types of slurries at different velocities are presented in this section. An analysis of the effect of near-wall lift on friction loss and the possible implications for erosion rate reduction are also described.

If a connection between friction loss and wear can be made –as was done in the previous section – then the research conducted by Wilson and co-workers on the near-wall lift force (e.g. Wilson et al. [141]; Wilson and Sellgren [142]; Whitlock et al. [143]; Wilson et al. [126]) provides a compelling case study, particularly for flows where Coulombic friction is important. The onset of the near-wall lift force often can be seen in the decrease in solids concentration near the pipe wall, as shown in Figure

---

[1] Ardalan Sadighian, Seyed Hashemi, Ryan Spelay, Randall Gillies and Sean Sanders:
Off-Bottom Solids Concentration Measurements: the Possible Implications of Wilson's Near-Wall Lift Force , September 2015, T&S 17 Conference, Delft, Netherlands.

4.23 for results recently obtained at the Saskatchewan Research Council. Similar "turnarounds" in the concentration profile have been observed by many others, as described by Wilson et al. [126]. In that same paper, the authors developed a friction loss model based on the reduction of the slurry stratification ratio, R, using a particle lift coefficient:

$$R = \frac{1}{C_L \theta} = \frac{0.7}{\theta \left(\mathrm{Re}^* \right)^{0.33}} \tag{4.12}$$

$$\theta = \frac{(3/32) f_w V^2}{g(S-1)d} \tag{4.13}$$

$$\mathrm{Re}^* = \frac{\rho_f u^* d}{\mu_f} \tag{4.14}$$

$$\mathrm{Re}^* = \frac{\rho_f u^* d}{\mu_f} \tag{4.15}$$

where C_L is Particle lift coefficient (-), θ is dimensionless ratio, Re^* is particle Reynolds number (-), f_w is Darcy friction factor for the carrier fluid (-), V is average velocity (m/s), g is acceleration of gravity (m/s^2), S is density ratio (solids/fluid), d is particle diameter (m), u^* is particle shear velocity (m/s), μ_f is fluid viscosity, ρ_f is fluid density and R is stratification ratio (i.e. the ratio of solids sliding bed pressure gradient to fluid forces on the particle) defined as:

171

$$R = \frac{i_m - i_w}{\left(\dfrac{\rho_s}{\rho_f} - 1\right) C} \tag{4.16}$$

where ρ_s is the solids density (kg/m^3), ρ_w is the fluid density (kg/m^3), C is the solids concentration (% by volume), i_m is the mixture hydraulic gradient and i_w is the equal flow of water hydraulic gradient in height of water per length of pipe.
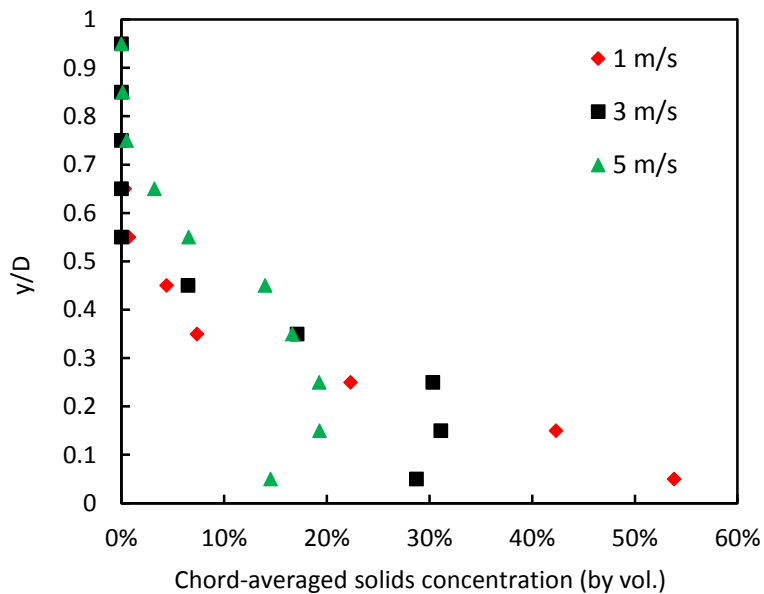
Figure 4.23 Concentration profiles for monosized Delrin spheres (d = 3.34 mm; ρ_s = 1400 kg/m^3) in water: Cr= 9.7%; D = 0.104 m; T = 19.6°C (unpublished SRC data)

The purpose of this set of experiments is to provide a preliminary evaluation of the potential effect that the near-wall lift force could have on wear rates in a slurry flow dominated by Coulombic (contact load) friction.

172

4.6.1 Near-wall concentration experimental details

Experiments were conducted on the 75 mm leg of the pipeloop. The details of the experimental setup can be found in Section 4.2.1. In this particular set of experiments, three key parameters were measured: slurry flow rate (magnetic flow meter), frictional pressure loss (differential pressure cell) and chord-averaged solids concentration at $y/D = 0.05$ (traversing nuclear densitometer).

The length of the pressure drop test section was 3 m and it was located more than 100 pipe diameters from the nearest upstream flow disturbance. Three different water-based slurries were tested: silica sand, aluminum oxide and zirconium silicate. The particle properties are given in Table 4.8. The particle size distributions for the sand and aluminum oxide particles were obtained from sieve analysis and are shown in Figure 3.3. No size distribution is shown for the zirconium silicate (referred to as 'Si-Zi' in Table 4.8 and all subsequent figures showing data for that particular slurry) as the particles are essentially monosized and spherical. The in situ concentration of each slurry tested was held constant at 10%, a value chosen because the near-wall lift force is not attenuated under these conditions [126].

The tests were conducted as follows: the desired mass of the chosen particle type was added to a water-filled loop (to provide the required in situ concentration) and then the loop was operated at a relatively high velocity to ensure the slurry concentration was uniform in the axial direction. The pump speed was then reduced slowly to determine the deposition velocity (V_c). The pump speed was then increased in step-wise increments. Each velocity condition was maintained for about 4 minutes to reduce particle degradation and consequent changes in carrier fluid properties. At each constant-velocity condition, the frictional pressure loss and chord-averaged solids concentration at $y/D = 0.05$ were measured. The pressure loss measurements are shown in Figure 4.24 and the same data are shown in the form of a stratification ratio plot in Figure 4.25. In the latter figure, the point at which the data cross the $R = i_w$ line indicates the operating conditions at which the lift force on a particle balances its submersed weight [126]. It also corresponds to the point at which a reversal in the concentration profile occurs [126]. The velocities at which $R = i_w$ for the three different slurries were 3.3 m/s (sand), 4 m/s (Al_2O_3) and 4.3 m/s (Si-Zi). In Figure 4.26, the variation of the off-bottom solids concentration (at $y/D = 0.05$) is shown as a function of mixture velocity. It is interesting that the "crossover" velocity, V_{NWL}, corresponds almost exactly with a discontinuity in the slope dc/dV for the

174

sand and Si-Zi particles. For the Al_2O_3 particles, the discontinuity can be observed as well, but occurs at a mixture velocity $V < V_{NWL}$. Clearly, the rather simplified approach that considers only particle immersed weight and particle lift (see Equations (4.12) to (4.15) and/or Wilson et al. [126]) cannot explain the behavior of the dc/dV curves. Since it is also not the main focus of the current paper, it must suffice to say that a more complete analysis of the vertical forces acting on a particle must be considered (e.g. Gillies and Shook [122]; Spelay et al. [125]).

Table 4.8 Particle properties

Particle	d_{50} (mm)	ρ_s (kg/m^3)	C_{max}	Circularity	V_c (m/s)
Sand	0.420	2650	0.60	0.80	1.9
Al2O3	0.425	3950	0.56	0.68	2.9
Si-Zi	0.45	3700	0.60	1	2.7
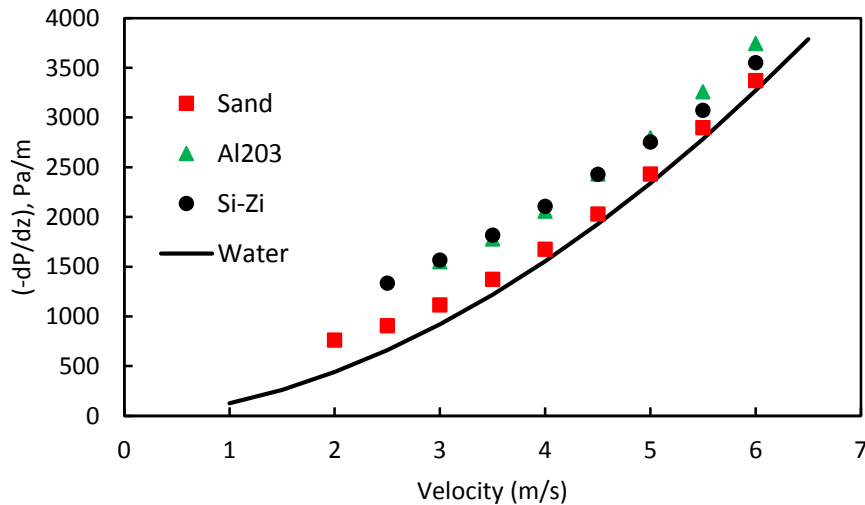
Figure 4.24 Measured pressure gradients for slurries flowing in horizontal test loop C_r = 10%, D = 75 mm; T = 20°C. Solid line shows pressure losses for water.
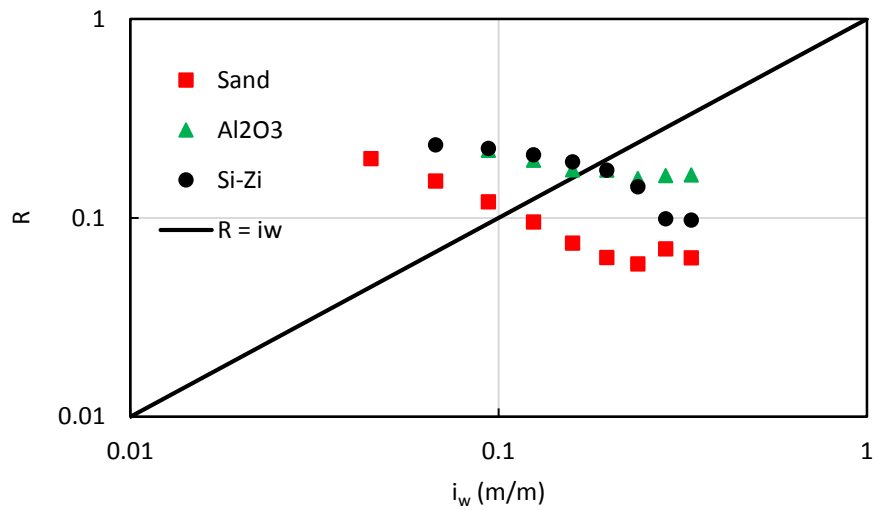
Figure 4.25 Stratification ratio plot for the slurries tested in the present study
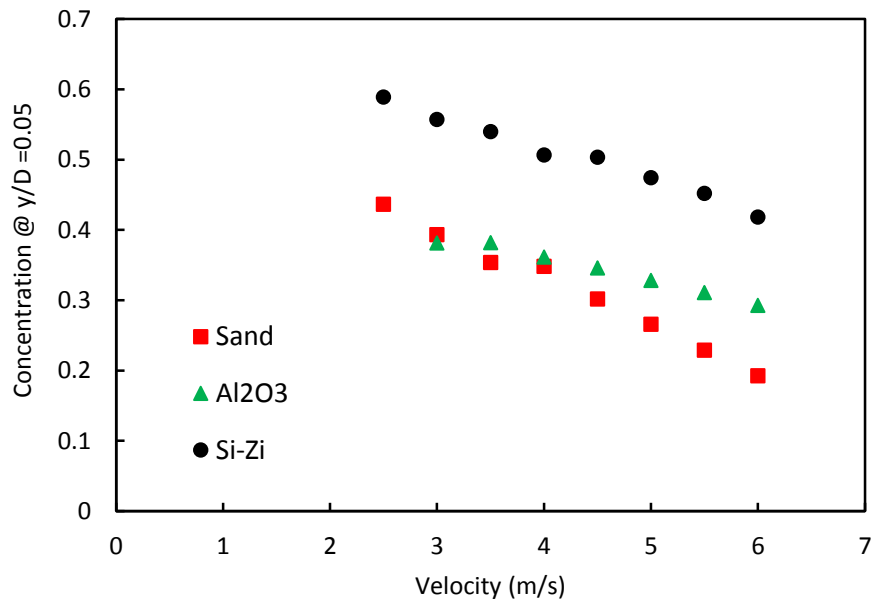
Figure 4.26 Chord-averaged solids concentration measured at a vertical position y/D = 0.05

176

4.6.2 Analysis

Predictions of the near-wall model

Friction loss predictions are not required to fulfill the main objective of the present study (which is presented in the next section); however, since the data are available, a brief analysis of the performance of the near-wall model developed by Wilson et al. [126] is provided. For the conditions tested here, the slurry concentration is relatively low and the particles are larger than the viscous sublayer thickness but not so large as to provide a relative particle diameter (d/D) effect, the near-wall model of Wilson et al. [126] is given by Equation (4.12), which was presented in Section 4.6 introduction. The performance of the near-wall model is illustrated in the parity plot, shown here as Figure 4.27. Generally, the model is better at extremes when the velocity is low (higher R values) or when the velocity is high and the near-wall lift effect is strong. The performance of the model observed here is similar to the results presented by Wilson et al. [126], where the predicted stratification ratios in the intermediate velocity region were not modeled as accurately as the low- and high-velocity conditions.

177
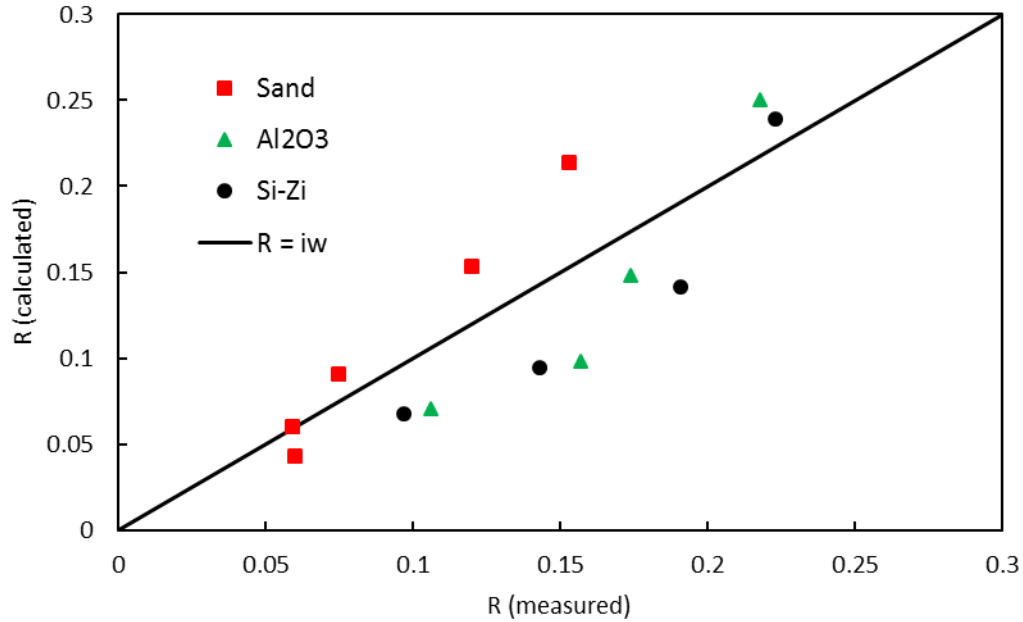
Figure 4.27 Comparison of the stratification ratios calculated from experimental measurements with predictions obtained using the near-wall model of Wilson et al.

Potential implications to erosive pipe wear

As described earlier, the study of Shook et al. [8] clearly showed that the product of wall contact particle flux (cv) and normal force (F) is proportional to erosive wear rate for contact load-dominated slurry flows. In such cases, the wear in the bottom part of the pipe (say, 140 to 220° if 0° and 180° represent the top and bottom of the pipe, respectively) will be 2 to 2.5 times greater than anywhere else on the pipe circumference [8]. In the following analysis, the change in the product [cvF] at the bottom of

178

the pipe with increasing mixture velocity (V) is estimated. To do so, two simplifying assumptions are required: (i) the "near-wall" concentration is taken to be the value measured at $y/D = 0.05$ during the experiments; and (ii) the magnitude of the normal force (F) is proportional to the stratification ratio, which is calculated from the pressure loss measurements (i.e. Figure 4.24).

Clearly, the "near-wall" particle velocity is also required for this analysis. In theory, one could make such a measurement using a wall surface probe [8] or using other methods such as dual-plane Electrical Impedance Tomography (EIT) [144]. One could also calculate the value using CFD simulations, but such predictions (for velocity) are generally poor, especially at lower solids concentrations and mixture velocities [145]. In this particular analysis, however, a notable feature of contact load-dominated slurries is used to develop a relatively simple yet effective method of estimating velocity distributions. For coarse particle slurries that are of interest in the present study, it is well-known that V_c scales with $D^{0.5}$ [121]. The implication is that one should be able to compare velocity distributions in different pipe sizes, provided that C_r and V/V_c are roughly constant. A comparison such as this is shown in Figure 4.28, where scaled velocity measurements in three different pipelines are shown

for conditions where $V/V_c \sim 1.3$ and $Cr \sim 20\%$. The convergence of the velocity measurements, particularly in the lower portion of the pipe, provide a method of estimating the "near-wall" velocity (taken at $y/D = 0.05$ to be consistent with the near-wall concentration assumption described earlier). Although only the scaled velocity distributions for $V/V_c \sim 1.3$ are shown here, a series of these curves was produced for a range of V/V_c values, which allowed for the prediction of the near-wall velocity for all the velocity conditions tested during the present study.
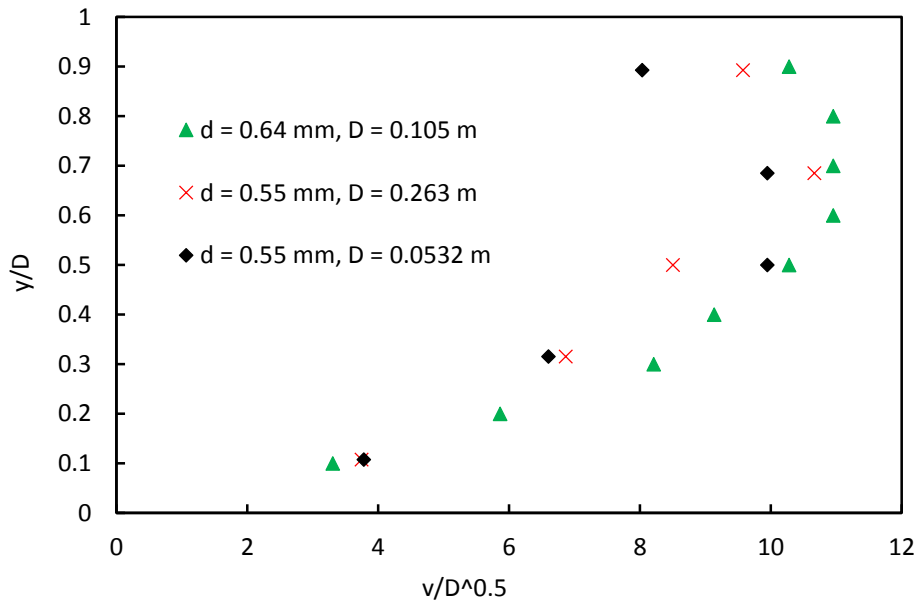
Figure 4.28 Scaled local velocities for slurries. 0.64 mm (0.105 mm pipe): C_r = 25%; V/V_c = 1.25; 0.55 mm (0.263 m pipe): C_r = 25%; V/V_c = 1.31, 0.55 mm (0.0532 m pipe): C_r = 15%; V/V_c = 1.35.

Figure 4.29 demonstrates the quality of the predictions that can be made using the velocity scaling approach, using wall velocity measurements taken from Shook et al. [8] for a slurry of 0.45 mm sand particles flowing in a 50 mm pipe at 2 m/s ($V/V_c = 1.15$) and an in situ solids concentration of 18%. For the comparison the centerline velocity predictions from the scaled velocity model were converted to near-wall velocities at the different circumferential positions using the "isovel" (isovelocity lines) approach outlined in Roco and Shook [146]. Considering the simplicity of the velocity scaling approach and the conversion from centerline velocity values to "near-wall" velocities, the agreement between the measurements and predictions is surprisingly good.

With the measured values of c ($y/D = 0.05$) and R, and the predictions of v from the scaled velocity maps, it is possible to show how the wear-indicating product [cvR] varies as the mixture velocity (and impact of the near-wall lift) increases. In Figure 4.30, the product [cvR] is normalized using the value calculated at an operating velocity that is "typical" for most coarse particle slurry pipelines operating in turbulent flow ($1.05 \leq V/V_c \leq 1.15$). The results show that the normalized wear-indicating product follows a clear trend: there is a slight increase (to about 1.05) at moderate values of V/V_c, and then a sharp decrease as V/V_c is increased

181

beyond $V/V_c \sim 1.75$. The implication is that the wear in the bottom portion of the pipe for contact load slurries should be reduced since the product of (flux × normal force) is substantially reduced. At this point, some healthy skepticism regarding the above is required, primarily for two reasons: a) supporting experimental measurements have not yet been made; and b) any reduction in wear at the pipe invert may be completely overshadowed by the increased overall wear rates. The best possible implementation of higher-velocity operation may in fact be to strike a balance such that overall wear rates are slightly higher but are more uniform over the pipe circumference.
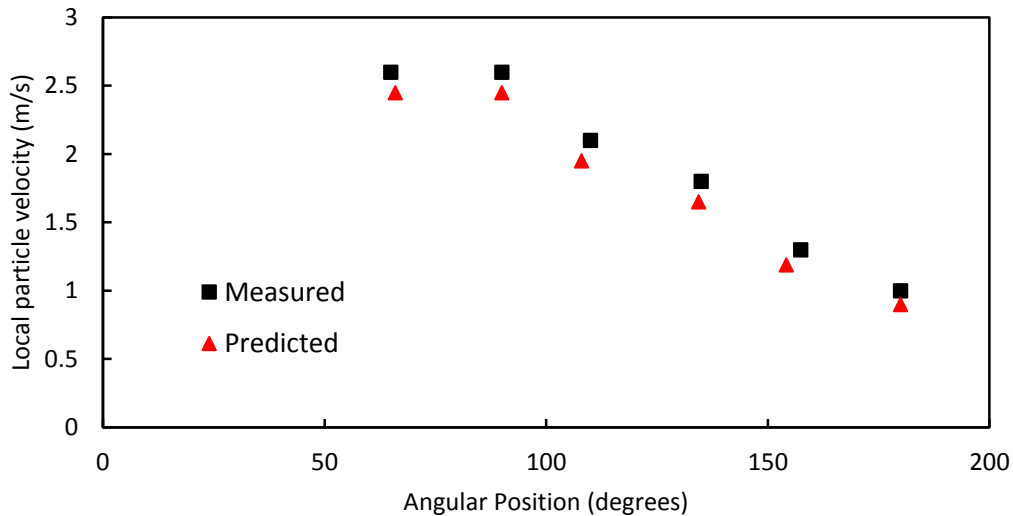
Figure 4.29 Comparison of the particle velocity measurements of Shook et al. (1990) with predictions obtained using the scaled velocity approach: D = 53 mm; d = 0.45 mm; C_r = 18%; V/V_c = 1.15.
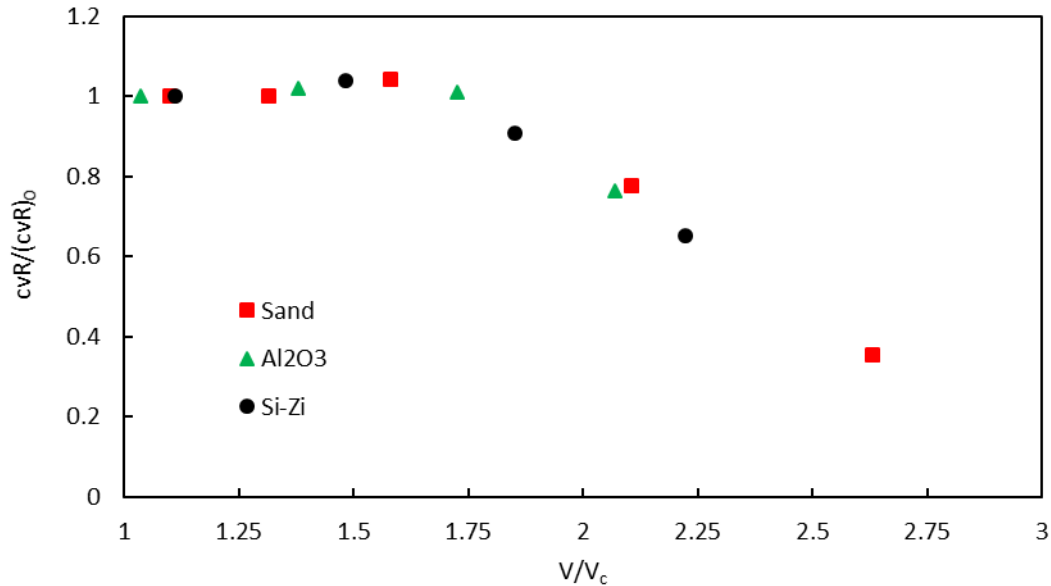
Figure 4.30 Variation of the contact-load wear parameter [cvR] normalized by the value obtained at "typical" operating velocities ($1.05 \leq V/V_c \leq 1.15$) for the three slurries tested during the present study.

In the present study, experiments were conducted using dilute, coarse particle slurries ($d \sim 0.425$ mm, $C_r = 10\%$) to evaluate the effect of high-velocity operation, and consequent onset of Wilson's near-wall lift, on stratification ratio (R) and the chord-averaged concentration near the bottom of the pipe (i.e. at $y/D = 0.05$). Since no local particle velocities were measured, a simple method for predicting velocity distributions in contact load-dominated slurries was proposed. The relative product of particle flux and normal force [cvR] was calculated as a function of mixture velocity. The relative product decreases substantially at operating velocities $V/V_c > 1.75$. This finding may have important implications in terms of selecting operating conditions that reduce the asymmetric wear

associated with coarse particle slurry flows, but most probably at the expense of increasing the overall wear rate.

5. Conclusions and recommendations for future work

5.1 Conclusions and novel contributions

The main goal of the present study was to investigate slurry pipeline erosion and the mechanisms governing this phenomenon. The research plan was built based on the hypothesis that slurry pipe wear has a direct relationship with pipe wall stress. To investigate the surface erosion and examine the hypothesis, the research was broken into two phases:

a) An investigation of carrier fluid viscosity and impact angle on erosion rate (Chapter 3).

b) A pilot-scale investigation of pipe wall erosion (Chapter 4).

In phase one (Chapter 3), a slurry pot tester was chosen to investigate the effect of carrier fluid viscosity and particle impact angle on erosion rate. Gupta et al. [54] showed that data obtained from slurry pot tester can be utilized to predict pipeline wear; therefore, slurry pot tester is a suitable tool for scale-up purposes (see Section 3.4 for details). In contrast with more traditional applications of the slurry pot tester, in this study the specimen alloy (X65 steel) was unchanged and slurry fluid properties

185

were instead the control parameters. Three types of particles were used and the carrier fluid viscosity was changed by changing the composition of the suspending liquid (see Section 4.2.2 for details). The main findings and achievements of this phase are:

1) By choosing slurry properties as the control parameter, a new application of slurry pot tester is introduced. Using the proposed method, the effect of slurry properties (i.e. carrier fluid viscosity, particle density and shape) on erosion rate were investigated.

2) Initially, the effect of solids shape and density on the erosion rate was investigated. It was observed that Al_2O_3 particles cause significantly higher erosion rates, which was attributed to their greater density and more angular shape. To isolate the effect of particle shape (i.e. circularity), erosion rates obtained using rounded sand were compared with those obtained using new sand. It was observed that the fresh sand produces higher erosion rates, which is associated with the sharp tips on the surface of the particles (i.e. higher surface roughness).

186

3) Erosion rates were measured at various impact angles. The maximum erosion rate was observed at an impact angle of 30°. This value was independent of particle type and carrier fluid viscosity.

4) The effect of carrier fluid viscosity on the specimen erosion rate was investigated. Initially, the erosion rate was observed to decrease with increasing carrier fluid viscosity, but after a certain viscosity, the erosion rate increased with increasing viscosity. This phenomenon was consistent for both Al_2O_3 and silica sand particles. To examine the original hypothesis of this study, the normal and shear stresses on the specimen surface were calculated using the Bagnold's methodology. It was observed that erosion rate is function of both normal and shear stresses. Effect of slurry properties (e.g. solids concentration and carrier fluid viscosity) on erosion rate can be predicted by analyzing their effect on shear stresses.

Erosion rates were obtained for Al_2O_3 particles and silica sand at various velocities ($V \approx$ 2-5 m/s) inside the pipe. To directly investigate the pipeline erosion mechanisms, a purpose-built pipeloop was utilized. The achievements of this phase can be categorized into two groups: development of a reliable and repeatable experimental procedure; and the

new insights into the mechanisms of slurry pipe erosion. The contributions in terms of experimental procedure development include the following:

a) As the slurry recirculates inside the loop, it will become less abrasive. This phenomenon is referred to as "particle degradation". Slurry pot tester results revealed that particles with similar shape and size (i.e. new silica sand and rounded sand) may have significantly different erosion rates; therefore, to monitor the particle degradation inside the pipeloop, it is critical to monitor carrier fluid viscosity in addition to particle shape and size.

b) Typically, for the purpose of wear studies, a relatively long test section is used so that entrance/edge effects are reduced. In present study, a new method to examine the presence of edge effects is introduced. Test spools with various lengths were used. It was observed that all the spools have relatively similar wear rate per surface area. By isolating the edge erosion rate (through data analysis), it was revealed that with proper alignment, test spools as short as 3 inch can also produce repeatable data.

188

By analyzing the pipeloop erosion rate data, insight into dominant mechanism affecting slurry pipeline erosion was gained. The main findings here can be itemized as:

a) Al_2O_3 particles showed significantly higher erosion rate. This phenomenon was attributed to low circularity and high density of these particles.

b) To examine the original hypothesis of the present study, the erosion rates were correlated against the associated pipe solids shear stress. It was observed that the erosion rate increases logarithmically with increasing the solids shear stress. This phenomenon is used as the basis for modeling approach proposed here for the first time.

c) The proposed model was validated using various data sets from the literature. It was observed that the proposed modeling approach was applicable to both vertical and horizontal slurry pipe. Also, polymer pipes and lower density particle pipelines were successfully modeled using the proposed approach. The capability of the model for predicting industrial pipeline erosion was also demonstrated. It should be noted that the model application is limited to pipeline

conditions similar to this study experimental conditions (see Section 4.5 for details)

d) The effect of near-wall lift on the solids concentration was analyzed. The product of particle flux and normal force (cvR) is calculated as an indicator of local pipe erosion rate. By analyzing the slurry flow friction loss-slurry pipe erosion connection, it was revealed that the asymmetric wear (i.e. greater erosion at the bottom of the pipe compared to the top) can be reduced by adjusting the pipeline operating conditions. Also, this analysis can be used to predict the local coarse particles settling rates.

5.2 Uncertainties and challenges

In the slurry pot experiments the stresses on the specimen surface were calculated using the Bagnold methodology. However, the experimental conditions are not identical to Bagnold apparatus; hence, direct force measurements on the specimen surfaces is highly recommended to improve the stress model proposed here.

190

As the particles circulate inside the loop they degrade. Specifically, the particle surface roughness (i.e. sharp edges on the surface) will be reduced. By using the degraded particles in the slurry pot tester, it was observed that the change in particle surface roughness will directly affect the erosion rate. In the present study to mitigate the particle degradation effect, slurry is replaced inside the pipeloop on a weekly basis. One pass through testing (i.e. no slurry recirculation) is ideal, but it is extremely resource-consuming.

The main challenge in this study was local erosion measurement on the pipe wall. Ultrasound probe was utilized to locally monitor the thickness of the pipe wall. The absolute value of pipe wall thickness did not reveal any meaningful trend within the course the experiments. This technique is more suitable for longer test durations with relatively larger changes in the pipe wall thickness.

5.3 Recommendations for future work

In this study the stresses on the specimen surface is calculated using Bagnold methodology. Current efforts are ongoing to directly measure both shear and normal stresses on the surface of the specimen. For

191

example, Noda et al. [135] and Ayaz et al. [136] have developed sensors which can be manufactured for this purpose. This will give the ability to correlate the erosion rate to the surface forces more accurately.

For the pipeloop tests, it is also recommended to locally measure the shear and erosion rate. As was previously described, there is a strong correlation between overall erosion rate and shear rate. Therefore, this approach should be used to describe local erosion rates.

Slurry pot tester data revealed the strong effect of particle surface roughness on erosion rate. It is recommended to quantify this parameter and study its effect in a more controlled environment. The results of such investigation may reveal insight into ranking various particles abrasivity.

All the experiments performed in this study eliminated the effect of corrosion by utilizing a corrosion inhibitor. To examine and understand the erosion-corrosion synergy in slurry pipelines, it is recommended to perform test with similar conditions but without the corrosion inhibitor.

Various lab-scale investigations have been performed to investigate the effect of alloy properties on erosion rate. It is highly recommended to

192

perform a similar investigation coupled with pipeloop wear testing. The ability to relate the results of lab-scale wear tester to pipeloop wear results is very valuable. This information can be used as an important new tool for analyzing lab-scale wear results.

Finally, by expanding the range of experiments and specifically altering the solids concentrations, one can collect more evidence for this hypothesis. This will increase the accuracy of the model for predicting the effect of various flow parameters on the wall erosion rate.

Bibliography

1.   ASTM, *ASTM G99 standard test method for wear testing with a pin-on-disk apparatus*. 2010, ASTM Internationl

2.   ASTM, *ASTM G77 standard test method for ranking resistance of materials to sliding wear using block-on-ring wear test*. 2010, ASTM Internationl

3.   Parent, L.L. and D.Y. Li, *Wear of hydrotransport lines in Athabasca oil sands*. Wear, 2013. **301**(1–2): p. 477-482.

4.   Neville, A. and F. Reza. *Erosion-corrosion of cast white irons for application in the oilsands industry*. in *Corrosion*. 2007. Nashville, TN, United states: National Assoc. of Corrosion Engineers International.

5.   Schaan, J., N. Cook, and R.S. Sanders. *On-line wear measurements for commercial-scale, coarse-particle slurry pipelines*. in *The 17th International Conference on the Hydraulic Transport of Solids*. 2007. Cape Town, South Africa: BHR Group Limited.

6.   McKibben, M.J., *Wall erosion in slurry pipelines*, in *ProQuest Dissertations and Theses*. 1992, The University of Saskatchewan (Canada): Ann Arbor. p. 190-190 p.

7.   Parslow, G.I., D.J. Stephenson, J.E. Strutt, and S. Tetlow, *Paint layer erosion resistance behaviour for use in a multilayer paint erosion indication technique*. Wear, 1997. **212**(1): p. 103-109.

8.   Shook, C.A., M. McKibben, and M. Small, *Experimental investigation of some hydrodynamic factors affecting slurry pipeline wall erosion*. Canadian Journal of Chemical Engineering, 1990. **68**(1): p. 17-23.

9.   Wood, R.J.K., J.C. Walker, T.J. Harvey, S. Wang, and S.S. Rajahram, *Influence of microstructure on the erosion and erosion–corrosion characteristics of 316 stainless steel*. Wear, 2013. **306**(1–2): p. 254-262.

10.   Tsai, W., J.A.C. Humphrey, I. Cornet, and A.V. Levy, *Experimental measurement of accelerated erosion in a slurry pot tester*. Wear, 1981. **68**(3): p. 289-303.

11.   Rajahram, S.S., T.J. Harvey, and R.J.K. Wood, *Electrochemical investigation of erosion-corrosion using a slurry pot erosion tester*. Tribology International. **44**(3): p. 232-240.

12.   Levy, A.V. and P. Crook, *The erosion properties of alloys for the chemical processing industries*. Wear, 1991. **151**(2): p. 337-350.

13.   Jiang, L.-F., S.-Z. Yang, X.-L. Ji, Y. Tang, P. Yuan, and Y.-L. Zhou, *Erosion-corrosion of electroplated Ni-based alloy coatings*. Zhendong yu Chongji/Journal of Vibration and Shock, 2012. **31**(21): p. 137-142.

14.   Dong, H., P.Y. Qi, X.Y. Li, and R.J. Llewellyn, *Improving the erosion-corrosion resistance of AISI 316 austenitic stainless steel by low-temperature plasma surface alloying with N and C*. Materials Science & Engineering A (Structural Materials: Properties, Microstructure and Processing), 2006. **431**(1-2): p. 137-45.

15.   Desale, G.R., B.K. Gandhi, and S.C. Jain, *Slurry erosion of ductile materials under normal impact condition.* Wear, 2008. **264**(3–4): p. 322-330.

16.   Chung, R.J., X. Tang, D.Y. Li, B. Hinckley, and K. Dolman, *Abnormal erosion-slurry velocity relationship of high chromium cast iron with high carbon concentrations.* Wear. **271**(10): p. 1454-1461.

17.   Wood, R.J.K., T.F. Jones, J. Ganeshalingam, and N.J. Miles, *Comparison of predicted and experimental erosion estimates in slurry ducts.* Wear, 2004. **256**(9): p. 937-947.

18.   Wood, R.J.K. and T.F. Jones, *Investigations of sand-water induced erosive wear of AISI 304L stainless steel pipes by pilot-scale and laboratory-scale testing.* Wear, 2003. **255**(6): p. 206-218.

19.   Shook, C.A., D.B. Haas, W.H.W. Husband, and M. Small, *Relative wear rate determinations for slurry pipelines.* Journal of Pipelines, 1981. **1**(4): p. 273-280.

20.   Huang, C., P. Minev, J. Luo, and K. Nandakumar, *A phenomenological model for erosion of material in a horizontal slurry pipeline flow.* Wear, 2010. **269**(3–4): p. 190-196.

21.   Cooke, R. *Pipeline Material Evaluation for the Mina Grande Hydrohoist System.* in *13th International Conference of Slurry Handling and Pipeline Transport.* 1996. Johannesburg: BHR.

22.   Hyppaenen, T., *Coating wall to achieve long-lasting abrasion-resistant coating - used in fluidised bed reactor to minimise erosion of walls near refractory lined portions, reducing shut-down time.* Ahlstroem Corp a (Ahls-C) Foster Wheeler Energia Oy (Fosx-C) Foster Wheeler Energia Oy (Fosx-C) Foster Wheeler Energy Co Ltd (Fosx-C). p. 777758-A1:.

23.   Mitsuishi, D., *Fluidized-bed reactor e.g. boiler for use in combustion chamber, determines maintenance time of combustion chamber when presumed wear amount is compared with preset threshold value and presumed wear amount reaches threshold value.* Sumitomo Heavy Ind Ltd (Sumh-C). p. 14.

24.   Fam, D., O. Scrivener, and J. Dodds, *RHEOLOGY AND FLOW OF PHOSPHATE SLURRIES (MINE TAILINGS) IN PIPES.* Chemical Engineering and Technology, 1987. **10**(5): p. 305-311.

25.   Kaushal, D.R., Y. Tomita, and R.R. Dighade, *Concentration at the pipe bottom at deposition velocity for transportation of commercial slurries through pipeline.* Powder Technology, 2002. **125**(1): p. 89-101.

26.   Takano, S., M. Ono, and S. Masanobu. *Evaluation of wearing pipe for subsea mining with large particles in slurry transportation.* in *ASME 2015 34th International Conference on Ocean, Offshore and Arctic Engineering, OMAE 2015, May 31, 2015 - June 5, 2015.* 2015. St. John's, NL, Canada: American Society of Mechanical Engineers (ASME).

27.   Yan, D., T. Parker, and S. Ryan, *Dewatering of fine slurries by the kalgoorlie filter pipe.* Minerals Engineering, 2003. **16**(3): p. 283-289.

28. Fuhr, A., M. Krantz, and B. Fotty. *An investigation into developing slurry flow conditions and their effect on wear profiles using a pilot scale flow loop* in *Hydrotransport 19*. 2014. Golden, Colorado: BHR Group.

29. Lovchev, V.N., D.F. Gutsev, G.V. Tomarov, and A.A. Shipkov, *Improvement and optimization of techniques for monitoring erosion-corrosion wear of equipment and pipelines at nuclear power stations.* Thermal Engineering (English translation of Teploenergetika), 2009. **56**(2): p. 134-141.

30. Stephens, M.P., *Productivity and Reliability-based Maintenance Management.* 2004: Prentice Hall.

31. Gandhi, B.K., S.N. Singh, and V. Seshadri, *Variation of wear along the volute casing of a centrifugal slurry pump.* JSME International Journal, Series B: Fluids and Thermal Engineering, 2001. **44**(2): p. 231-237.

32. Wu, J., B. Ngyuen, L. Graham, Y. Zhu, T. Kilpatrick, and J. Davis, *Minimizing Impeller Slurry Wear through Multilayer Paint Modelling.* The Canadian Journal of Chemical Engineering, 2005. **83**(5): p. 835-842.

33. McNeill, L.S. and M. Edwards, *Iron pipe corrosion in distribution systems.* Journal American Water Works Association, 2001. **93**(7): p. 88-+.

34. Nesic, S., *Key issues related to modelling of internal corrosion of oil and gas pipelines - A review.* Corrosion Science, 2007. **49**(12): p. 4308-4338.

35. Tian, H.H. and G.R. Addie, *Experimental study on erosive wear of some metallic materials using Coriolis wear testing approach.* Wear, 2005. **258**(1-4): p. 458-69.

36. Finnie, I., *Some observations on the erosion of ductile metals.* Wear, 1972. **19**(1): p. 81-90.

37. Benchaita, M.T., P. Griffith, and E. Rabinowicz, *Erosion of metallic plate by solid particles entrained in a liquid jet.* Journal of Engineering for Industry, 1983. **104**(3): p. 215-222.

38. Neville, A. and T. Hodgkiess. *Characterisation of high-grade alloy behaviour in severe erosion-corrosion conditions.* 1999. Cambridge, UK: Elsevier S.A.

39. El-Sayed, S., *Measuring wall forces in a slurry pipeline*, in *Mechanical engineering.* 2010, University of Alberta (Canada): Canada. p. 146.

40. Kesana, N.R., S.A. Grubb, B.S. McLaury, and S.A. Shirazi. *Ultrasonic measurement of multiphase flow erosion patterns in a standard elbow.* in *Fluids Engineering Summer Meeting* 2012. Rio Grande, Puerto Rico: ASME.

41. Kesana, N.R., J.M. Throneberry, B.S. McLaury, S.A. Shirazi, and E.F. Rybicki, *Effect of Particle Size and Liquid Viscosity on Erosion in Annular and Slug Flow.* Journal of Energy Resources Technology, 2013. **136**(1): p. 012901-012901.

42. Neville, A., F. Reza, S. Chiovelli, and T. Revega, *Assessing metal matrix composites for corrosion and erosion-corrosion applications in the oil sands industry.* Corrosion, 2006. **62**(8): p. 657-675.

43. Liang, G.C., X.Y. Peng, L.Y. Xu, and Y.F. Cheng, *Erosion-Corrosion of Carbon Steel Pipes in Oil Sands Slurry Studied by Weight-Loss Testing and CFD*

Simulation. Journal of Materials Engineering and Performance, 2013. **22**(10): p. 3043-3048.

44. Kleis, I. and P. Kulu, *Solid Particle Erosion*. 1 ed. Vol. 1. 2008: Springer.

45. Gandhi, B.K., S.N. Singh, and V. Seshadri, *A study on the effect of surface orientation on erosion wear of flat specimens moving in a solid-liquid suspension.* Wear, 2003. **254**(12): p. 1233-1238.

46. McKibben, M.J. and C.A. Shook, *Slurry Handling: Design of solid-liquid systems Chapter 20*. 1991: Springer Netherlands.

47. Cooke, R. and G. Johnson. *Laboratory apparatus for evaluating slurry pipeline wear*. in *Sait Seminar, Economics of Wear Materials*. 2000.

48. Goosen, P. and I. Maglas. *An experimental investigation into aspects of wear in boiler ash disposal pipelines*. in *14th International Conference on Slurry Handling and Pipeline Transport* 1999. Maastricht, The Netherlands: BHR.

49. Faddick, B. *Wear in pipes*. in *BHRA hydrotransport 9 short course*. 1984. Cranfield, UK.

50. De Pellegrin, D.V. and G.W. Stachowiak, *Assessing the role of particle shape and scale in abrasion using 'sharpness analysis' Part I. Technique development.* Wear, 2002. **253**(9-10): p. 1016-1025.

51. Finnie, I., *Some reflections on the past and future of erosion.* Wear, 1995. **186-187**(1): p. 1-10.

52. Clark, H.M. and K.K. Wong, *Impact angle, particle energy and mass loss in erosion by dilute slurries.* Wear, 1995. **186-187**(2): p. 454-464.

53. Okita, R., Y. Zhang, B.S. McLaury, and S.A. Shirazi, *Experimental and Computational Investigations to Evaluate the Effects of Fluid Viscosity and Particle Size on Erosion Damage.* Journal of Fluids Engineering, 2012. **134**(6): p. 061301-061301.

54. Gupta, R., S.N. Singh, and V. Sehadri, *Prediction of uneven wear in a slurry pipeline on the basis of measurements in a pot tester.* Wear, 1995. **184**(2): p. 169-178.

55. Colwell, J.M. and C.A. Shook, *Entry length for slurries in horizontal pipeline flow.* Canadian Journal of Chemical Engineering, 1988. **66**(5): p. 714-720.

56. Lester, D.R., L.A. Graham, and J. Wu, *High precision suspension erosion modeling.* Wear, 2010. **269**(5–6): p. 449-457.

57. Graham, L.J.W., D.R. Lester, and J. Wu, *Quantification of erosion distributions in complex geometries.* Wear, 2010. **268**(9–10): p. 1066-1071.

58. Chen, X., B.S. McLaury, and S.A. Shirazi, *Application and experimental validation of a computational fluid dynamics (CFD)-based erosion prediction model in elbows and plugged tees.* Computers & Fluids, 2004. **33**(10): p. 1251-1272.

59. Gnanavelu, A., N. Kapur, A. Neville, and J.F. Flores, *An integrated methodology for predicting material wear rates due to erosion.* Wear, 2009. **267**(11): p. 1935-1944.

60. Zhang, Y., B.S. McLaury, and S.A. Shirazi, *Improvements of particle near-wall velocity and erosion predictions using a commercial CFD code.* Journal of Fluids Engineering, Transactions of the ASME, 2009. **131**(3): p. 0313031-0313039.

61. Grant, G. and W. Tabakoff, *Erosion Prediction in Turbomachinery Resulting from Environmental Solid Particles.* Journal of Aircraft, 1975. **12**(5): p. 471-478.

62. Hu, X. and A. Neville, *The effect of an impinging liquid-solid jet on the electrochemical corrosion of stainless steels.* Materials and Corrosion, 2001. **52**(8): p. 598-606.

63. Oka, Y.I., H. Ohnogi, T. Hosokawa, and M. Matsumura, *The impact angle dependence of erosion damage caused by solid particle impact.* Wear, 1997. **203-204**(1): p. 573-579.

64. Brown, N.P. and N.I. Heywood, *Slurry Handling: Design of solid-liquid systems.* 1991: Springer Netherlands.

65. Huang, X.C., H. Lu, H.B. He, X.G. Yan, and D.Y. Li, *Correlation between the wear resistance of Cu-Ni alloy and its electron work function.* Philosophical Magazine, 2015. **95**(34): p. 3896-3909.

66. Ye, H.Z., D.Y. Li, and R.L. Eadie, *Improvement in wear resistance of TiNi-based composites by hot isostatic pressing.* Materials Science and Engineering a-Structural Materials Properties Microstructure and Processing, 2002. **329**: p. 750-755.

67. Ye, H.Z., R. Liu, D.Y. Li, and R.L. Eadie, *Wear and friction of a new wear-resistant material: TiNi-based composites.* Composites Science and Technology, 2001. **61**(7): p. 987-994.

68. Ye, H.Z., D.Y. Li, and R.L. Eadie, *Influences of porosity on mechanical and wear performance of pseudoelastic TiNi-matrix composites.* Journal of Materials Engineering and Performance, 2001. **10**(2): p. 178-185.

69. Shook, C.A., S.K. Ghosh, and F.E. Pilling. *Wall erosion in slurry couette flow.* in *Liquid-Solid Flows and Erosion Wear in Industrial Equipment. Presented at Energy Sources Technology Conference.* 1984. New Orleans, LA, USA: ASME.

70. Shook, C.A. and F.E. Pilling, *Simulating boundary erosion with slurry couette flow* Journal of pipelines, 1987. **6**(1): p. 83-88.

71. Wiedenroth, W. *Experimental study of wear of centrifugal pumps and pipeline components.* in *Liquid-solid flows and erosion wear in industrial equipment. presented at energy sources technology conference.* 1984. New Orleans, LA, USA: ASME.

72. Drury, J.C., *Corrosion monitoring and thickness measurement - What are we doing wrong?* Insight, 1997. **39**(1): p. 17-&.

73. Rudlin, J.R., *Review of existing and possible techniques for corrosion under insulation and wall thickness measurement in steel pressure containments.* Insight, 1997. **39**(6): p. 413-417.

74.	Honarvar, F., F. Salehi, V. Safavi, A. Mokhtari, and A.N. Sinclair, *Ultrasonic monitoring of erosion/corrosion thinning rates in industrial piping systems.* Ultrasonics, 2013. **53**(7): p. 1251-1258.

75.	Yassen, Y., M.P. Ismail, A.A. Jemain, and A.R. Daud, *Reliability of ultrasonic measurement of thickness loss caused by corrosion.* Insight, 2011. **53**(12): p. 658-663.

76.	Scanimetrics. *Scanimetrics Pipe Wear Monitoring* Available from: http://www.scanimetrics.com/solutions/pipeline-integrity-monitoring/pipe-wear.

77.	CiDRA. *HALO Wear Sensor.* Available from: http://www.cidra.com/resource-center/halo-smartring-pipe-wear-measurement-characterization.

78.	Henday, G. *Predicting wear in slurry transport systems* in *Antiwear* 1988. London, UK.

79.	Wu, J., L.J.W. Graham, D. Lester, C.Y. Wong, T. Kilpatrick, S. Smith, and B. Nguyen, *An effective modeling tool for studying erosion.* Wear, 2011. **270**(9–10): p. 598-605.

80.	Noui-Mehidi, M.N., L.J.W. Graham, J. Wu, B.V. Nguyen, and S. Smith, *Study of erosion behaviour of paint layers for multilayer paint technique applications in slurry erosion.* Wear, 2008. **264**(7–8): p. 737-743.

81.	Loewen, D.J., *Characterization of Wear in a Laboratory-Scale Slurry Pipeline.* 2013, University of Alberta (Canada): Ann Arbor. p. 242.

82.	Bajwa, R.S., Z. Khan, V. Bakolas, and W. Braun, *Effect of bath ionic strength on adhesion and tribological properties of pure nickel and Ni-based nanocomposite coatings.* Journal of Adhesion Science and Technology, 2016. **30**(6): p. 653-665.

83.	Dong, S.R., J.P. Tu, and X.B. Zhang, *An investigation of the sliding wear behavior of Cu-matrix composite reinforced by carbon nanotubes.* Materials Science and Engineering a-Structural Materials Properties Microstructure and Processing, 2001. **313**(1-2): p. 83-87.

84.	Singh, B., J. Kumar, and S. Kumar, *Investigation of the Tool Wear Rate in Tungsten Powder-Mixed Electric Discharge Machining of AA6061/10%SiCp Composite.* Materials and Manufacturing Processes, 2016. **31**(4): p. 456-466.

85.	Guilemany, J.M., S. Dosta, and J.R. Miguel, *The enhancement of the properties of WC-CoHVOF coatings through the use of nanostructured and microstructured feedstock powders.* Surface & Coatings Technology, 2006. **201**(3-4): p. 1180-1190.

86.	Lima, R.S., A. Kucuk, and C.C. Berndt, *Evaluation of microhardness and elastic modulus of thermally sprayed nanostructured zirconia coatings.* Surface & Coatings Technology, 2001. **135**(2-3): p. 166-172.

87.	Farshad, F.F., T.C. Pesacreta, J.D. Garber, and S.R. Bikki, *A comparison of surface roughness of pipes as measured by two profilometers and atomic force microscopy.* Scanning, 2001. **23**(4): p. 241-248.

88.	Buschinelli, P.D.V., J.R.C. Melo, A. Albertazzi, J.M.C. Santos, and C.S. Camerini, *Optical Profilometer Using Laser Based Conical Triangulation for*

Inspection of Inner Geometry of Corroded Pipes in Cylindrical Coordinates, in *Optical Measurement Systems for Industrial Inspection Viii*, P.H. Lehmann, W. Osten, and A. Albertazzi, Editors. 2013, Spie-Int Soc Optical Engineering: Bellingham.

89. Buchely, M.F., J.C. Gutierrez, L.M. Leon, and A. Toro, *The effect of microstructure on abrasive wear of hardfacing alloys.* Wear, 2005. **259**(1-6): p. 52-61.

90. Gee, M.G., A. Gant, and B. Roebuck, *Wear mechanisms in abrasion and erosion of WC/Co and related hardmetals.* Wear, 2007. **263**: p. 137-148.

91. Guilemany, J.M., S. Dosta, J. Nin, and J.R. Miguel, *Study of the properties of WC-Co nanostructured coatings sprayed by high-velocity oxyfuel.* Journal of Thermal Spray Technology, 2005. **14**(3): p. 405-413.

92. ASTM, *ASTM G65 Standard Test Method for Measuring Abrasion Using the Dry Sand/Rubber Wheel Apparatus*. 2010, ASTM Internationl

93. Wood, R.J.K. and D.W. Wheeler, *Design and performance of a high velocity air-sand jet impingement erosion facility.* Wear, 1998. **220**(2): p. 95-112.

94. Zu, J.B., I.M. Hutchings, and G.T. Burstein, *Design of a slurry erosion test rig.* Wear, 1990. **140**(2): p. 331-344.

95. Lin, F.Y. and H.S. Shao, *Effect of impact velocity on slurry erosion and a new design of a slurry erosion tester.* Wear, 1991. **143**(2): p. 231-240.

96. Feng, Z. and A. Ball, *The erosion of four materials using seven erodents — towards an understanding.* Wear, 1999. **233–235**(0): p. 674-684.

97. McLaury, B.S., S.A. Shirazi, V. Viswanathan, Q.H. Mazumder, and G. Santos, *Distribution of sand particles in horizontal and vertical annular multiphase flow in pipes and the effects on sand erosion.* Journal of Energy Resources Technology, Transactions of the ASME, 2011. **133**(2).

98. Tang, X., L.Y. Xu, and Y.F. Cheng. *A fundamental understanding of erosion-corrosion of hydrotransport pipes in oil sands slurry*. in *2008 ASME International Pipeline Conference, IPC 2008, September 29, 2008 - October 3, 2008*. 2009. Calgary, AB, Canada: American Society of Mechanical Engineers.

99. Yu, B., D.Y. Li, and A. Grondin, *Effects of the dissolved oxygen and slurry velocity on erosion-corrosion of carbon steel in aqueous slurries with carbon dioxide and silica sand.* Wear, 2013. **302**(1-2): p. 1609-1614.

100. Rajahram, S.S., T.J. Harvey, and R.J.K. Wood, *Evaluation of a semi-empirical model in predicting erosion–corrosion.* Wear, 2009. **267**(11): p. 1883-1893.

101. Clark, H.M., *On the impact rate and impact energy of particles in a slurry pot erosion tester.* Wear, 1991. **147**(1): p. 165-183.

102. Clark, H.M., *Specimen diameter, impact velocity, erosion rate and particle density in a slurry pot erosion tester.* Wear, 1993. **162-164**(0): p. 669-678.

103. Clark, H.M., *Particle velocity and size effects in laboratory slurry erosion measurements OR... do you know what your particles are doing?* Tribology International, 2002. **35**(10): p. 617-624.

104. Abouel-Kasem, A., Y.M. Abd-elrhman, K.M. Emara, and S.M. Ahmed, *Design and Performance of Slurry Erosion Tester.* Journal of Tribology-Transactions of the Asme, 2010. **132**(2).

105. Desale, G.R., B.K. Gandhi, and S.C. Jain, *Improvement in the design of a pot tester to simulate erosion wear due to solid–liquid mixture.* Wear, 2005. **259**(1–6): p. 196-202.

106. Madsen, B.W., *A Portable Slurry Wear Test for the Field.* Journal of Fluids Engineering, 1989. **111**(3): p. 324-330.

107. Tuzson, J.J., *Laboratory slurry erosion tests and pump wear rate calculations.* Journal of Fluids Engineering, Transactions of the ASME, 1984. **106**(2): p. 135-140.

108. Tuzson, J.J., J. Lee, and K.A. Scheibe-Powell. *Slurry erosion tests with centrifugal erosion tester.* 1984. New Orleans, LA, USA: ASME.

109. Llewellyn, R.J., S.K. Yick, and K.F. Dolman, *Scouring erosion resistance of metallic materials used in slurry pump service.* Wear, 2004. **256**(6): p. 592-599.

110. Tian, H.H. and G.R. Addie. *Evaluation of abrasive/erosive wear resistance of some hard coating materials by Coriolis wear testing.* 2006. St. Paul, MN, United states: ASM International.

111. Tian, H.H., G.R. Addie, and E.P. Barsh, *A new impact erosion testing setup through Coriolis approach.* Wear, 2007. **263**(1-6): p. 289-94.

112. Tian, H.H., G.R. Addie, and K.V. Pagalthivarthi, *Determination of wear coefficients for erosive wear prediction through Coriolis wear testing.* Wear, 2005. **259**(1-6): p. 160-170.

113. Clark, H.M. and R.J. Llewellyn, *Assessment of the erosion resistance of steels used for slurry handling and transport in mineral processing applications.* Wear, 2001. **250-251**(PART 1): p. 32-44.

114. Worster, R.C. and D.F. Denny. *The Hydraulic Transport of Solid Material in Pipes.* in *General Meeting of the Institution of Mechanical Engineers.* 1955. London.

115. Henday, G., *A comparison of commercial pipe materials intended for the hydraulic transport of solids: report prepared on behalf of: pipe wear consortium.* 1988: BHRA, the Fluid Engineering Centre.

116. Wood, R.J.K., T.F. Jones, and J. Ganeshalingam. *Erosion in swirl-inducing pipes.* 2002. Montreal, Que., United states: American Society of Mechanical Engineers.

117. Shook, C.A., R.G. Gillies, and R.S.S. Sanders, *Pipeline Hydrotransport: With Applications in the Oil Sand Industry.* 2002: SRC Pipe Flow Technology Centre.

118. Bagnold, R.A., *Experiments on a gravity-free dispersion of large solid spheres in a newtonian fluid under shear. Proceedings of the royal society of London. Series A, mathematical and physical sciences*, 1954. **225**(1160): p. 49-63.

119. Gillies, R.G., C.A. Shook, and K.C. Wilson, *Improved two layer model for horizontal slurry pipeline flow.* Canadian Journal of Chemical Engineering, 1991. **69**(1): p. 173-178.

120. Gillies, D.P., *Particle Contributions to Kinematic Friction in Slurry Pipeline Flow*. 2013, University of Alberta (Canada): Ann Arbor. p. 94.

121. Gillies, R.G., J. Schaan, R.J. Sumner, M.J. McKibben, and C.A. Shook. *Deposition velocities for Newtonian slurries in turbulent flow*. 2000. Canadian Society for Chemical Engineering.

122. Gillies, R.G. and C.A. Shook, *Concentration distributions of sand slurries in horizontal pipe flow*. Particulate Science and Technology, 1994. **12**(1): p. 45-45.

123. Shook, C.A. and A.S. Bartosik, *Particle—wall stresses in vertical slurry flows*. Powder Technology, 1994. **81**(2): p. 117-124.

124. Spelay, R., S.A. Hashemi, R.G. Gillies, R. Hegde, R.S. Sanders, D.G. Gillies, and Asme, *Governing Friction Loss Mechanisms And The Importance Of Off-Line Characterization Tests In The Pipeline Transport Of Dense Coarse-Particle Slurries*. Proceedings of the Asme Fluids Engineering Division Summer Meeting, 2013, Vol 1c: Symposia. 2014, New York: Amer Soc Mechanical Engineers.

125. Spelay, R.B., S.A. Hashemi, R.G. Gillies, and R.S. Sanders, *Concentration distributions for slurries of particles having broad size and/or density distributions*. Int. J. Multiphase Flow 2015.

126. Wilson, K.C., R.S. Sanders, R.G. Gillies, and C.A. Shook, *Verification of the near-wall model for slurry flow*. Powder Technology, 2010. **197**(3): p. 247-253.

127. Wilson, K.C. *Stationary Deposits and Sliding Beds in Pipes Transporting Solids*. in *1st Int. Symp on Dredging Technology*. 1975. Cranfield, U.K.: BHRA.

128. Shook, C.A., R.G. Gillies, and R.S. Sanders, *Pipeline hydrotransport*. 2002: SRC.

129. Lindgren, M. and J. Perolainen, *Slurry pot investigation of the influence of erodent characteristics on the erosion resistance of austenitic and duplex stainless steel grades*. Wear, 2014. **319**(1-2): p. 38-48.

130. Lu, B.T., L.C. Mao, and J.L. Luo, *Hydrodynamic effects on erosion-enhanced corrosion of stainless steel in aqueous slurries*. Electrochimica Acta, 2010. **56**(1): p. 85-92.

131. Jerome, F.S., J.T. Tseng, and L.T. Fan, *Viscosities of aqueous glycol solutions*. Journal of Chemical & Engineering Data, 1968. **13**(4): p. 496-496.

132. Neville, A., F. Reza, S. Chiovelli, and T. Revega. *Assessing MMCs for corrosion and erosion-corrosion applications in the oil sands industry*. in *NACE Meeting Papers*. 2004. New Orlean, LA.

133. Hutchings, I.M. and R.E. Winter, *The erosion of ductile metals by spherical particles*. Journal of Physics D: Applied Physics, 1975. **8**(1): p. 8-14.

134. Hunt, M.L., R. Zenit, C.S. Campbell, and C.E. Brennen, *Revisiting the 1954 suspension experiments of R. A. Bagnold*. Journal of Fluid Mechanics, 2002. **452**: p. 1-24.

135. Noda, K., K. Hoshino, K. Matsumoto, and I. Shimoyama, *A shear stress sensor for tactile sensing with the piezoresistive cantilever standing in elastic material*. Sensors and Actuators A: Physical, 2006. **127**(2): p. 295-301.

136. Ayaz, U.K., T. Ioppolo, and M.V. Ötügen, *Direct measurement of wall shear stress in a reattaching flow with a photonic sensor.* Measurement Science and Technology, 2013. **24**(12): p. 1-9.

137. Rodbard, D., *STATISTICAL QUALITY-CONTROL AND ROUTINE DATA-PROCESSING FOR RADIOIMMUNOASSAYS AND IMMUNORADIOMETRIC ASSAYS.* Clinical Chemistry, 1974. **20**(10): p. 1255-1270.

138. Nesic, S. and J. Postlethwaite, *Relationship Between the Structure of Disturbed Flow and Erosion—Corrosion.* Corrosion, 1990. **46**(11): p. 874-880.

139. Figgis, D.L. and A.D. Sarkar, *Method of calculating steady-state wear rate of metals from profilometric traces.* Wear, 1977. **43**(3): p. 351-365.

140. Churchill, S.W., *FRICTION-FACTOR EQUATION SPANS ALL FLUID-FLOW REGIMES.* Chemical Engineering, 1977. **84**(24): p. 91-92.

141. Wilson, K.C., A. Sellgren, and G.R. Addie. *Near-wall fluid lift of particles in slurry pipelines*. in *10th Conf. on Transport and Sedimentation of Solid Particles*. 2000. Wrocław, Poland.

142. Wilson, K.C. and A. Sellgren, *Interaction of Particles and Near-Wall Lift in Slurry Pipelines.* Journal of Hydraulic Engineering, 2003. **129**(1): p. 73-76.

143. Whitlock, L., K.C. Wilson, and A. Sellgren. *Effect of near-wall lift on frictional characteristics of sand slurries*. in *Proc. HYDROTRANSPORT16*. 2004. Cranfield, UK: BHR Group.

144. Hashemi, S.A., A. Sadighian, S.I.A. Shah, and R.S. Sanders, *Solid velocity and concentration fluctuations in highly concentrated liquid-solid (slurry) pipe flows.* International Journal of Multiphase Flow, 2014. **66**: p. 46-61.

145. Hashemi, R., R. Spelay, K.F. Adane, and R.S. Sanders, *Solids Velocity Fluctuations in Concentrated Slurries.* Hydrotransport, 2014. **19**.

146. Roco, M.C. and C.A. Shook, *A MODEL FOR TURBULENT SLURRY FLOW.* Journal of Pipelines, 1984. **4**(1): p. 3-13.

Appendix A

Pipeloop pump curve
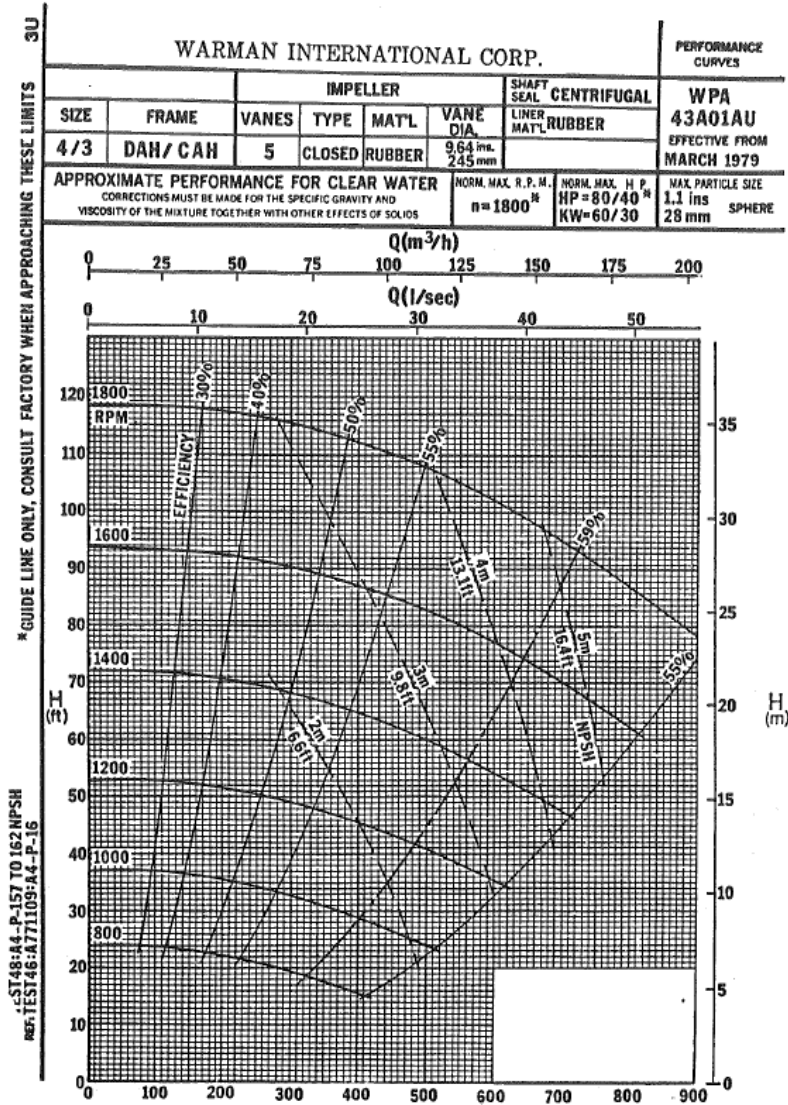
Appendix B

Ultrasound thickness measurement data sets:
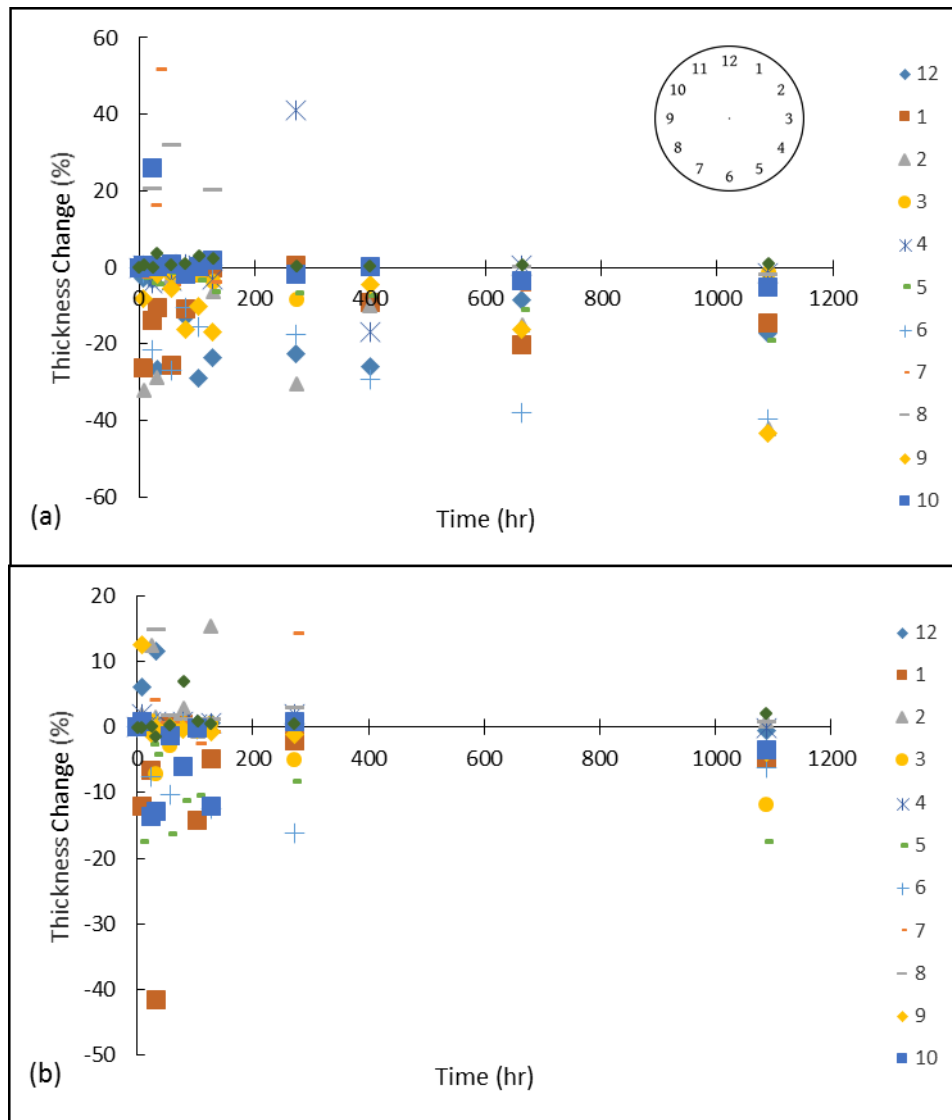
Figure B.1 Ultrasound thickness measurements on 12 angular positions, 20% sand
(a) pipe ID = 63 mm, velocity = 4.03 m/s (b) pipe ID = 75 mm, velocity = 2.65 m/s
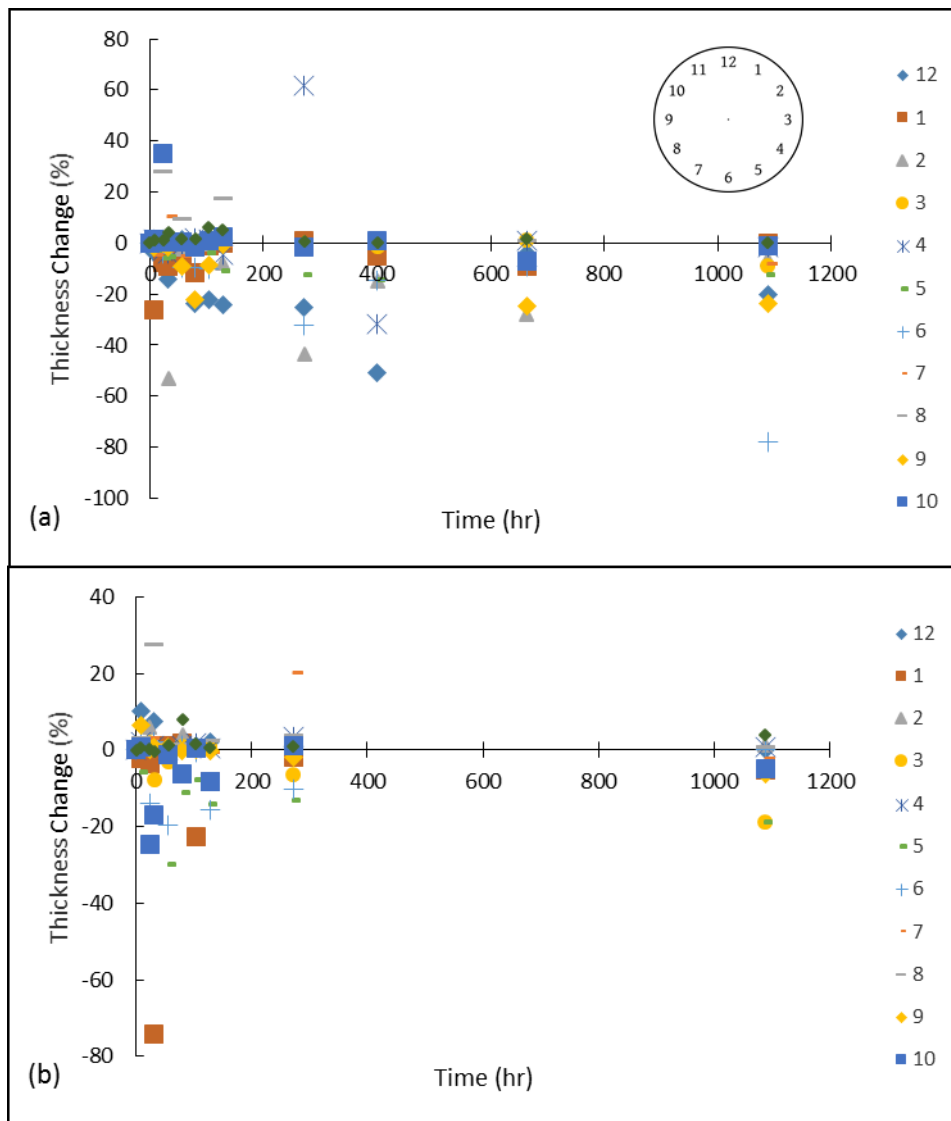
Figure B.2 Ultrasound thickness measurements on 12 angular positions, 20% sand
(a) pipe ID = 63 mm, velocity = 3.47 m/s (b) pipe ID = 75 mm, velocity = 2.28 m/s

206

Appendix C

Model inputs for model validation (see Section 4.5.2)

McKibben [6]

Case #	1	2	3
Pipe ID (mm)	25.8	25.8	25.8
Velocity (m/s)	2.7	2.6	1.9
Solids Density (kg/m³)	2650	2650	2650
Particle d_{50} (mm)	0.47	0.47	0.47
Solids Concentration (% by volume)	20	30	30
Viscosity (mPa.s)	1	1	1

Shook et al. [19]

Case #	1	2	3	4	5	6
Pipe ID (mm)	40	40	40	40	40	40
Velocity (m/s)	2.286	2.286	4.420	2.286	2.286	4.420
Solids Density (kg/m³)	2650	2650	2650	2650	2650	2650
Particle d_{50} (mm)	0.250	0.250	0.250	0.250	0.250	0.250
Solids Concentration (% by volume)	50	30	30	50	30	30
Viscosity (mPa.s)	1	1	1	1	1	1

Goosen and Maglas [48]

Case #	1	2	3	4	5	6
Pipe ID (mm)	91	77	64	91	77	64
Velocity (m/s)	2.22	3.32	4.78	2.22	3.32	4.78
Solids Density (kg/m³)	2000	2000	2000	2000	2000	2000
Particle d_{50} (mm)	0.300	0.300	0.300	0.300	0.300	0.300
Solids Concentration (% by volume)	40	40	40	40	40	40
Viscosity (mPa.s)	1.5	1.5	1.5	1.5	1.5	1.5

Appendix D

Slurry pot raw data

Test Condition		Date	20-Nov-12	
Mixer RPM	660			
Temperature (c)	29.5			
Test Time (min)	45			
Solid (gr)	2960			
Solid Type	Sil4 Sand			
Water (Liter)	6			
EG (Liter)	0			
Position	Angle	Initial Weight (gr)	Final Weight (gr)	Weight loss (gr)
1	0	19.312	19.295	0.017
2	30	19.4437	19.419	0.025
3	60	19.353	19.326	0.027
4	90	19.372	19.3526	0.019

Test Condition		Date	20-Nov-12	
Mixer RPM	660			
Temperature (c)	29.5			
Test Time (min)	45			
Solid (gr)	2960			
Solid Type	Sil4 Sand			
Water (Liter)	4.8			
EG (Liter)	1.2			
Position	Angle	Initial Weight (gr)	Final Weight (gr)	Weight loss (gr)
1	0	19.295	19.282	0.013
2	30	19.419	19.4014	0.018
3	60	19.326	19.3057	0.020
4	90	19.3526	19.3384	0.014

Test Condition		Date	20-Nov-12	
Mixer RPM	660			
Temperature (c)	31			
Test Time (min)	45			
Solid (gr)	2960			
Solid Type	Sil4 Sand			
Water (Liter)	4.2			
EG (Liter)	1.8			
Position	Angle	Initial Weight (gr)	Final Weight (gr)	Weight loss (gr)
1	0	19.282	19.267	0.015
2	30	19.4014	19.383	0.018
3	60	19.3057	19.284	0.022
4	90	19.3384	19.322	0.016

Test Condition		Date		22-Nov-12	
Mixer RPM	660				
Temperature (c)	30.5				
Test Time (min)	45				
Solid (gr)	2960				
Solid Type	Sil4 Sand				
Water (Liter)	3				
Glycerol(Liter)	3				
Position	Angle	Initial Weight (gr)	Final Weight (gr)	Weight loss (gr)	
1	0	19.267	19.247	0.020	
2	30	19.383	19.361	0.022	
3	60	19.284	19.258	0.026	
4	90	19.322	19.3	0.022	

Test Condition		Date	20-Jun-13	
Mixer RPM	660			
Temperature (c)	30.5			
Test Time (min)	45			
Solid (gr)	2960			
Solid Type	Sil4 Sand			
Water (Liter)	3.35			
Glycerol(Liter)	2.65			
Position	Angle	Initial Weight (gr)	Final Weight (gr)	Weight loss (gr)
1	0	19.426	19.408	0.018
2	30	19.475	19.455	0.020
3	60	19.842	19.818	0.024
4	90	19.671	19.65	0.021

Test Condition		Date	20-Jun-13	
Mixer RPM	660			
Temperature (c)	30.5			
Test Time (min)	45			
Solid (gr)	2960			
Solid Type	Sil4 Sand			
Water (Liter)	3.93			
Glycerol(Liter)	2.07			
Position	Angle	Initial Weight (gr)	Final Weight (gr)	Weight loss (gr)
1	0	19.408	19.391	0.017
2	30	19.455	19.436	0.019
3	60	19.818	19.795	0.023
4	90	19.65	19.629	0.021

Test Condition		Date	22-Nov-12	
Mixer RPM	660			
Temperature (c)	29.5			
Test Time (min)	45			
Solid (gr)	4400			
Solid Type	AlO2			
Water (Liter)	6			
EG (Liter)	0			
Position	Angle	Initial Weight (gr)	Final Weight (gr)	Weight loss (gr)
1	0	19.247	19.2006	0.046
2	30	19.3055	19.2378	0.068
3	60	19.28	19.2056	0.074
4	90	19.3	19.246	0.054

Test Condition		Date	26-Nov-12	
Mixer RPM	660			
Temperature (c)	29.5			
Test Time (min)	45			
Solid (gr)	4400			
Solid Type	AlO2			
Water (Liter)	4.8			
EG (Liter)	1.2			
Position	Angle	Initial Weight (gr)	Final Weight (gr)	Weight loss (gr)
1	0	19.2006	19.1684	0.032
2	30	19.2378	19.1809	0.057
3	60	19.2056	19.1422	0.063
4	90	19.246	19.209	0.037

Test Condition		Date	26-Nov-12	
Mixer RPM	660			
Temperature (c)	33			
Test Time (min)	45			
Solid (gr)	4400			
Solid Type	AlO2			
Water (Liter)	4.2			
EG (Liter)	1.8			
Position	Angle	Initial Weight (gr)	Final Weight (gr)	Weight loss (gr)
1	0	19.1684	19.14	0.028
2	30	19.1809	19.13	0.051
3	60	19.1422	19.085	0.057
4	90	19.209	19.175	0.034

Test Condition		Date	6-Dec-12	
Mixer RPM	660			
Temperature (c)	30.5			
Test Time (min)	45			
Solid (gr)	4400			
Solid Type	AlO2			
Water (Liter)	3			
Glycerol(Liter)	3			
Position	Angle	Initial Weight (gr)	Final Weight (gr)	Weight loss (gr)
1	0	19.14	19.088	0.052
2	30	19.13	19.053	0.077
3	60	19.085	19.002	0.083
4	90	19.175	19.108	0.067

Test Condition		Date	19-Jun-13	
Mixer RPM	660			
Temperature (c)	30.5			
Test Time (min)	45			
Solid (gr)	4400			
Solid Type	AlO2			
Water (Liter)	3.35			
Glycerol(Liter)	2.65			
Position	Angle	Initial Weight (gr)	Final Weight (gr)	Weight loss (gr)
1	0	19.391	19.345	0.046
2	30	19.436	19.367	0.069
3	60	19.795	19.717	0.078
4	90	19.629	19.57	0.059

Test Condition		Date	19-Jun-13	
Mixer RPM	660			
Temperature (c)	30.5			
Test Time (min)	45			
Solid (gr)	4400			
Solid Type	AlO2			
Water (Liter)	3.93			
Glycerol(Liter)	2.07			
Position	Angle	Initial Weight (gr)	Final Weight (gr)	Weight loss (gr)
1	0	19.345	19.308	0.037
2	30	19.367	19.305	0.062
3	60	19.717	19.648	0.069
4	90	19.57	19.521	0.049

Test Condition		Date	6-Dec-12	
Mixer RPM	660			
Temperature (c)	28.5			
Test Time (min)	45			
Solid (gr)	2960			
Solid Type	Sil4 Sand 4 week in rotation			
Water (Liter)	6			
EG(Liter)	0			
Position	Angle	Initial Weight (gr)	Final Weight (gr)	Weight loss (gr)
1	0	19.088	19.08	0.008
2	30	19.053	19.045	0.008
3	60	19.002	18.988	0.014
4	90	19.108	19.103	0.005

Test Condition		Date	6-Dec-12	
Mixer RPM	660			
Temperature (c)	35.5			
Test Time (min)	45			
Solid (gr)	2960			
Solid Type	Sil4 Sand 4 week in rotation			
Water (Liter)	4.8			
EG(Liter)	1.2			
Position	Angle	Initial Weight (gr)	Final Weight (gr)	Weight loss (gr)
1	0	19.08	19.073	0.007
2	30	19.045	19.032	0.013
3	60	18.988	18.976	0.012
4	90	19.103	19.095	0.008

Appendix E

Pipeloop Raw Data

Pipe ID (m)	0.0867918	
Pipe Length (m)	0.61	
Pump RPM	1048	
Pump Flow Meter m3	0.01353	
Velocity	2.28691764	
Solid Type	Sil 4 Sand	
Pipe Area	0.166325334	
Slurry Change Interval	1 week	
D50 (mm)	0.45	
Date	13/06/2012	
Time (hr)	272	1500
Weight (kg)	3.597	3.586

Pipe ID (m)	0.0867918	
Pipe Length (m)	0.61	
Pump RPM	1245	
Pump Flow Meter m3	0.01797	
Velocity	3.037391721	
Solid Type	Sil 4 Sand	
Pipe Area	0.166325334	
Slurry Change Interval	1 week	
D50 (mm)	0.45	
Date	25/07/2012	
Time (hr)	0	493
Weight (kg)	3.586	3.578

Pipe ID (m)	0.0867918	
Pipe Length (m)	0.61	
Pump RPM	1133	
Pump Flow Meter m3	0.015715	
Velocity	2.656238781	
Solid Type	Sil 4 Sand	
Pipe Area	0.166325334	
Slurry Change Interval	1 week	
D50 (mm)	0.45	
Date	22/08/2012	
Time (hr)	0	450
Weight (kg)	3.578	3.57333

Pipe ID (m)	0.0867918	
Pipe Length (m)	0.61	
Pump RPM	1133	
Pump Flow Meter m3	0.015715	
Velocity	2.656238781	
Solid Type	Sil 4 Sand	
Pipe Area	0.166325334	
Slurry Change Interval	4 week	
D50 (mm)	0.45	
Date	19/09/2012	
Time (hr)	0	493
Weight (kg)	3.57333	3.56992

Pipe ID (m)	0.0867918	
Pipe Length (m)	0.61	
Pump RPM	1092	
Pump Flow Meter m3	0.01354	
Velocity	2.288607897	
Solid Type	AlO2	
Pipe Area	0.166325334	
Slurry Change Interval	1 week	
D50 (mm)	0.45	
Date	03/10/2012	
Time (hr)	0	264
Weight (kg)	3.56992	3.56341

Pipe ID (m)	0.0867918	
Pipe Length (m)	0.61	
Pump RPM	**1364**	
Pump Flow Meter m3	0.02025	
Velocity	3.422770304	
Solid Type	Sil 4 Sand	
Pipe Area	0.166325334	
Slurry Change Interval	1 week	
D50 (mm)	0.45	
Time (hr)	0	750
Weight (kg)	3.55885	3.54087

Pipe ID (m)	0.0867918	
Pipe Length (m)	0.61	
Pump RPM	1092	
Pump Flow Meter m3	0.01578	
Velocity	2.667225451	
Solid Type	AlO2	
Pipe Area	0.166325334	
Slurry Change Interval	none	
D50 (mm)	0.45	
Date	03/10/2012	
Time (hr)	0	160
Weight (kg)	3.54087	3.52713

Pipe ID (m)	0.0867918	
Pipe Length (m)	0.61	
Pump RPM	1092	
Pump Flow Meter m3	0.02029	
Velocity	3.429531331	
Solid Type	AlO2	
Pipe Area	0.166325334	
Slurry Change Interval	none	
Date	03/10/2012	
Time (hr)	0	190
Weight (kg)	3.52713	3.51017

Pipe ID (m)	0.0709168	
Pipe Length (m)	0.61	
Pump RPM	1048	
Pump Flow Meter m3	0.01353	
Velocity	3.42538707	
Solid Type	Sil 4 Sand	
Pipe Area	0.135902936	
Slurry Change Interval	1 week	
D50 (mm)	0.45	
Date	13/06/2012	
Time (hr)	272	1500
Weight (kg)	1.414	1.374

Pipe ID (m)	0.0709168	
Pipe Length (m)	0.61	
Pump RPM	1245	
Pump Flow Meter m3	0.01797	
Velocity	4.549460876	
Solid Type	Sil 4 Sand	
Pipe Area	0.135902936	
Slurry Change Interval	1 week	
D50 (mm)	0.45	
Date	25/07/2012	
Time (hr)	0	493
Weight (kg)	1.384	1.358

Pipe ID (m)	0.0709168	
Pipe Length (m)	0.61	
Pump RPM	1133	
Pump Flow Meter m3	0.015715	
Velocity	3.978563031	
Solid Type	Sil 4 Sand	
Pipe Area	0.135902936	
Slurry Change Interval	1 week	
D50 (mm)	0.45	
Date	22/08/2012	
Time (hr)	0	450
Weight (kg)	1.358	1.33778

Pipe ID (m)	0.0709168	
Pipe Length (m)	0.61	
Pump RPM	1133	
Pump Flow Meter m3	0.015715	
Velocity	3.978563031	
Solid Type	Sil 4 Sand	
Pipe Area	0.135902936	
Slurry Change Interval	1 week	
Time (hr)	0	493
Weight (kg)	1.33578	1.32024

Pipe ID (m)	0.0709168	
Pipe Length (m)	0.61	
Pump RPM	1092	
Pump Flow Meter m3	0.01354	
Velocity	3.427918768	
Solid Type	AlO2	
Pipe Area	0.135902936	
Slurry Change Interval	1 week	
Time (hr)	0	442
Weight (kg)	1.32024	1.27382

Pipe ID (m)	0.0709168	
Pipe Length (m)	0.61	
Pump RPM	**1364**	
Pump Flow Meter m3	0.02025	
Velocity	5.126687966	
Solid Type	Sil 4 Sand	
Pipe Area	0.135902936	
Slurry Change Interval	1 week	
D50 (mm)	0.45	
Time (hr)	0	750
Weight (kg)	1.2535	1.16107

Pipe ID (m)	0.0709168	
Pipe Length (m)	0.61	
Pump RPM	1092	
Pump Flow Meter m3	0.01578	
Velocity	3.995019067	
Solid Type	AlO2	
Pipe Area	0.135902936	
Slurry Change Interval	1 week	
Time (hr)	0	160
Weight (kg)	1.16107	1.14312

Pipe ID (m)	0.0709168	
Pipe Length (m)	0.61	
Pump RPM	1092	
Pump Flow Meter m3	0.02029	
Velocity	5.136814757	
Solid Type	AlO2	
Pipe Area	0.135902936	
Slurry Change Interval	1 week	
Time (hr)	0	190
Weight (kg)	1.14312	1.1173

Appendix F

Model Sample Calculation

In this section the presented model (details available in Section 4.5) is used to predict the erosion rate in a typical oil sands tailings pipeline.

Step 1: The erosion model (4.9) is built based on experimental erosion data acquired for a representative slurry pipeline (details available in Section 4.5).

$$ w = w_0 + 3.1 \ln\left(\frac{(dP/dz)_s}{(dP/dz)_{s,o}}\right) $$

where w is the pipeline erosion rate (cm/yr), $(dp/dz)_s$ is the pipeline solids pressure gradient (Pa/m), w_0 is the baseline erosion rate and $(dP/dz)_{s,o}$ is the solids pressure gradient.

Step 2 and 3: Acquire baseline pressure gradient and erosion rate. Pipeline baseline conditions are presented in Table F.1:

Table F.1 pipeline properties

Pipe Diameter (m)	0.60
Velocity (m/s)	4.84
Viscosity (Pa.s)	0.001
Sand d_{50} (μm)	250
Solids %(by volume)	25
Solids Density (kg/m^3)	2650
Carrier Fluid Density (kg/m^3)	1000
Erosion Rate (cm/yr)	8
Pressure Gradient (Pa/m)	516

As presented in Table F.1 currently pipeline wall is facing 8 cm/yr erosion rate. As a result of process modifications the feed to the pipeline has altered to the following conditions:

Table F.2 pipeline properties

Pipe Diameter (m)	0.71
Velocity (m/s)	5.31
Viscosity (Pa.s)	0.0011
Sand d_{50} (μm)	280
Solids %(by volume)	35
Solids Density (kg/m^3)	2650
Carrier Fluid Density (kg/m^3)	1000
Erosion Rate (cm/yr)	?
Pressure Gradient (kPa/m)	?

Step 4: Using available models (e.g. SRC two-layer model) or direct measurement the pressure gradient for the tailings pipeline at the secondary is calculated/measured. The new pressure gradient is 683 Pa/m.

Step 5: Using the model built in Step 1 the erosion rate for new pipeline condition will be calculated:

$$w = w_0 + 3.1 \ln\left(\frac{(dP/dz)_s}{(dP/dz)_{s,o}}\right) = 8 + 3.1 \ln\left(\frac{683}{516}\right) = 8.89$$

One can observe that by altering the velocity, concentration, viscosity and particle size the erosion rate has increased from 8 cm/yr to 8.89 cm/yr.